UNIVERSITÀ DEGLI STUDI DI UDINE
hic sunt futura

www.uniud.it

Phd Course in
Computer Science, Mathematics And Physics

CYCLE XXXII

Periodic solutions and chaotic dynamics in a Duffing equation model of charged particles

Dottorando

Oltiana Gjata

Supervisore

Fabio Zanolin

YEAR 2020

Universitá degli studi di Udine
Dipartimento di Scienze Matematiche, Informatiche e Fisiche

Tesi di Dottorato

Informatica e Scienze Matematiche e Fisiche
XXXII Ciclo

Periodic solutions and chaotic dynamics in a Duffing equation model of charged particles

Author:
Oltiana Gjata

Supervisor:
Prof. Fabio Zanolin

A.A. 2020

UNIVERSITÁ DEGLI STUDI DI UDINE

Abstract

Dipartimento di Scienze Matematiche, Informatiche e Fisiche

Dottorato di Ricerca

Periodic solutions and chaotic dynamics in a Duffing equation model of charged particles

by Oltiana Gjata

The emergence of chaotic behavior in many physical systems has triggered the curiosity of scientists for a long time. Their study has been concentrated in understanding which are the underlying laws that govern such dynamics and eventually aim to suppress such (often) undesired behavior. In layman terms, a system is defined chaotic when two orbits that initially are very near to each other will diverge in exponential time. Clearly, this translates to the fact that a chaotic system can hardly have regular behavior, a property that is also often required even for human-made systems. An example is that of particle accelerators used a lot in the study of experimental physics. The main principle is that of forcing a large number of particles to move periodically in a toroidal space in order to collide with each other. Another example is that of the tokamak, a particular accelerator built to generate plasma, one of the states of the matter. In both cases, it is crucial for the sake of the accelerating process, to have regular periodic behavior of the particles instead of a chaotic one.

In this dissertation, we have studied the question of chaos in mathematical models for the motion of magnetically charged particles inside the tokamak in the presence or absence of plasma. We start by a model introduced by Cambon et al., which describes in general mathematical terms, also known as the Duffing modes, the formalism of the above problem. The central core of this work reviews the necessary mathematical tools to tackle this problem, such as the theorem of the Linked Twisted maps and the variational Hamiltonian equations which describe the evolutionary dynamics of the system under consideration. Extensive analytical and numerical tools are required in this thesis work to investigate the presence of chaos, known as chaos indicator. The main ones we have used here are the Poincaré Map, the Maximum Lyapunov Exponent (MLE), and the SALI and GALI methods.

Using the techniques mentioned above, we have studied our problem analytically and validated our results numerically for the particular case of the Duffing equation, which applies to the motion of charged particles in the tokamak. In detail, we first discuss the presence of chaotic dynamics of charged particles inside an idealized magnetic field, suggested by a tokamak type configuration. Our model is based on a periodically perturbed Hamiltonian system in a half-plane r ¿ 0. We propose a simple mechanism producing complex dynamics, based on the theory of Linked Twist Maps jointly with the method of stretching along the paths. A key step in our argument relies on the monotonicity of the period map associated with the unperturbed planar system. In the second part of our results, we give an analytical proof of the presence of complex dynamics for a model of charged particles in a magnetic field. Our method is based on the theory of topological horseshoes and applied to a periodically perturbed Duffing equation. The existence of chaos is proved for sufficiently large, but explicitly computable, periods. In the latter part, we study the generalized aforementioned Duffing equations and study

the chaoticity using the Melnikov topological method and verify the results numerically for the models of Wang & You and the tokamak one.

I declare that this thesis has been composed by myself and that the work has not be submitted for any other degree or professional qualification. I confirm that the work in preparation is my own, except where work which has formed part of jointly-authored publications has been included. My contribution and those of other authors to this work have been explicitly indicated. I confirm that appropriate credit has been given within this thesis where reference has been made to the work of others.

Udine, June 9 2020

Acknowledgements

Nella realizzazione di questo lavoro sono stata aiutato e supportato da molte persone alle quali esprimo la mia immensa gratitudine. In particolare, voglio ringraziare il Prof. Zanolin che mi ha seguito con tanta devozione passo dopo passo e mi ha capito anche nei momenti più difficili.

Contents

Introduction

The growth of the population has increased the depletion of natural resources, becoming one of the most problems in nowadays society. Regardless, recycling and no wasting politics, our interests are to find and to develop new methods and technology as the grand challenge of the future centuries.

An important task is to use fission reactors to provide replacement of fossil fuel considered as an unsustainable source and a global warming main factor. The development of this new renewable energy source depends on the amount of uranium available on earth. According to Professor Cohen [1] , it is estimated to have enough energy for another 5 billion years extracting uranium at a higher cost from the seawater and from eroding earth crust by river water, and from other types of hard rock mining like in-situ leach, underground, open pit, and heap leaching mining methods. The fast-breeder reactor, are potentially more vulnerable to accidents and would produce large amounts of plutonium that can be used in nuclear weapon production (proliferating bomb-making capacity) and deals with the problems of storing radioactive waste. In 2017, in the United Kingdom, the share of generation from non-fossil fuel was 46%, where 19% is composed of nuclear energy. In 2018 the share of fuel was increased by 2% driven by renewables form of energy.

Fusion reactors offer another way of energy production without disadvantages of fossil and non-fossil fuel. The tokamak, invented in the Soviet Union in the late 1950s by Igor Tamm and Andrei Sakharov, was one of the grand engineering challenges of the last century providing us energy from fusion reactor using deuterium and tritium in equal part in the development of the thermonuclear reaction. Deuterium is a stable isotope of hydrogen. One in 6700 atoms of hydrogen in seawater is deuterium. This amounts to 33 grams of D per m^3, or a total resource of 4.6×10^{19} g in the oceans of the world. Meanwhile, tritium is a radioactive isotope of hydrogen. It can be produced by irradiating lithium metal. However, the serious problem with fusion is the enormous temperature required to overcome the repulsive force between colliding charged particles achieved at temperatures exceeding 2×10^8K, round 12 times hotter than the center of the sun which operates on fusion, but at densities some 10^{12}times greater than reactor values. It is mind-boggling that the deuterium contained in 0.5 liters of ordinary water can provide enough energy for a single family house in Europe for a year when properly fused with tritium in a fusion reactor. The first prototype of tokamak called stellarator was proposed by Spitzer in 1951 using the notion of magnetic confinement, where the solenoidal coils encircling a toroidal tube generate a strong magnetic field. In the 1960s the first tokamak, named T-3 was built at Kurchatov Institute in Moscow with a minor radius of 15 cm and a major radius of 100 cm. Some years later, it was built the JET (joint European torus), remaining until now the largest tokamak in the world.

The study of confined plasma within tokamak remains the main topic of this thesis. Charged particle motion in magnetic field configurations has been proved theoretically to give rise to chaotic dynamics and has been related to ionospheric plasmas [2]. It is shown increasing the number of particles the system becomes more chaotic.

What is chaos? Usually, a dynamical system is called chaotic if small changes to its initial conditions can create large changes to the behavior of the solutions. This is the so-called *sensitive dependence on initial conditions*. Such instability property is not enough to capture the true meaning of deterministic chaos. Indeed, also the linear equation $\dot{x} = x$ of exponential growth presents the same instability features. Typically the condition on sensitive dependence is paired with some other conditions, like the density of periodic orbits, or, more in general, some form of compactness (boundedness) of the solutions. By analogy, a dynamical system is called structurally chaotic if small changes to the equations describe the evolution of the system producing large changes in its behavior. This thesis considers the numerical and theoretical part of chaos detection, with applications to a second-order differential equation model introduced in the study of the dynamics of charged particles confined in a toroidal magnetic field.

Following standard numeric methods (Maximal Lyapunov exponent, SALI, and GALI) supposing small changes of initial conditions, one is able to discriminate between regular and chaotic orbits. The smaller and the generalized alignment index (SALI and GALI) introduced recently by H. Skokos [4] tends to zero for chaotic orbits and approximately remain constant round non zero values in the case of regular orbits. Meanwhile, Maximal Lyapunov exponent tends to zero for regular orbits and remains constant for chaotic orbits.

Other theories treat the same argument but from the topological point of view. One of the first pioneering works of chaos theory was made by Poincaré in the study of transversal homoclinic points, an example becoming the trademark of chaos. But the person who made a revolution in this field was the famous topologist Smale. He was involved in the study of this topic after the preceding pioneering research by Cartwright-Littlewood-Levinson, who encountered some form of chaotic phenomena in the analysis of a set of equations involving radio waves (the periodically forced van der Pol equations). As a topologist, Smale translated some peculiar features concerning the solutions of these equations in terms of the language of geometry, visually interpreted by a horseshoe shape.

Smale said –

"... Sometimes a horseshoe is considered an omen of good luck. The horseshoe that I found on the beaches of Rio certainly seemed to have such a property ..."

Knowing the paper of Birkhoff, he panned out to prove that if a dynamic system possesses a homoclinic point, then it also contains a horseshoe. Continuing on the traces of A. Andronov and L. Pontryagin, he started to develop the theory of hyperbolic dynamical system referring to the concept of structural stability.

Smale continues –

"*... Thus the mathematics created on the beaches of Rio was the horseshoe and the higher dimensional Poincaré's conjecture ...*"

Smale's horseshoe, together with his researches on the Poincaré's conjecture, led him to the Fields medal, transforming Smale into an icon of the science.

An important consequence related to our work is the Stretching along a path or shortly SAP method that when it applies to a couple of oriented rectangular regions (homeomorphic with horseshoe shapes) causes chaotic dynamics following the Linked Twist Maps theorem. Chapter 3 is entirely dedicated to numerical indicators of chaos such as the Maximal Lyapunov Exponent, SALI, and GALI methods, which can discriminate between regular and chaotic orbits as a consequence of small changes in the initial conditions. In particular, the Smaller and the Generalized Alignment Indices (respectively SALI and GALI) were introduced in recent times by H. Skokos [4]. Their measures tend to zero for chaotic orbits and approximately remain constant around non zero values in the case of regular orbits. Meanwhile, Maximal Lyapunov Exponent tends to zero for regular orbits and remains constant for chaotic ones. The latter numerical methods allow fast and precise chaos detection even for higher dimensional systems. In fact, as part of the original contribution, using these methods, I have shown the existence of chaos for a model of charged particles in the absence of plasma in the case of two particles. A survey paper on this topic is in the state of preparation [G]. For the sake of clarity, the original work of Vittot et al. has been limited to the case of a single particle. The same model with a single particle has also been the focus of the original study we present in Chapter 4. As a first step, we have proved the monotonic behavior of the orbits of such a system in the absence of plasma by studying the corresponding Time Mapping function. For more, we also show the minimal conditions for the existence of kT-periodic orbits. These aspects are essential to understand the eventual chaoticity of the system. Using the Linked Twist Map theorem, we prove that our model is chaotic for a particular region of parameters. Based on the topological concept of the horseshoe map, we generalize the results related to the chaoticity of the motion of the charged particles, but now in the presence of plasma. The contributions in this direction, in collaboration with F. Zanolin, which can be founded in [GZ01] and [GZ02].

One of the first followers of Poincaré's theory was V. Melnikov, who continued to work in this direction and introduced a theoretical tool, nowadays known as the " Melnikov method," to predict if the smooth system exhibits chaotic behavior. In other words, if the Melnikov function has simples zeros, then the stable and unstable manifold of the perturbed system intersect transversally. Then by Moser's theorem or the Smale-Birkoff homoclinic theorem, in turn, it has been shown that a smooth system exhibits chaotic dynamics. We applied this theory to a general case of non-smooth Duffing systems. As an illustration, we present an application for a piecewise linear oscillator. These results are presented in [GZ03]. In Chapter 5, we use the Maximal Lyapunov Exponent and the Poincaré map to study the chaoticity of the charged particles model and a more general class of Duffing equations by varying some control parameters. It is observed that for the general Duffing model, the system behaves chaotically only for small values of the frequency, here the control parameter. On the contrary, the tokamak model shows a robust chaoticity for a wide range of the studied control parameter. The Poincaré map also validates these results, where islands of irregularity appear for indicating the presence of chaos. The original contribution to this thesis work has been organized in the following articles:

[GZ01] O.Gjata, F. Zanolin, *An example of chaotic dynamics for the motion of charged particle in a magnetic field*, submitted (2020)

[GZ02] O.Gjata, F. Zanolin, *Complicated dynamics in a model of charged particles*, accepted for publication (2020)

[GZ03] O.Gjata, F. Zanolin, *An application of the Melnikov method to a piecewise linear oscillator*, in preparation (2020)

[G] O. Gjata *Numerical investigation of the chaotic behaviour of charged particles in the tokamak*, in preparation (2020)

Chapter 1

Mathematical model

1.1 Definition, properties and applications of Plasma

Any ionized gas cannot be called a plasma; of course, there is always some small degree of ionization in any gas. A useful definition is as follows [5]

"*A plasma is a quasineutral gas of charged and neutral particles which exhibits collective behavior* "

By collective behavior, we mean motions that depend not only on local conditions but on the state of the plasma in remote regions as well. A plasma is quasineutral it the density of positively charged ions is approximately equal to the density of negatively charged electrons such that electromagnetic forces control their collision. An ionized gas to be called a plasma must satisfy the following property:

1. should be dense enough such that the quantity λ_D called Debye length is much smaller than the dimension of the system L. The quantity Debye length represents the number of charge carriers within a sphere (called the Debye sphere whose radius is the Debye screening length) surrounding a given charged particle is sufficiently high as to shield the electrostatic influence of the particle outside of the sphere.
2. the number of particles N_D in a "Debye sphere" must be greater than 1.
3. we require $\omega\tau_E > 1$ where ω is the frequency of typical plasma oscillations and τ_E is the mean time between collisions with neutral atoms.

Plasmas can be characterized by the two parameters n and KT_e where n is the density, K Bolzman's constant, and T_e temperature of the electron. Plasma applications cover an extremely wide range of n and KT_e: n varies over 28 orders of magnitude from 10^6 to 10^{34} m^{-3} and KT can vary over seven orders from 0.1 to 10^6 eV. Plasma usually exists only in a vacuum. In the laboratory, we need to pump the air out of the vacuum chamber. There are many applications of plasma-like in gas discharges lamp, controlled thermonuclear fusion, atmospheric plasmas, particle accelerators, gas lasers, MHD energy conversion, and ion propulsion.

Plasma is called the fourth state of matter. It is estimated that 99% of the matter in the observable universe is in the plasma state. Just to mention the stellar interior, plasma of sun, solar, wind, ionospheres and magnetospheres of the earth, gaseous nebulas, entire galaxies, and Aurora Borealis.

1.2 Tokamak

A tokamak is a toroidal chamber which uses a strong magnetic field, B_ϕ, to contain hight temperature plasma within the torus. Charged particles cannot easily move across a strong magnetic field. If the fields are closed into nested surfaces, then deuterium and tritium ions trapped in this way colliding with sufficient energy to overcome their repulsive Coulomb potential will fuse liberate energy. The toroidal field is produced by external electric currents flowing in coils around the torus, as shown in Figure 4.13. Superimposed on the toroidal field is much weaker than the poloidal field, B_θ, generated by an electric current I_p flowing in the plasma around the torus. The plasma forms the secondary circuit of a transformer so that I_p is induced by changing the magnetic flux B_T passing through the torus, which is usually carried by an iron core, as indicated in the figure.

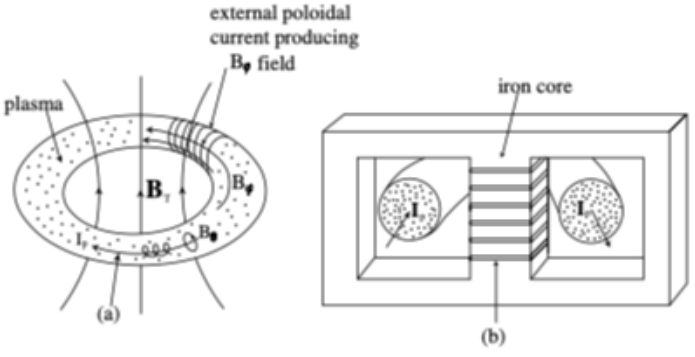

FIGURE 1.1: Tokomak currents and fields: (a) toroidal plasma current induced by transformer, (b) primary winding.This figure has been reproduced from [6]

In a plasma consisting of deuterium, or deuterium mixed with tritium, the fusion reactions

$$D^2 + D^2 \longrightarrow He^3 + n^1 + 3.27MeV$$
$$D^2 + D^2 \longrightarrow T^3 + H^1 + 4.03MeV$$
$$D^2 + He^3 \longrightarrow He^4 + H^1 + 18.3MeV$$
$$D^2 + T^3 \longrightarrow He^4 + n^1 + 17.6MeV$$

will occur frequently if the ion temperature, T_i, and the ion number density, n_i, are large enough. Furthermore, in a fusion reactor, these high values of T_i and n_i must be maintained long enough for the energy liberated by fusion to more than balance the energy losses due to radiation, conduction, convection and neutron flux. Let τ_E be the time it takes these loss processes to remove all the energy from the system than for a given value of $n_i\tau_E$ there is a minimum temperature at which the plasma is said to ignite, i.e., at which the liberated fusion energy is just adequate to balance all losses. As D-D plasmas require a considerably higher temperature to achieve ignition, almost all reactor proposals have concentrated on D-T fusion.

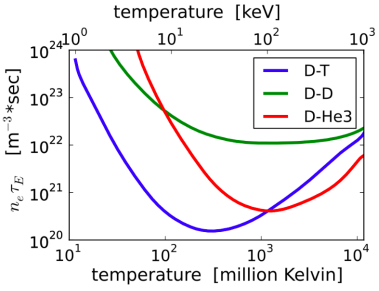

FIGURE 1.2: Ignition curve for a D-D, a D-T and a D-He plasma. This figure has been reproduced from [7]

Figure 4.14 shows the ignition curve for a D-T plasma. It has a minimum at a temperature of about 30 keV, where for ignition we need $n_i\tau_E > 1.5 \times 10^{20}\ m^{-3}s$.

1.3 Physical model of charged particells inside tokamak

In this section, we will study the motion of charged particles in the presence and absence of plasma in terms of the laboratory toroidal coordinates (r, θ, ϕ) where r denotes the distance from the magnetic axis, which is located at a distance R, from the axis of

symmetry, θ denotes poloidal angle, and ϕ indicates a toroidal angle. The the following relation gives the toroidal coordinates:

$$(x, y, z) = (r, r\theta, (R + r\cos\theta)\phi) \tag{1.1}$$

Furthermore, we shall adopt a Lagrangian approach to describe the dynamics of charged particles In a tokamak magnetic field as in [**?**]. Since the corresponding the element of length ds satisfies

$$ds^2 = r^2 + r^2 d\theta^2 + (R + r\cos\theta)^2 d\phi^2$$

and magnetic field $\vec{B}$ satisfies

$$\vec{B} = (0, B_\phi, B_\theta) = (0, \psi_T(r, \theta), \psi_P(r, \phi))$$

for a particle of unit mass and charge e in a tokamak magnetic field, with an electrostatic potential V also present one can easily define the toroidal coordinate Lagrangian function

$$L = \frac{1}{2}r^2 + \frac{1}{2}r^2\dot{\theta}^2 + \frac{1}{2}(R + r\cos\theta)^2\dot{\phi}^2 + e\Big(\dot{\theta}\psi_T(r, \theta) + \dot{\phi}\psi_P(r, \phi)\Big) + eV \tag{1.2}$$

In eq. (1.2) the first three terms describe the particle kinetic energy and the last ones the particle potential energy. The Euler- Langrage equations

$$\frac{d}{dt}\frac{\partial L}{\partial \dot{q}_i} - \frac{\partial L}{\partial q_i} = 0 \tag{1.3}$$

when applied to the Lagrangian of eq. (1.2), yields the evolution equations

$$\ddot{r} - r\dot{\theta}^2 - \cos\theta(R + r\cos\theta)\dot{\phi}^2 - e\Big(\dot{\theta}\frac{\partial\psi_T}{\partial r} - \dot{\phi}\frac{\partial\psi_p}{\partial r}\Big) - e\frac{\partial V}{\partial r} = 0 \tag{1.4}$$

$$\frac{d}{dt}(r^2\dot{\theta}) + e\dot{r}\frac{\partial\psi_T}{\partial r} + r\sin\theta(R + r\cos\theta)\dot{\phi}^2 - e\frac{\partial V}{\partial r} = 0 \tag{1.5}$$

$$\frac{d}{dt}((R + r\cos\theta)^2\dot{\phi}) - e\dot{r}\frac{\partial\psi_p}{\partial r} - e\frac{\partial V}{\partial r} = 0 \tag{1.6}$$

respecting the flux conservation of the magnetic field $\nabla \cdot \vec{B} = 0$.

We write

$$r = r_0 + r_s + r_f, \qquad \theta = \theta_s + \theta_f, \qquad \phi = \phi_s + \phi_f \tag{1.7}$$

Here the subscripts f and s refer to rapidly oscillatory and nonoscillatory terms respectively with $\langle \dot{\phi}_f \rangle = 0$ and $\langle \dot{\phi}_s \rangle \neq 0$, where $\langle\rangle$ denotes the slow time scale average and $r_f, r_s \ll r_0$, which is a costant corresponding to the average distance of the particle from the magnetic axis.

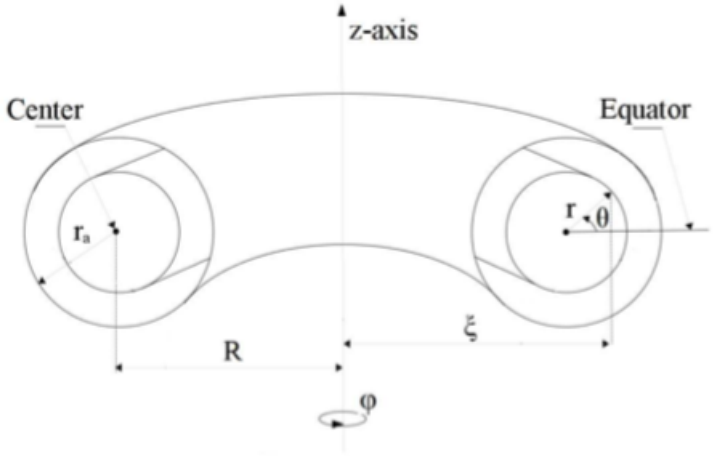

FIGURE 1.3: Toroidal geometry and notations. This figure has been reproduced by [8]

In eqs. (1.4) to (1.6) for convenience we shall assume that

- the electrostatic potential is weak that it does not perturb the fast time scale motion; that is, recognizable cyclotron orbits exist,
- we will consider the linear terms in oscillatory quantities and otherwise involve the zeroth-order quantities r_0, ψ_T and ψ_P,
- , we will consider only the radial centrifugal force associated with poloidal motion.

$$\ddot{r} - r\dot{\theta}^2 - e\Big(\dot{\theta}\frac{\partial \psi_T}{\partial r} - \dot{\phi}\frac{\partial \psi_p}{\partial r}\Big) = 0 \tag{1.8}$$

$$\frac{d}{dt}(r^2\dot{\theta}) + e\dot{r}\frac{\partial \psi_T}{\partial r} = 0 \tag{1.9}$$

$$\frac{d}{dt}((R + r\cos\theta)^2\dot{\phi}) - e\dot{r}\frac{\partial \psi_p}{\partial r} = 0 \tag{1.10}$$

Similarly, integrating eqs. (1.9) and (1.10) we can easily express in (r, θ, z) coordinates the evolutions eqs. (1.8) to (1.10)

$$\ddot{r} - r\dot{\theta}^2 - e\Big(\dot{\theta}\frac{\partial \psi_T}{\partial r} - \dot{\phi}\frac{\partial \psi_p}{\partial r}\Big) = 0 \tag{1.11}$$

$$r^2\dot{\theta} + \psi_T r^2 = C \tag{1.12}$$

$$\dot{z} = e\psi_p \tag{1.13}$$

where C is a costant.

Let's suppose for example that the magnetic potential, written in polar coordinates (r, θ, ϕ) is given by

$$A(r) = \frac{B_0 R F(r)}{\epsilon}\vec{e}_\theta - B_0 \log\frac{\epsilon}{R}\vec{e}_z \tag{1.14}$$

where $\epsilon = R + r\cos(\theta)$ and $F(r) = \int^r f(\epsilon)d\epsilon$. Since $B = \bigtriangledown A$ then the magneric field is

$$B = \frac{B_0 R}{\epsilon}(\vec{e}_z + f(r)\vec{e}_\theta) \tag{1.15}$$

A very similar calculation to eqs. (1.11) to (1.13) can be made in the case of cylindrical geometry. In this case when $R \to \infty$ the magnetic field is given by

$$B = B_0\vec{e}_z + B_0 f(r)\vec{e}_\theta \tag{1.16}$$

In polar coordinates (r, θ, z) we have:

$$\ddot{r} - r\dot{\theta}^2 = e(B_0\dot{\theta} - B_0 f(z)\dot{z}) \tag{1.17}$$

$$r^2\dot{\theta} + \frac{eB_0}{2m}r^2 = C \tag{1.18}$$

$$\dot{z} = \frac{e}{m}F(r) \tag{1.19}$$

where C is a costant and $F(r) = \int^r f(r)dx$.

In the simple case, when there is no plasma inside the tokamak, we can write the magnetic filed as:

$$B = \frac{B_0 R}{\epsilon} e_z \tag{1.20}$$

Similarly to eqs. (1.11) to (1.13) in polar coordinates (r, θ, z) we have:

$$\ddot{r} - r\dot{\theta}^2 = -\frac{B_0 R e}{r}\dot{z} \tag{1.21}$$

$$r^2\dot{\theta} = C \tag{1.22}$$

$$\dot{z} = \frac{B_0 R q}{m} + C' \tag{1.23}$$

where C and C' are two costants.

The eqs. (1.17) to (1.19) and (1.21) to (1.23) are in accordance to the plasma model proposed by [3].

Chapter 2

Definitions of chaos and topological methods

2.1 On various definitions of chaos

In this section, we provide some tools from symbolic dynamics that will be useful to investigate more deeply the relationship between the different notions of chaos. This part of chapter follows the Ph.D thesis of [9].

We start by introducing a model of a continuous map in a compact metric space, the so-called *Bernoulli shift*, which presents all the features which are usually associated with the concept of chaos. Understanding this model is important because different definitions of chaotic dynamics are then related to the Bernoulli shifts via a procedure of *conjugation*.

Given an integer $m \geq 2$, we denote by $\Sigma_m = \{0, \ldots, m-1\}^{\mathbb{Z}}$ the set of two-sided sequences of m symbols and by $\Sigma_m^+ = \{0, \ldots, m-1\}^{\mathbb{Z}}$ the set of one-sided sequences of m symbols. These compact spaces are usually endowed with the distance

$$\hat{d}(s', s'') = \sum_{i \in \mathbb{I}} \frac{\mid s_i^{'} - s_i^{''} \mid}{m^{|i|+1}}, \quad for \;\; s' = (s'_i)_{i \in \mathbb{I}}, s'' = (s''_i)_{i \in \mathbb{I}}, \tag{2.1}$$

where $\mathbb{I} = \mathbb{Z}$ or $\mathbb{I} = \mathbb{N}$ respectively. The metric in (2.1) could be replaced with

$$\hat{d}(s', s'') = \sum_{i \in \mathbb{I}} \frac{d(s'_i, s''_i)}{m^{|i|+1}}, \quad for \;\; s' = (s'_i)_{i \in \mathbb{I}}, s'' = (s''_i)_{i \in \mathbb{I}},$$

where $d(\cdot, \cdot)$ is the discrete distance on $\{0, \ldots, m-1\}$,that is, $d(s'_i, s''_i) = 0$ for $s'_i = s''_i$ and $d(s'_i, s''_i) = 1$ for $s'_i \neq s''_i$. The significance of this second choice reveals when one

needs to look at the elements from $0, \ldots, m-1$ as symbols instead of numbers. On such spaces we define one-sided Bernoulli shift $\sigma : \Sigma_m^+ \to \Sigma_m^+$ and the two-sided Bernoulli shift $\sigma : \Sigma_m \to \Sigma_m$ on m symbols as $\sigma((s)_i)_i = (s_{i+1})_i$, $\forall i \in \mathbb{I}$ for $\mathbb{I} = \mathbb{Z}$ or $\mathbb{I} = \mathbb{N}$ respectively. Both maps are continuous and the two-sided shift is a homeomorphism.

A precious tool for the detection of complex dynamics is the topological entropy and indeed its positivity is generally considered as one of the trademarks of chaos. Such object can be introduced for any continuous self-map f of a compact topological space X and we indicate it with the symbol $h_{top}(f)$. More precisely, for an open cover α of X, we define the entropy of α as $H(\alpha) = \log N(\alpha)$, where $N(\alpha)$ is the minimal number of elements in a finite open subcover of α. Given two open covers α and β of X, we define their join $\alpha \vee \beta$ as the open cover of X made by all sets of the form $A \cap B$ with $A \in \alpha$ and $B \in \beta$. Similarly one can define the join $\vee_{i=1}^n \alpha_i$ of any finite collection of open covers of X. If α is an open cover of X and $f : X \to X$ a continuous map, we denote by $f^{-1}\alpha$ the open cover consisting of all sets $f^{-1}(A)$, with $A \in \alpha$. By $\vee_{i=0}^{n-1} f^{-1}\alpha$ we mean $\alpha \vee f^{-1}\alpha \vee \cdots \vee f^{-n+1}\alpha$. Finally we have

$$h_{top}(f) = \sup_{\alpha}(\lim_{n\to\infty} \frac{1}{n}(H(\vee_{i=0}^{n-1} f^{-i}\alpha)))$$

where α ranges over all open covers of X. Among the several properties of the topological entropy, we recall just the ones that are useful in view of the subsequent discussion.

In regard to the (one-sided or two-sided) Bernoulli shift σ on m symbols, it holds that

$$h_{top}(\sigma) = log(m)$$

Given a continuous self-map f of a compact topological space X and a invariant subset $\mathcal{I} \subseteq X$,i.e. such that $f(\mathcal{I}) = \mathcal{I}$ then

$$h_{top}(f) \geq h_{top}(f \mid_{\mathcal{I}}) \tag{2.2}$$

Denoting by f^n the n-th iterate of the continuous self map f of a compact topological space X, we have

$$h_{top}(f^n) = n h_{top}(f),\ \forall n \geq 1. \tag{2.3}$$

Given two continuous self maps $f : X \to X$ and $g : Y \to Y$ of the compact topological spaces X and Y and a continuous onto map $\phi : X \to Y$ which makes the diagram

$$\begin{array}{ccc} X & \xrightarrow{f} & X \\ {\scriptstyle\phi}\downarrow & & \downarrow{\scriptstyle\phi} \\ Y & \xrightarrow[g]{} & Y \end{array} \tag{2.4}$$

commute, i.e. such that $\phi \circ f = g \circ \phi$, then it holds that

$$h_{top}(f) \geq h_{top}(g).$$

If ϕ is also injective, the above inequality is indeed an equality. When the diagram in (2.4) commutes, we say that f and g are topologically semi-conjugate and ϕ is a semiconjugacy between them. If ϕ is also one-to-one, then f and g are topologically conjugate and ϕ is named conjugacy. Thus,when for a continuous self-map f of a compact topological space X and a invariant (positively) subset $\mathcal{I} \subseteq X$ it holds that $f\mid_{\mathcal{I}}$ is semiconjugate to the (one sided or two sided) Bernoulli shift σ on m symbols,then

$$h_{top}(f) \geq h_{top}(f\mid_{\mathcal{I}}) \geq h_{top}(\sigma). = \log(m) \tag{2.5}$$

If $f\mid_{\mathcal{I}}$ is conjugate to σ, then the second inequality is indeed an equality. We notice that, although the topological entropy can be defined for continuous self-maps of topological spaces, we confine ourselves to the case of metric spaces. More precisely, when dealing with chaotic dynamics, we will consider dynamical systems, i.e. couples (X, f), where X is a compact metric space and $f : X \to X$ is continuous and surjective.

We will show the mutual relationships among some of the most classical definitions of chaos (such as the ones by Li-Yorke, Devaney, etc.), considering also the notion of chaotic dynamics in the coin-tossing sense that will be presented later on in Definition 2.8. In [10] it has been proven that the presence of a point of period three for a continuous self-map f which is defined on a compact interval, is a condition that ensures the existence of periodic points of any period. The existence of a point of period three also implies the positivity of the topological entropy for f. This result which is due to Li and Yorke is often considered as a particular case of the Sharkovskii Theorem [11] but, actually, the authors in [10] proved much more than simply the conditions for the existence of positivity of the topological entropy. In fact, for this particular map they showed the existence of an uncountable scrambled set (cf. Definition 2.1), which was called "chaotic" in [10] for the first time in the literature, although the precise corresponding definition of chaos nowadays known as Li-Yorke chaos, was not given there.

Definition 2.1. Let (X, d_X) be a metric space and $f : X \to X$ be a continuous map. We say that $S \subseteq X$ is a scrambled set for f if for any $x, y \in S$ with $x \neq y$, it holds that

$$\liminf_{n\to\infty} d_X(f^n(x), f^n(y)) = 0 \ \ and \ \ \limsup_{n\to\infty} d_X(f^n(x), f^n(y)) > 0$$

If the set S is uncountable, we say that f is chaotic in the sense of $Li - Yorke$.

Let us remark that according to [10] the scrambled set S should satisfy an extra assumption, i.e.

$$\limsup_{n\to\infty} d_X(f^n(x), f^n(p)) > 0$$

for any $x \in S$ and for any periodic point $p \in X$. However, this further condition is usually omitted since it has been proven in [12] to be redundant in any compact metric space. We also point out that the original framework in [10] was one-dimensional. The later extension to generic metric spaces has been done by different authors (see e.g. [12, 13]) that have compared the concept of chaos from [10] to other ones available in the literature. The aim of the following pages is to try to present some of these connections. We warn the reader that, in what follows, the term chaotic will be referred without distinction to a dynamical system, meant as a couple (X, f), where X is the compact metric space and $f : X \to X$ is the continuous and surjective map. In case we need to specify the distance d_X on X, then we will write (X, f, d_X) in place of (X, f). If we are in the framework of Theorem 2.12 and since the map f has to be onto, the dynamical system we usually consider is given by $(I, \psi\,|_{\mathcal{I}})$, where $\mathcal{I}$ is the invariant set.

In order to understand the relationship between the kind of chaos expressed in Definition 2.10 and the Li-Yorke chaos, a key role is played by the topological entropy. Indeed, as we have seen in Theorem 2.12, conclusion (iv), thanks to the semi-conjugacy with the Bernoulli shift, the topological entropy of ψ is positive in the setting described in Definition 2.10. On the other hand, in [13] it is established that any dynamical system with positive topological entropy admits an uncountable scrambled set and therefore it is chaotic in the sense of Li-Yorke. Hence, we can conclude that our notion of chaos is stronger than the one in Definition 2.1, since any system chaotic according to Definition 2.10 is also Li-Yorke chaotic, while the vice versa is not true in general. In fact, there exist maps Li-Yorke chaotic but with zero topological entropy; such an example on the unit interval is given in [14].

In perspective of the following discussion and also for the reader's convenience, we present the complete definition of Devaney chaos, although we will focus at first only on the third condition.

Definition 2.2. Given a metric space (X, d_X) and a continuous function $f : X \to X$, we say that f is chaotic in the sense of Devaney if:

- f is topologically transitive, i.e. for any couple of nonempty open subsets $U, V \subseteq X$ there exists an integer $n \geq 1$ such that $U \cap f^n(V) \neq \emptyset$;
- the set of periodic points for f is dense in X;
- f is sensitive with respect to initial data on X, i.e. there exists $\delta > 0$ such that for any $x \in X$ there is a sequence $(x_i)_{i\in\mathbb{N}}$ of points in X such that $x_i \to x$ when $i \to \infty$ and for each $i \in \mathbb{N}$ there exists a positive integer m_i with $d_X(f^{m_i}(x_i), f^{m_i}(x)) \geq \delta$

So, the positivity of the topological entropy and the sensitivity on initial conditions are related in some way, being both signals of a certain instability of the system. The topological entropy is however, a "locally detectable" feature, in the sense that, according to (2.2), it is sufficient to find a (positively) invariant subset of the domain where it is positive in order to infer its positivity on the whole domain. Therefore, in general, we cannot expect the system to be sensitive at each point if the entropy is positive. In order to make this implication true we should also add a global property, such as transitivity. Indeed in [13] it is argued that any transitive map with positive topological entropy displays sensitivity with respect to initial data. On the other hand, some authors have obtained results with the presence of sensitivity only on an invariant subset of the domain by considering, instead of the positivity of the entropy, the stronger property of chaos in the sense of coin-tossing, or at least the semi-conjugacy to the Bernoulli shift σ for the map f defining the dynamical system or one of its iterates. For example, the already cited [15] (Chaos Lemma), under hypotheses for a map f similar to the ones for ψ in Theorem 2.10, establishes the existence of a compact f-invariant set Q_* , on which f is sensitive and such that each forward itinerary on m symbols is realized by the itinerary generated by some point of Q_* (here m is the crossing number). A similar result is mentioned, without proof, by Aulbach and Kieninger in [12] and it asserts that if a continuous self-map f of a compact metric space X is chaotic in the sense of Block and Coppel, that is, if there exist an iterate f^K (with $k \geq 1$) of f and a compact subset $Y \subseteq X$ positively f^k -invariant, such that $f^k \mid_Y$ is semi-conjugate to the one-sided Bernoulli shift on two symbols , then $f \mid_Z$ is Block-Coppel chaotic, transitive and sensitive on Z, where Z is a suitable compact positively f-invariant subset of X. To conclude this discussion, we should also observe that, as proved independently by Banks et al in [16] and by Silverman in [17]

Based on the references [12, 18], we notice that any map chaotic according to Definition 2.10 is also chaotic in the sense of Block-Coppel, thanks to Theorem 2.12 conclusion (ii).

More precisely, the later result consitutes a stronger property than the notion of chaos in the sense of Block-Coppel. Indeed, the semi-conjugacy with the Bernoulli shift is established for the map ψ itself and not for one of its iterates. The same remark applies to Theorem 2.12, conclusion (v), where again a sharper feature than the Block-Coppel chaos is deduced. Pursuing further this discussion on the Block-Coppel chaos, we notice that every system (X, f) Block-Coppel chaotic has positive topological entropy. Indeed, by the postulated semi-conjugacy between an iterate f^k (with $k \geq 1$) of the map f, restricted to a suitable positively invariant subset of the domain, and the one-sided Bernoulli shift on two symbols, by (2.3) and (2.4) it follows that $kh_{top}(f) = h_{top}(f^k) \geq log(2)$, from which$h_{top}(f) \geq \log(2)/k > 0$. Thus, based on the previously quoted [13], any such system is also Li-Yorke chaotic. However, we observe that the Block-Coppel chaos is strictly weaker than chaos in the sense of coin-tossing and, a fortiori, also than the concept introduced in Definition 2.10. In fact, according to [12], there exist systems (X, f) such that f^2 restricted to some f-invariant subset of X is semi-conjugate to the one-sided Bernoulli shift on two symbols, while such property does not hold for f.

Regarding the analysis of the relationship between the topological entropy and the sensitivity on initial conditions, we recall that, except for the particular case of continuous self-mappings of compact intervals, in general, the sensitivity does not imply a positive entropy [12]. Actually, if instead of the sensitivity alone, we take into account the definition of Devaney chaos in its completeness, then it is possible to prove that the Devaney chaoticity and the positivity of topological entropy are independent, as none of the two implies the other [19, 20]. In this sense it means that, in generic metric spaces, Devaney definition does not imply chaos in the sense of Definition 2.10 because, otherwise, the topological entropy would be positive in any Devaney chaotic system. On the other hand, we cannot conclude if our notion of chaos implies the one by Devaney. In fact, in [12] it is presented a dynamical system Block-Coppel chaotic, but not chaotic according to Devaney, since it has no periodic points. So, although we have already pointed out that our notion of chaos is strictly stronger than the one of Block-Coppel, we cannot state the same compared to the definition of Devaney.

When we restrict ourselves to the one-dimensional case, most of the definitions of chaos are known to be equivalent, while it is in the higher dimensional setting that these relationships become more involved. Indeed, in [21] it has been proved that for a continuous self-mapping f of a compact interval to have positive topological entropy is equivalent to be chaotic in the sense of Devaney on some closed (positively) invariant subset of the domain. The positivity of the topological entropy is also equivalent to the fact that some iterate of f is turbulent or to the chaoticity in the Block-Coppel sense [12]. However, such equivalence, is not valid with the definition of Li-Yorke, because as we have

already pointed out, there exist interval maps which are Li-Yorke chaotic, but with zero topological entropy [14].

The previous discussion suggests that for more general frameworks, several links among the various notions of chaos can be lost, although something can still be said for particular cases. For instance, in addition to the facts already exposed (e.g., chaos according to Definition 2.10 $\Rightarrow$ chaos in the sense of coin-tossing $\Rightarrow$ Block-Coppel chaos $\Rightarrow$ $h_{top} > 0 \Rightarrow$ Li-Yorke chaos), we mention that Devaney chaos implies Li-Yorke chaos in any compact metric space. In order to prove this implication, the hypothesis on the density of periodic points in Definition of Devaney chaos could be replaced with the weaker condition that at least one periodic point does exist [22]. On the other hand this weaker condition is necessary, because transitivity and sensitivity alone are not sufficient to imply Li-Yorke chaos and vice versa, as shown in [13]. Let us notice that a dynamical system that is both sensitive and transitive is sometimes called Auslander-Yorke chaotic [13, 18]. Therefore we can rephrase the previous sentence by saying that the concepts of Li-Yorke chaos and Auslander-Yorke chaos are independent.

2.2 Stretching along the paths and variants

Before introducing the main concepts of the "Stretching Along the Paths" method, let us recall some facts about generalized rectangle.

Given a metric space X, we call generalized rectangle any set $R \subseteq X$ homeomorphic to the unit square $\mathcal{Q} := [0,1]^2$ of $\mathbb{R}^2$. If $\mathcal{R}$ is a generalized rectangle and $h : \mathcal{Q} \to h(\mathcal{Q}) = R$ is a homeomorphism defining it, we call contour $v\mathcal{R}$ of $\mathcal{R}$ the set $v\mathcal{R} = h(\partial\mathcal{Q})$, where $\partial\mathcal{Q}$ is the usual boundary of the unit square. Notice that the contour $v\mathcal{R}$ is well defined as it does not depend on the choice of the homeomorphism h. Indeed, if $h_1 : \mathcal{Q} \to h_1(\mathcal{Q}) = R$ and $h_2 : \mathcal{Q} \to h_2(\mathcal{Q}) = R$ are two homeomorphisms from the square onto the same rectangle $\mathcal{R}$, then $h_2^{-1} \circ h_1$ is a homeomorphism of the unit square $\mathcal{Q}$ onto itself. In this case, $h_2^{-1} \circ h_1(\partial\mathcal{Q}) = \partial\mathcal{Q}$ and hence $h_1(\partial\mathcal{Q}) = h_2(\partial\mathcal{Q})$. Then $v\mathcal{R}$ is also a homeomorphic image of S^1, that is a Jordan curve. When $X = \mathbb{R}^2$ is the plane, then the contour $v\mathcal{R}$ actually coincides with the boundary of $\mathcal{R}$, but, in general, they are different (for instance when $\mathcal{R}$ is a part of two-dimensional surface embedded in $\mathbb{R}^3$.

By an oriented rectangle we mean a pair

$$\widehat{\mathcal{R}} = (\mathcal{R}, \mathcal{R}^-)$$

where $\mathcal{R} \subseteq X$ is a generalized rectangle and

$$\mathcal{R}^- = \mathcal{R}_l^- \cup \mathcal{R}_r^-$$

is the union of two disjoint arcs $\mathcal{R}_l^-, \mathcal{R}_r^- \subseteq v\mathcal{R}$, that we call the left and the right sides of $\mathcal{R}^-$. Since $v\mathcal{R}$ is a Jordan curve it follows that $v\mathcal{R}\backslash$ $(mathcalR_l^- \cup \mathcal{R}_r^-)$ consists of two open arcs. We denote by $\mathcal{R}^+$ the closure of such open arcs, that we name $\mathcal{R}_d^+$ and $\mathcal{R}_u^+$ (the down and the up sides of $\mathcal{R}^+$). It is important to notice that we always can label the arcs $\mathcal{R}_d^+$, $\mathcal{R}_u^+$,$\mathcal{R}_l^+$ and $\mathcal{R}_r^+$ following this orientation $l - d - r - u - l$, and take a homeomorphism $g : \mathcal{Q} \to g(\mathcal{Q}) = \mathcal{R}$ so that

$$g(\{0\} \times [0,1]) = \mathcal{R}_l^- \qquad g(\{1\} \times [0,1]) = \mathcal{R}_r^-$$
$$g([0,1] \times \{0\}) = \mathcal{R}_d^- \qquad g([0,1] \times \{1\}) = \mathcal{R}_u^-$$

The notation $\mathcal{R}^-$ is inspired by the concept of exist set in the Conley-Waėwski theory [23]. For example, given in the plane a flow defined by an autonomous differential system $\dot{x} = f(x)$, the sets labeled as $[\cdot]^-$, or as $[\cdot]^+$, are made by those points of $\partial\mathcal{R}$ which are moved by the flow outward/inward, with respect to $\mathcal{R}$ (see [24, 25]).

Definition 2.3. Let X be a metric space and let $\psi : X \supseteq D_\psi \to X$ be a map defined on a set D_ψ. Assume that $\widehat{\mathcal{A}} = (\mathcal{A}, \mathcal{A}^-)$ and $\widehat{\mathcal{B}} = (\mathcal{B}, \mathcal{B}^-)$ are oriented rectangles of X and let $\mathcal{K} \subseteq \mathcal{A} \cap D_\psi$ be a compact set. We say that $(\mathcal{K}, \psi)$ stretches $\widehat{\mathcal{A}}$ to $\widehat{\mathcal{B}}$ along the paths and write

$$(\mathcal{K}, \psi) : \widehat{\mathcal{A}} \twoheadrightarrow \widehat{\mathcal{B}},$$

if any path γ in $\mathcal{A}$ connecting the opposite sides of $\mathcal{A}^-$ has a sub-path σ contained in $\mathcal{K}$ and such that $\psi \circ \sigma$ is a path contained in $\mathcal{B}$ and connecting the opposite sides of $\mathcal{B}^-$.

When $\mathcal{K} = \mathcal{A}$ we simply write

$$\psi : \widehat{\mathcal{A}} \twoheadrightarrow \widehat{\mathcal{B}}.$$

In the applications an important case is when the "SAP"-property is satisfied with respect to different compact subsets of an oriented rectangle. With this respect, we have also the following definition.

Definition 2.4. Let X be a metric space and let $\psi : X \supseteq D_\psi \to X$ be a map defined on a set D_ψ. Assume that $\widehat{\mathcal{A}} = (\mathcal{A}, \mathcal{A}^-)$ and $\widehat{\mathcal{B}} = (\mathcal{B}, \mathcal{B}^-)$ are oriented rectangles of X. Let also $m \geq 1$ be an integer. We say that $(\mathcal{D}, \psi)$ stretches $\widehat{\mathcal{A}}$ to $\widehat{\mathcal{B}}$ along the paths with crossing number m and write

$$\psi : \widehat{\mathcal{A}} \twoheadrightarrow^m \widehat{\mathcal{B}},$$

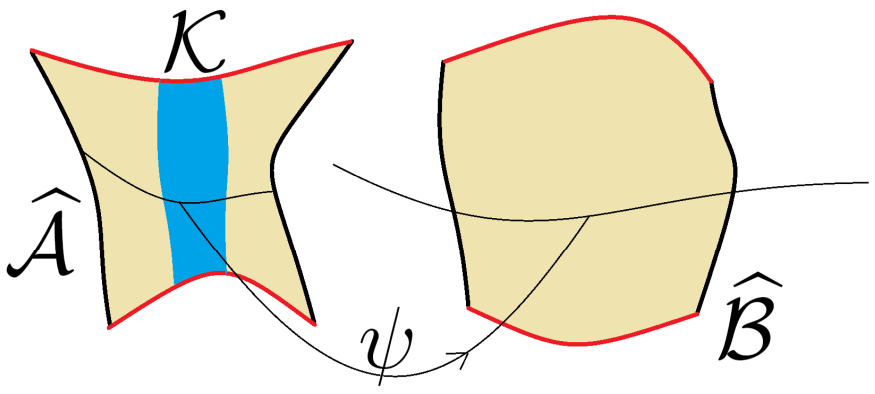

FIGURE 2.1: A pictorial comment to Definition 2.3. The rectangles $\mathcal{A}$ and $\mathcal{B}$ have been oriented by selecting the sets $\mathcal{A}^-$ and $\mathcal{B}^-$ (drawn with thicker black lines), respectively. We represent a case in which the relation $(\mathcal{K}, \psi) : \widehat{\mathcal{A}} \Subset \widehat{\mathcal{B}}$. For a generic path $\gamma : [0,1] \to \mathcal{A}$ with $\gamma(0)$ and $\gamma(1)$ belonging to different components of $\mathcal{A}^-$, we have a sub-paths σ in $\mathcal{K}$ which is mapped by ψ across $\mathcal{B}$ and joining the two sides of $\mathcal{B}^-$.

if there exists m pairwise disjoint compact sets

$$\mathcal{K}_0, \dots, \mathcal{K}_{m-1} \subseteq \mathcal{D}$$

such that

$$(\mathcal{K}_i, \psi) : \widehat{\mathcal{A}} \Subset \widehat{\mathcal{B}}, \quad i = 0, \dots, m-1. \tag{2.6}$$

The role of the compact sets $\mathcal{K}$ (respectively the compact sets $\mathcal{K}_i$) is fundamental in the applications of Definition 2.3 and Definition 2.4. For instance, if 2.3 is satisfied with $\widehat{\mathcal{B}} = \widehat{\mathcal{A}}$ we are able to prove the existence of a fixed point for ψ in $\mathcal{K}$. If, in particular Definition 2.4 is satisfied with respect to two or more pairwise disjoint compact sets $\mathcal{K}_i$ we get e multiplicity of fixed point. On the other hand, when Definition 2.4 holds for some iterate of ψ, the existence of periodic points is ensured.

Theorem 2.5. *Let X be a metric space and let $\psi : X \supseteq D_\psi \to X$ be a map defined on a set D_{psi}. Assume that $\widehat{\mathcal{R}} = (\mathcal{R}, \mathcal{R}^-)$ is an oriented rectangle of X. If $\mathcal{K} \subseteq \mathcal{R} \cap D_{psi}$ is*

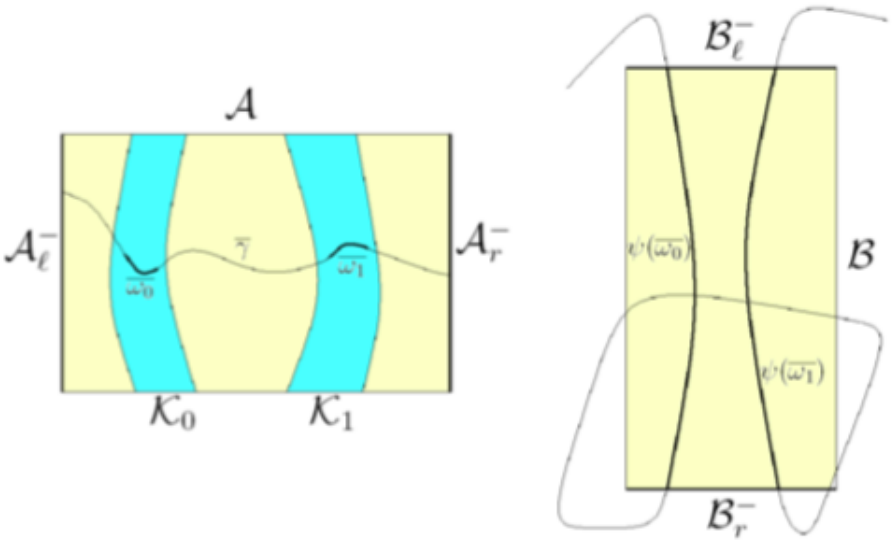

FIGURE 2.2: A pictorial comment to Definition 2.4. The rectangles $\mathcal{A}$ and $\mathcal{B}$ have been oriented by selected the sets $\mathcal{A}^-$ and $\mathcal{B}^-$ (drown with thicker lines), respectively. We represent a case in which the relation $(\mathcal{K}_i, \psi) : \widehat{\mathcal{A}} \overset{m}{\Subset} \widehat{\mathcal{B}}, \quad i = 0, 1$, is satisfied for a map $\psi : \mathbb{R}^2 \supseteq \mathcal{A} \to \mathbb{R}^2$ and for the two darker compact subsets $\mathcal{K}_0$ and $\mathcal{K}_1$ of $\mathcal{A}$, on which ψ is continuous. For a generic path $\gamma : [0, 1] \to \mathcal{A}$ with $\gamma(0)$ and $\gamma(1)$ belonging to different components of $\mathcal{A}^-$, we have highlighted two sub-paths ω_0 and ω_1 with range in $\mathcal{K}_0$ and $\mathcal{K}_1$,respectively, such that their composition with ψ determines two new paths (drawn by bolder vertical lines) with values in $\mathcal{B}$ and joining the two sides of $\mathcal{B}^-$. In this framework according to the Definition 2.4 we could also write $\psi : \widehat{\mathcal{A}} \overset{2}{\Subset} \widehat{\mathcal{B}}$. This figure has been reproduced from [9].

a compact set for which it holds that

$$(\mathcal{K}, \psi) : \widehat{\mathcal{R}} \Subset \widehat{\mathcal{R}} \tag{2.7}$$

then there exists at least one point $z \in \mathcal{K}$ with $\psi(z) = z$.

Proof. By the definition of oriented rectangle, there exists a homeomorphism $h : \mathbb{R}^2 \supseteq \mathcal{Q} \to h(\mathcal{Q}) = \mathcal{R} \subseteq X$ mapping in a correct way the sides of $\mathcal{Q} = [0, 1]^2$ into the arcs that compose the sets $\mathcal{R}^-$ and $\mathcal{R}^+$. Then passing to the planar map $\phi = h^{-1} \circ \psi \circ h$ defined on $D_\phi := h^{-1}(D_\psi) \subseteq \mathcal{Q}$ we can confine ourselves to the search of a fixed point for ϕ in the compact set $\mathcal{H} := h^{-1}(K) \subseteq \mathcal{Q}$. T he stretching assumption on ψ is now translated to

$$(\mathcal{H}, \phi) : \widehat{\mathcal{Q}} \Subset \widehat{\mathcal{Q}}.$$

On $\widehat{\mathcal{Q}}$ we consider the natural "left-right" orientation, by choosing

$$\mathcal{Q}^- = (0 \times [0, 1]) \cup (1 \times [0, 1])$$

A fixed point for *phi* in $\mathcal{H}$ corresponds to a fixed point for ψ in $\mathcal{K}$. For $\phi = (\phi_1, \phi_2)$ and $x = (x_1, x_2)$ we define the compact set

$$V := \{x \in \mathcal{H} : 0 \leq \phi_2(x) \leq 1, \;\; x_1 - \phi_1(x) = 0\}$$

The proof consists in showing that V contains a continuum $\mathcal{C}$ which joins in $\mathcal{Q}$ the lower side $[0,1] \times \{0\}$ to the upper side $[0,1] \times \{1\}$. To this end, it is sufficient to prove that V acts as a "cutting surface" between the left and right sides of $\mathcal{Q}$, that is, V intersects any path in $\mathcal{Q}$ joining the left side $\{0\} \times [0,1]$ to the right side $\{1\} \times [0,1]$. Such cutting property can be checked via the intermediate value theorem by observing that if $\gamma = (\gamma_1, \gamma_2) : [0,1] \to \mathcal{Q}$ is a continuous map with $\gamma(0) \in 0 \times [0,1]$ and $\gamma(1) \in 1 \times [0,1]$,then the stretching hypothesis $(\mathcal{H}, \phi) : \widehat{\mathcal{Q}} \twoheadrightarrow \widehat{\mathcal{Q}}$ implies that there exists an interval $[t', t''] \subseteq [0,1]$ such that $\gamma(t)\mathcal{H}$, $\phi(\gamma(t)) \in \mathcal{Q}$, $\forall t \in [t', t'']$ and $\gamma_1(t') - \phi_1(\gamma(t')) \geq 0 \geq \gamma_1(t'') - \phi_1(\gamma(t''))$ or $\gamma_1(t') - \phi_1(\gamma(t')) \leq 0 \leq \gamma_1(t'') - \phi_1(\gamma(t''))$. Notice that, by the definition of V it follows that $\phi_2(z) \in [0,1]$, $\forall z \in \mathcal{C}$. Hence for every point $p = (p_1, p_2) \in \mathcal{C} \cap ([0,1] \times 0)$ we have $p_2 - \phi_2(p) \leq 0$ and, similarly, $p_2 - \phi_2(p) \geq 0$ for every $p = (p_1, p_2) \in \mathcal{C} \cap ([0,1] \times 1)$. Applying Bolzano Theorem we obtain the existence of at least a point $v = (v_1, v_2) \in \mathcal{C} \subseteq V \subseteq \mathcal{H}$ such that $v_2 - \phi_2(v) = 0$. Hence v is a fixed point ϕ in $\mathcal{H}$ and $z = h(v)$ is a fixed point for ψ in $\mathcal{K} \subseteq \mathcal{R}$. □

Remark 2.6. Notice that, for the validity of Theorem 2.5, it is fundamental that the orientation of the generalized rectangle $\mathcal{R}$ in Definition 2.7 remains the same for $\mathcal{R}$ considered as "starting set" $\mathcal{A}$ and "target set" $\mathcal{B}$ of the map ψ. Indeed, if one chooses two different orientations for $\mathcal{R}$, in general the above result does not hold anymore and the existence of fixed points for ψ is no longer ensured, not only in $\mathcal{K}$, but even in $\mathcal{R}$, as shown by the example depicted in Figure 2.3.

The next result shows that the "SAP" property is preserved by composition of maps.

Theorem 2.7. *Let X be a metric space and let $\phi : X \supseteq D_{phi} \to X$ and $\psi : X \supseteq D_{psi} \to X$ be maps defined on the sets D_ϕ and D_ψ, respectively. Assume that $\widehat{\mathcal{A}} = (\mathcal{A}, \mathcal{A}^-)$, $\widehat{\mathcal{B}} = (\mathcal{B}, \mathcal{B}^-)$ and $\widehat{\mathcal{C}} = (\mathcal{C}, \mathcal{C}^-)$ are oriented rectangles of X. If $\mathcal{H} \subseteq \mathcal{A} \cap D_\phi$ and $\mathcal{K} \subseteq \mathcal{B} \cap D_\psi$ are compact sets such that*

$$(\mathcal{H}, \phi) : \widehat{\mathcal{A}} \twoheadrightarrow \widehat{\mathcal{B}} \quad \textit{and} \quad (\mathcal{K}, \psi) : \widehat{\mathcal{B}} \twoheadrightarrow \widehat{\mathcal{C}}$$

then it follows that

$$(\mathcal{H} \cap \phi^{-1}(\mathcal{K}), \psi \circ \phi) : \widehat{\mathcal{A}} \twoheadrightarrow \widehat{\mathcal{C}}$$

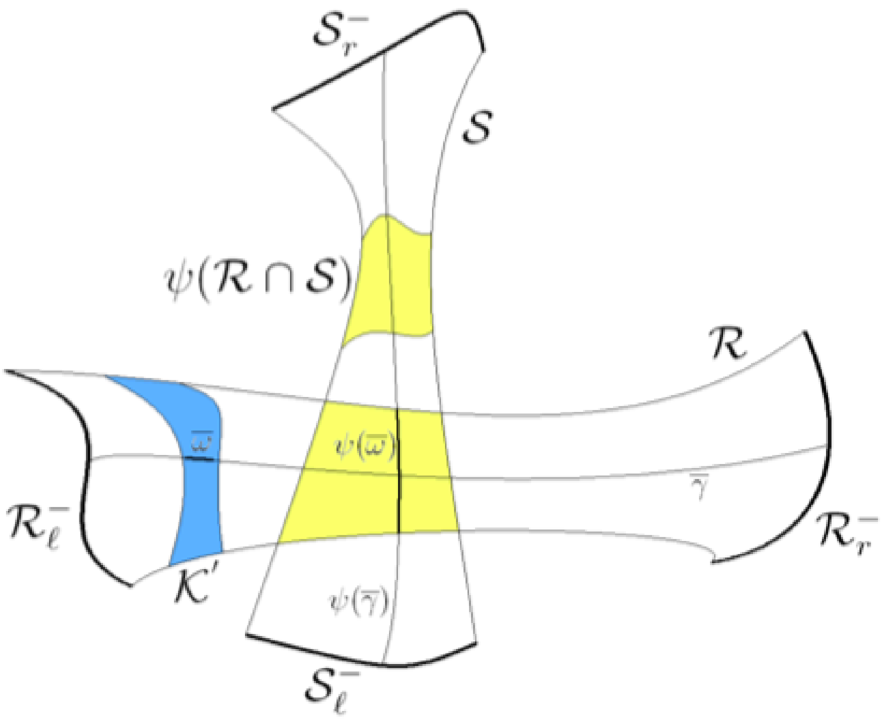

FIGURE 2.3: The generalized rectangle $\mathcal{R}$ is transformed by a continuous planar map ψ onto the generalized rectangle $\mathcal{S} = \psi(\mathcal{R})$, so that, in particular, $\mathcal{S}_l^- = \psi(\mathcal{R}_l^-)$ and$\mathcal{S}_r^- = \psi(\mathcal{R}_r^-)$. The boundary sets $\mathcal{R}^- = \mathcal{R}_l^- \cup \mathcal{R}_r^-$ and $\mathcal{S}^- = \mathcal{S}_l^- \cup \mathcal{S}_r^-$ are drawn with thicker lines. As it is immediate to verify, for $\widehat{\mathcal{R}} = (\mathcal{R}, \mathcal{R}^-)$ and $\widehat{\mathcal{S}} = (\mathcal{S}, \mathcal{S}^-)$,it holds that $\psi : \widehat{\mathcal{R}} \Leftrightarrow\!\!\!\rightarrow \widehat{\mathcal{S}}$. On the other hand, calling $\widehat{\widehat{\mathcal{R}}}$ the generalized rectangle $\mathcal{R}$ oriented by choosing $v\mathcal{R} \,\overline{\setminus}\, \mathcal{R}^-$ as $[\cdot]^-$-set, it also holds that $(\mathcal{K}', \psi) : \widehat{\mathcal{R}} \Leftrightarrow\!\!\!\rightarrow \widehat{\widehat{\mathcal{R}}}$, where $\mathcal{K}'$ is the subset of $\mathcal{R}$ depicted with darker color. However, since $\mathcal{R} \cap \mathcal{S}$ is mapped by ψ outside $\mathcal{R}$ (both $\mathcal{R} \cap \mathcal{S}$ and $\psi(\mathcal{R} \cap \mathcal{S})$ are drawn with the same light color),there cannot exist fixed points for ψ in $\mathcal{R}$ and, a fortiori, neither in $\mathcal{R}$. Notice that Theorem 2.5 does not apply because we have taken two different orientation of $\mathcal{R}$. This figure has been reproduced from [9].

Proof. Let $\gamma : [0,1] \to \mathcal{A}$ be a path such that $\gamma(0)$ and $\gamma(1)$ belong to the different sides of $\mathcal{A}^-$. Then,since $(\mathcal{H}, \phi) : \widehat{\mathcal{A}} \Leftrightarrow\!\!\!\rightarrow \widehat{\mathcal{B}}$, there exists a subinterval $[t', t''] \subset [0,1]$ such that

$$\gamma(t) \in \mathcal{H}, \quad \phi(\gamma(t)) \in \mathcal{B}, \quad \forall t \in [t', t'']$$

and, moreover, $\phi(\gamma(t'))$ and $\phi(\gamma(t''))$ belong to different components of $\mathcal{B}^-$. Let us call ω the restriction of γ to $[t', t'']$ and define $\nu : [t', t''] \to \mathcal{B}$ as $\nu := \phi \circ \omega$. Notice that $\nu(t')$ and $\nu(t'')$ belong to the different sides of $\mathcal{B}^-$ and so, by the stretching hypothesis $(\mathcal{K}, \psi) : \widehat{\mathcal{B}} \Leftrightarrow\!\!\!\rightarrow \widehat{\mathcal{C}}$ there is a subinterval $[s', s''] \subseteq [t', t'']$ such that

$$\nu(t) \in \mathcal{K}, \quad \psi(\nu(t)) \in \mathcal{C}, \quad \forall t \in [s', s'']$$

with $\psi(\nu(s'))$ and $\psi(\nu(s''))$ belonging to different components of $\mathcal{C}^-$. Rewriting all in terms of γ, this means that we have found a subinterval $[s', s''] \subseteq [0,1]$ such that

$$\gamma(t) \in \mathcal{H} \cap \phi^{-1}(\mathcal{K}), \quad \psi(\phi(\gamma(t))) \in \mathcal{C}, \quad \forall t \in [s', s'']$$

and $\psi(\phi(\gamma(s')))$ and $\psi(\phi(\gamma(s'')))$ belonging to different sides of $\mathcal{C}^-$. By the arbitrariness of the path γ, the stretching property

$$(\mathcal{H} \cap \phi^{-1}(\mathcal{K}), \psi \circ \phi) : \widehat{\mathcal{A}} \twoheadrightarrow \widehat{\mathcal{C}}$$

is thus fulfilled. We just point out that the continuity of the composite mapping $\psi \circ \phi$ on the compact set $\mathcal{H} \cap \phi^{-1}(\mathcal{K})$ follows from the continuity of ϕ on $\mathcal{H}$ and of ψ on $\mathcal{K}$, respectively. □

Theorem 2.8. *Assume there is a double sequence of oriented rectangles $(\widehat{\mathcal{R}}_i)_{i\in\mathbb{Z}}$ (with $\widehat{\mathcal{R}}_i = (\mathcal{R}_i, \mathcal{R}_i^-)$) of a metric space X and a sequence $((\mathcal{K}_i, \psi_i))_{i\in\mathbb{Z}}$, with $\mathcal{K}_i \subseteq \mathcal{R}_i$ compact sets, such that*

$$(\mathcal{K}_i, \psi_i) : \widehat{\mathcal{R}}_i \twoheadrightarrow \widehat{\mathcal{R}}_{i+1}, \quad i \in \mathbb{Z}$$

Let us denote by $\mathcal{R}_l^i$ and $\mathcal{R}_r^i$ the two components of $\mathcal{R}_i^-$ and by $\mathcal{R}_d^i$ and $\mathcal{R}_u^i$ the two components of $\mathcal{R}_i^-$. Then the following conclusions hold:

- *There is a sequence $(\omega_k)_{k\in\mathbb{Z}}$ such that $\omega_k \in \mathcal{K}_k$ and $\psi_k(\omega_k) = \omega_{k+1}$ for all $k \in \mathbb{Z}$;*
- *For each $j \in \mathbb{Z}$ there exists a compact connected set $\mathcal{C}_j \subseteq \mathcal{K}_j$ satisfying*

$$\mathcal{C}_j \cap \mathcal{R}_d^j \neq \emptyset \qquad \mathcal{C}_j \cap \mathcal{R}_u^j \neq \emptyset$$

and such that, for every $w \in \mathcal{C}_j$, t here is a sequence $(y_i)_{i\geq j}$ with $y_j = w$ and

$$y_i \in \mathcal{K}_i, \quad \psi_i(y_i) = y_{i+1}, \quad i \geq j;$$

- *If there are integers h and l, with $h < l$, such that $\widehat{\mathcal{R}}_h = \widehat{\mathcal{R}}_l$, then there exists a finite sequence $(z_i)_{h\leq i\leq l-1}$, with $z_i \in \mathcal{K}_i$ and $\psi_i(z_i = z_{i+1}$ for each $i = h, \ldots, l-1$ such that $z_l = z_h$, that is, z_h is a fixed point of $\psi_{l-1} \circ \cdots \circ \psi_h$ in $\mathcal{K}_h$.*

Theorem 2.9. *Let X be a metric space and $\psi : X \supseteq D_\psi \to X$ be a map defined on a set D_ψ. Assume that $\widehat{\mathcal{R}} = (\mathcal{R}, \mathcal{R}^-$ is an oriented rectangle of X. If $\mathcal{K}_0, \dots, \mathcal{K}_{m-1}$ are $m \geq 2$ pairwise disjoint compact subsets of $\mathcal{R} \cap D_\psi$ and*

$$(\mathcal{K}_i, \psi) : \widehat{\mathcal{R}} \overset{\circ}{\Rightarrow} \widehat{\mathcal{R}}, \quad for \;\; i = 0, \dots, m-1, \quad i \in \mathbb{Z}$$

then the following conclusion hold:

- *The map ψ has at least a fixed point in $\mathcal{K}_i$, $i = 0, \dots, m-1$;*
- *For each two-side sequence $(s_h)_{h\in\mathbb{Z}} \in 0, \dots, m-1^{\mathbb{Z}}$ there exists a sequence of point $(x_h)_{h\in\mathbb{Z}}$ such that $\psi(x_{h-1}) = x_h \in \mathcal{K}_{s_h}$,$\forall k \in \mathbb{Z}$;*
- *For each sequence $s = (s_n)_n \in 0, \dots, m-1^{\mathbb{N}}$,there exists a compact connected set $\mathcal{C}_s \subseteq \mathcal{K}_{s_0}$ satysfying*

$$\mathcal{C}_s \cap \mathcal{R}_d^+ \neq \emptyset \qquad \mathcal{C}_s \cap \mathcal{R}_u^+ \neq \emptyset$$

and such that $\psi^i(x) \in \mathcal{K}_{s_i}$, $\forall i \geq 1$, $\forall x \in \mathcal{C}_s$

- *Given an integer $j \geq 2$ and a $j+1$-uple $(s_0, \dots, s_j)$,$s_i \in 0, \dots, m-1$, for $i = 0, \dots, j$ and $s_0 = s_j$, then there exists a point $w \in \mathcal{K}_{s_0}$ such that*

$$\psi^i(w) \in \mathcal{K}_{s_i}, \;\; \forall i = 1, \dots, j \;\; and \;\; \psi^j(w) = w.$$

2.3 Linked Twist Maps

Definition 2.10. Let X be a metric space, $\psi : X \supseteq D_\psi \to X$ be a map and let $\mathcal{D} \subseteq D_\psi$. Let also $m \geq 2$ be an integer. We say that *psi* induces chaotic dynamics on m symbols on the set $\mathcal{D}$ if there exists m nonempty pairwise disjoint compact sets

$$\mathcal{K}_0, \dots, \mathcal{K}_{m-1} \subseteq \mathcal{D}$$

such that for each two sided sequence $(s_i)_{i\in\mathbb{Z}} \in 0, \dots, m-1^{\mathbb{Z}}$, there exists a corresponding sequence $w_i)_{i\in\mathbb{Z}} \in \mathcal{D}^{\mathbb{Z}}$ such that

$$w_i \in \mathcal{K}_{s_i} \;\; and \;\; w_{i+1} = \psi(w_i), \;\; \forall i \in \mathbb{Z} \tag{2.8}$$

and whenever $(s_i)_{i\in\mathbb{Z}}$ is a k-periodic sequence (that is, $s_{i+k} = s_i, \forall i \in \mathbb{Z}$) for some $k \geq 1$, there exists a corresponding k- periodic sequence $w_i)_{i\in\mathbb{Z}} \in \mathcal{D}^{\mathbb{Z}}$ satisfying 2.8. When we want to emphasize the role of the sets $\mathcal{K}_j$'s, we also say that ψ induces chaotic dynamics on m symbols on the set $\mathcal{D}$ relatively to $\mathcal{K}_0, \ldots, \mathcal{K}_{m-1}$.

For example let us take in consideration a coin-flipping experiment such that we can associate the nme "head" $= H$ to the set $\mathcal{K}_0$ and the name "tail" $= T$ to $\mathcal{K}_1$. If we consider any sequence of symbols

$$(s_i)_{i\in\mathbb{Z}} \in \{0,1\}^{\mathcal{Z}} \equiv \{H,T\}^{\mathcal{Z}}$$

so that for each i, s_i is either "head" or "tail", then we have the same itinerary of heads and tails realized through the map ψ. For instance, there exists a fixed point of ψ in the set $\mathcal{K}_1$ corresponding to the costant sequence of symbols $s_i =$ "tail", $\forall i \in \mathbb{Z}$. There is also a point $w \in \mathcal{K}_0$ of period three with $\psi(w) \in \mathcal{K}_0$ and $\psi^2(w) \in \mathcal{K}_1$ corresponding to the periodic sequence $\ldots HHT\ HHT\ HHT \ldots$, and so on.

The Theorem below shows the link between the method of stretching along the paths and the notion of chaotic dynamics in the sense of Definition 2.10.

Theorem 2.11. *Let $\widehat{\mathcal{R}} = (\mathcal{R}, \mathcal{R}^-)$ be an oriented rectangle of a metric space X and let $\mathcal{D} \subseteq \mathcal{R} \cap D_\psi$ the domain of a map $\psi : X \supseteq D_\psi \to X$. If $\mathcal{K}_0, \ldots, \mathcal{K}_{m-1}$ are $m \geq 2$ pairwise disjoint compact sets contained in $\mathcal{D}$ and*

$$(\mathcal{K}_i, \psi) : \widehat{\mathcal{R}} \not\Rightarrow \widehat{\mathcal{R}}, \quad for\ \ i = 0, \ldots, m-1, \quad i \in \mathbb{Z}$$

then psi induces chaotic dynamics on m symbols on the set $\mathcal{D}$ relatively to $\mathcal{K}_0, \ldots, \mathcal{K}_{m-1}$.

Proof. Recalling Definition 2.10, the thesis is just a reformulation of the second and forth conclusions in the Theorem 2.9. □

Theorem 2.12. *Let ψ be a map inducing chaotic dynamics on $m \geq 2$ symbols on a set $\mathcal{D} \subseteq X$ and which is continuous on*

$$\mathcal{K} = \bigcup_{i=0}^{m-1} \mathcal{K}_i \subseteq \mathcal{D}$$

where $\mathcal{K}_0, \ldots, \mathcal{K}_{m-1}, \mathcal{D}$ and X are as in Definition 2.10. Setting

$$\mathcal{I}_{\inf} = \bigcap_{n=0}^{\inf} \psi^{-n}(\mathcal{K}), \tag{2.9}$$

then there exists a nonempty compact set

$$\mathcal{I} \subseteq \mathcal{I}_{\text{inf}} \subseteq \mathcal{K}$$

on which the following are fulfilled:

1. *$\mathcal{I}$ is invariant for ψ (that is, $\psi(\mathcal{I} = \mathcal{I})$;*

2. *$\psi \mid_{\mathcal{I}}$ is semi-conjugate to the one-sided Bernoulli shift on m symbols, i.e. there exists a continuous map π of $\mathcal{I}$ onto $\Sigma_m^+ = \{0, \ldots, m-1\}^{\mathbb{N}}$, endowed with the distance*

$$\hat{d}(s', s'') = \sum_{i \in \mathbb{N}} \frac{\mid s_i' - s_i'' \mid}{m^{i+1}} \tag{2.10}$$

   for $s' = (s_i')_{i \in \mathbb{N}}$ and $s'' = (s_i'')_{i \in \mathbb{N}}$ such that the diagram

$$\begin{array}{ccc} \mathcal{I} & \xrightarrow{\psi} & \mathcal{I} \\ \pi \downarrow & & \downarrow \pi \\ \Sigma_m^+ & \xrightarrow[\sigma]{} & \Sigma_m^+ \end{array}$$

   commutes, i.e. $\pi \circ \psi = \sigma \circ \pi$, where $\sigma : \Sigma_m^+ \to \Sigma_m^+$ is the Bernoulli shift defined by $\sigma((s_i)_i) = (s_{i+1})_i$, $\forall i \in \mathbb{N}$

3. *The set $\mathcal{P}$ of periodic points of $\psi \mid \mathcal{I}_\infty$ is dense in $\mathcal{I}$ and the preimage $\pi^{-1}(s) \subseteq \mathcal{I}$ of every k-periodic sequence $s = (s_i)_{i \in \mathbb{N}} \in \Sigma_m^+$ contain at least on $k-$periodic point.*
   Furthermore, from conclusion 2) it follows that:

4. $$h_{top}(\psi) \geq h_{top}(\psi \mid \mathcal{I}) \geq h_{top}(\Sigma) = log(m), \tag{2.11}$$

   where h_{top} is the topological entropy;

5. *There exists a compact invariant set $\Lambda \subseteq \mathcal{I}$ such that $\psi \mid \mathcal{I}$ is semiconjugate to the one-sided Bernoulli shift on m symbols, topologically transitive and has sensitive dependence on initial conditions.*

Theorem 2.13. *Let X be a metric space and assume that $\phi : X \sqsubseteq D_\phi \to X$ and $\pi : X \sqsubseteq D_\psi \to X$ are continuous maps defined on the sets D_ϕ and D_ψ, respectively. Let also $\widehat{\mathcal{A}} = (\mathcal{A}, \mathcal{A}^-)$ and $\widehat{\mathcal{B}} = (\mathcal{B}, \mathcal{B}^-)$ be oriented rectangles of X. Suppose that the following conditions are satisfied:*

(H_ϕ) There are $m \geq 2$ pairwise disjoint compact sets $\mathcal{H}_0, \ldots, \mathcal{H}_{m-1} \subseteq \mathcal{A} \cap D_\psi$ such that $(\mathcal{H}_i, \phi) : \widehat{\mathcal{A}} \overset{\phi}{\Rightarrow} \widehat{\mathcal{B}}$ for $i = 0, \ldots, m-1$;

(H_ψ) $\mathcal{B} \subseteq D_\psi$ and $\psi : \widehat{\mathcal{B}} \overset{\psi}{\Rightarrow} \widehat{\mathcal{A}}$

Then the map $\varphi = \psi \circ \phi$ induces chaotic dynamics on m symbols in the set $\mathcal{H} \cap \phi^{-1}(\mathcal{B})$ where $\mathcal{H} = \bigcup_{i=0}^{m} \mathcal{H}_i$ and thus satisfies properties from Theorem 2.12.

Proof. We show that

$$(\mathcal{H} \cap \phi^{-1}(\mathcal{B}), \varphi) : \widehat{\mathcal{A}} \overset{\varphi}{\Rightarrow} \widehat{\mathcal{A}} \ \forall\, i = 0, \ldots, m-1 \tag{2.12}$$

from which the thesis about the chaotic dynamics is an immediate consequence of Theorem 2.11. To check condition 2.12 let us consider a path $\gamma : [0,1] \to \mathcal{A}$ such that $\gamma(0) \in \mathcal{A}_l^-$ and $\gamma(1) \in \mathcal{A}_r^-$ or otherwise and let us fix $i \in 0, \ldots, m-1$. By (H_ϕ) there exists a compact interval $[t', t''] \subseteq [0,1]$ such that $\gamma(t) \in \mathcal{H}_i$ and $\phi(\gamma(t)) \in \mathcal{B}$ for every $t \in [t', t'']$, and $\phi(\gamma(t'))$ and $\phi(\gamma(t''))$ belonging to different components of $\mathcal{B}^-$. Define now

$$\omega : [t', t''] \to \mathcal{B}, \ \ \omega(t) = \phi(\gamma(t)).$$

By (H_ψ) there is a compact interval $[s', s''] \subseteq [t', t'']$ such that $\psi(\omega(t)) \in \mathcal{A}$ for every $t \in [s', s'']$, with $\psi(\omega(s'))$ and $\psi(\omega(s''))$ belonging to different components of $\mathcal{A}^-$. Rewriting all in terms of γ we have thus proved that

$$\gamma(t) \in \mathcal{H} \cap \phi^{-1}(\mathcal{B}) \text{ and } \varphi(\gamma(t)) \in \mathcal{A} \ \ \forall t \in [s', s'']$$

with $\varphi(\gamma(s'))$ and $\varphi(\gamma(s''))$ belonging to different components of $\mathcal{A}^-$. THe continuity of the composite mapping $\varphi = \psi \circ \phi$ on $\mathcal{H} \cap \phi^{-1}(\mathcal{B})$ follows from the continuity of ϕ on $D_\phi \supseteq \mathcal{H}_i$ and from continuity of ψ on $D_\psi \supseteq \mathcal{B}$. By the arbitrariness of the path γ and of $i \in 0, \ldots, m-1$ the verification of 2.12 is complete. □

Theorem 2.14. *Let X be a metric space and assume that $\phi : X \sqsubseteq D_\phi \to X$ and $\pi : X \sqsubseteq D_\psi \to X$ are continuous maps defined on the sets D_ϕ and D_ψ, respectively. Let also $\widehat{\mathcal{A}} = (\mathcal{A}, \mathcal{A}^-)$ and $\widehat{\mathcal{B}} = (\mathcal{B}, \mathcal{B}^-)$ be oriented rectangles of X. Suppose that the following conditions are satisfied:*

(H_ϕ) There are $m \geq 1$ pairwise disjoint compact sets $\mathcal{H}_0, \ldots, \mathcal{H}_{m-1} \subseteq \mathcal{A} \cap D_\psi$ such that $(\mathcal{H}_i, \phi) : \widehat{\mathcal{A}} \overset{\phi}{\Rightarrow} \widehat{\mathcal{B}}$ for $i = 0, \ldots, m-1$;

(H_ψ) There are $l \geq 1$ pairwise disjoint compact sets $\mathcal{K}_0, \ldots, \mathcal{K}_{l-1} \subseteq \mathcal{B} \cap D_\psi$ such that $(\mathcal{K}_i, \psi) : \widehat{\mathcal{B}} \overset{\psi}{\Rightarrow} \widehat{\mathcal{A}}$ for $i = 0, \ldots, l-1$;

If at least one between m and l is greater or equal than 2, then the composite map $\varphi = \psi \circ \phi$ induces chaotic dynamics on $m \times l$

$$H^* = \bigcup_{i,j} \mathcal{H}_l^{i,j} \text{ with } \mathcal{H}_l^{i,j} = \mathcal{H}_i \cap \phi^{-1}(\mathcal{K}_j),\ i = 0, \dots, m-1, j = 0, \dots, m-1. \quad (2.13)$$

and thus satisfies properties from Theorem 2.12.

Proof. In order to get the thesis,it suffices to show that

$$(\mathcal{H}'_{i,j}, \phi) : \widehat{\mathcal{A}} \twoheadrightarrow \widehat{\mathcal{A}},\ \forall i = 0, \dots, m-1,\ \text{and } j = 0, \dots, l-1$$

Such condition can be checked by steps analogous to the ones in Theorem 2.12. The details are omitted since they are straightforward. □

Chapter 3

Chaos indicators and numerical methods

In this chapter, we will discuss several numerical methods that have been developed with the intent to detect chaotic behavior in Hamiltonian systems. In particular and different from the standard Poincaré map or the Lyapunov exponents, we will present two relatively recent numerical indicators of chaos. The two methods, named SALI (Smaller ALignment Index) and GALI (Generalised ALignment Index), have been developed by C. Skokos and coworkers and are based on the alignment of the unit vectors defined on the orbits of the system under investigation [26]. Studying how the angle (SALI) of two unit vectors or the volume (GALI) of n unit vectors evolve over the orbits contributes to establishing the chaoticity of the conservative system. In this chapter, we will extensively refer to the paper of C. Skokos [26, 27] when we discuss the part regarding the maximum Lyapunov Characteristic Exponents (mLCE), and the SALI and GALI chaos detectors. As an original contribution, at the end of this chapter, we discuss also the application of the SALI and GALI methods to the case of the dynamical system that describes the motion of two charged particles inside the tokamak. The peculiarity of these methods is due to the fact that they can be used to investigate the behavior of the system even for higher dimensional systems as in this case. In fact, such results cannot be obtained with the analytical methods described in the previous chapter.

3.1 Hamiltonian systems

The first idea of a dynamical system emerged with the seminal work of Isaac Newton while formulating his famous laws (in particular the second one) of mechanics. Newton mechanics was initially successfully used to explain Kepler's laws for the motion of the

planets. From the mathematical point of view, we represent the evolution of the state, so the variables that characterize a given physical, biological, chemical system, by a set of differential equations which can be either of the deterministic or stochastic nature. In other words, a system in which the state is a function of time is called "dynamical." To determine the state for all future times requires iterating the system many times—each advancing time a small step. The iteration procedure is referred to as solving the system or integrating the system. For integrable systems, given an initial point it is possible to determine analytically all its future positions, a collections of points known as a trajectory or orbit.

Euler, Lagrange, Laplace, and Hamilton did further development and generalization of the theory that studied the mechanics of dynamical systems representing the state as a geometric variable associating a spatial position with a given temporal point. In particular, the Hamiltonian formulation of dynamical systems is widely used nowadays to describe many physical systems. In modern times, a major contribution to the standard mathematical definition of dynamical systems is due to the work of Poincaré, who studied the stability of the system, e.g., that of the three-body problem, with the eventual chaoticity of the orbits. In particular, he introduced his recurrence theorem that we have extensively used even in this thesis. Later on, respectively, Lyapunov and Lorenz formalized the idea of stability and chaoticity of dynamical systems. The study of dynamical systems is still a significant research field of mathematics with many essential applications in everyday life spanning from medicine to social behavior.

Definition 3.1. A dynamical system consists of a phase space $\mathcal{S}$ and a family of continuous transformations $\phi_t : \mathcal{S} \to \mathcal{S}$, depending by the parameter t where t is the time and may be either discrete, $t \in \mathbb{Z}$ or continuous $t \in \mathbb{R}$. For arbitrary states $x \in \mathcal{S}$ the following must hold

1. $\phi_0(\mathbf{x}) = \mathbf{x}$ identity
2. $\phi_t(\phi_s(\mathbf{x})) = \phi_{t+s}(\mathbf{x}) \forall t, s \in \mathbb{R}$ additivity

A dynamical system can be of a continuous or discrete nature, depending on the way the state of the system evolves. So, if the state evolves as a function of a (continuous or discrete) variable, usually representing time, in a continuous domain, then it is a continuous (state) system. Otherwise, if the state space is a discrete one and the evolution of the system is described by a succession of points in the discrete state space, then the system is considered to be discrete.

Definition 3.2. Let $\mathcal{S} \subset \mathbb{R}^n$ be an open set, $n \in \mathbb{N}$, $\mathbf{x} = (x^1, \ldots, x^n) \in \mathcal{S}$,$t \in \mathbb{R}$ Then

$$F : \mathcal{S} \to \mathcal{S}, \;\; \dot{\mathbf{x}} = F(\mathbf{x}(t)) = F(\mathbf{x}) \tag{3.1}$$

is called a vector field. It can be written as a system of n first order, autonomus (i.e., not explicitely time - dependent), ordinary differential equations.

$$\begin{aligned} \frac{dx^1}{dt} &= F^1(x^1, \ldots, x^n) \\ \frac{dx^2}{dt} &= F^2(x^1, \ldots, x^n) \\ &\vdots \\ \frac{dx^n}{dt} &= F^n(x^1, \ldots, x^n) \end{aligned}$$

The formal solution of (3.3) satisfying the initial condition $\mathbf{x}(0) = \mathbf{z}$ is defined as

$$\mathbf{x}(t) = \phi_t(\mathbf{z}) \tag{3.2}$$

and is called the flow of the vector field.

A single path in phase space followed by $\mathbf{x}(t)$ in time is called the *trajectory* or *orbit* of the dynamical system.

Definition 3.3. Let $\mathcal{S} \subset \mathbb{R}^N$, $N \in \mathbb{N}$, $\mathbf{x}_n \in \mathcal{S}$,$n \in \mathbb{Z}$ Then given a map

$$M : \mathcal{S} \to \mathcal{S}, \;\; \text{such that} \;\; \mathbf{x}_{n+1} = M(\mathbf{x}_n) \tag{3.3}$$

we have a discrete dynamical system, setting $\phi_n(w) = M^n(w)$ with $M^0(w) = Id$. The relation $\mathbf{x}_{n+1} = M(\mathbf{x}_n)$ defines equations of motion of the dynamical system.

A *Hamiltonian system* is a system of $2N$ ordinary differential equations of the form

$$\dot{q}_i = \frac{\partial H}{\partial p_i}(t, \mathbf{q}, \mathbf{p}), \;\; \dot{p}_i = -\frac{\partial H}{\partial p_i}(t, \mathbf{q}, \mathbf{p}), \; i = 1, \ldots, N \tag{3.4}$$

where $H = H(t, \mathbf{q}, \mathbf{p})$, known as the Hamiltonian is a smooth real-valued function defined for $(t, \mathbf{q}, \mathbf{p})$ in an open set of $\mathbb{R}^1 \times \mathbb{R}^N \times \mathbb{R}^N$.

The vectors $\mathbf{q} = (q_1, \ldots, q_N)$ and $\mathbf{p} = (p_1, \ldots, p_N)$ traditionally denote the position and momentum vectors, respectively. The integer N is the number of degrees of freedom of the system. Equations (3.4) are also formulated in matrix form as following:

$$\dot{\mathbf{x}} = \mathbf{F}(\mathbf{x}) = \left[\frac{\partial H}{\partial \mathbf{p}}, -\frac{\partial H}{\partial \mathbf{q}}\right]^T = \mathbf{J}_{2N} \cdot \mathbf{DH}(\mathbf{x}) \tag{3.5}$$

with $\mathbf{q} = (q_1(t), q_2(t), ...q_N(t))$, $\mathbf{p} = (p_1(t), p_2(t), ..., p_N(t))$ and

$$\mathbf{DH}(\mathbf{x}) = \left[\frac{\partial H}{\partial q_1}, \frac{\partial H}{\partial q_2}, \dots \frac{\partial H}{\partial q_N}, \frac{\partial H}{\partial p_1}, \frac{\partial H}{\partial p_2}, \dots \frac{\partial H}{\partial p_N}\right]^T$$

Matrix $\mathbf{J}_{2N}$ has the following block form:

$$\mathbf{J}_{2N} = \begin{bmatrix} \mathbf{0}_N & \mathbf{I}_N \\ -\mathbf{I}_N & \mathbf{0}_N \end{bmatrix}$$

with $\mathbf{I}_N$ being the $N \times N$ identity matrix and $\mathbf{0}_N$ being the $N \times N$ matrix with all its elements equal to zero. Let's see now the following example:

Example 3.1. *Using eqs.* (1.18) *and* (1.19) *in eq.* (1.17) *which we multiply by* $\dot{r}$ *before integration we end up with the Hamiltonian function of a charge* e *with mass* m *in cylindrical geometry*

$$H(r, \dot{r}) = m\frac{\dot{r}^2}{2} + \frac{mA^2}{2r^2} + \frac{(eB_0)^2}{8m}r^2 + \frac{e^2}{m}F^2(r) \tag{3.6}$$

meanwhile, similarly one can easily obtain the Hamiltonian function in the case without plasma for a particle with charge e *with mass* m *as*

$$H(r, \dot{r}) = \frac{\dot{r}^2}{2} + \frac{C^2}{2r^2} + \frac{(\frac{B_0 Rq}{m}\log(r))^2}{2} + \frac{B_0 Rq}{m}C'\log(r) \tag{3.7}$$

For further details refer to [8].

3.2 Variational equations

Let us now turn our attention to the (continuous or discrete) time evolution of deviation vectors $\mathbf{w}$ from a given reference orbit of a dynamical system. These vectors evolve on the tangent space $\mathcal{T}_{\mathbf{x}}\mathcal{S}$ of the set $\mathcal{S}$. We denote by $d_{\mathbf{x}}\Phi^t$ the linear mapping which maps the tangent space of $\mathcal{S}$ at a point x onto the tangent space at point $\Phi^t(\mathbf{x})$ and so we have $d_{\mathbf{x}}\Phi^t : \mathcal{T}_{\mathbf{x}}\mathcal{S} \to \mathcal{T}_{\Phi^t(\mathbf{x})}\mathcal{S}$ with

$$\mathbf{w}(t) = d_x\Phi^t\mathbf{w}(0) \tag{3.8}$$

where $\mathbf{w}(0)$, $\mathbf{w}(t)$ are deviation vectors with respect to the given orbit at times $t = 0$ and $t > 0$, respectively and the followed property are satisfied:

1. If t and s are two successive time intervals, then the composition property $d_{\mathbf{x}}\phi^{t+s} = d_{\phi^s(\mathbf{x})}\phi^t \circ d_{\mathbf{x}}\phi^s$ holds;
2. $d_{\mathbf{x}}\phi^t(a\mathbf{w}) = a d_{\mathbf{x}}\phi^t \mathbf{w}$, for any $a \in \mathbb{R}$.

In the case of Hamiltonian systems (eq. (3.5)) an initial deviation vector

$$\mathbf{w}(0) = (\delta x_1(0), \delta x_2(0), ..., \delta x_{2N}(0))$$

from the solution $\mathbf{x}(t)$ (eq. (3.2)) evolves on the tangent space $\mathcal{T}_{\mathbf{x}}\mathcal{S}$ according to the so-called variational equations:

$$\begin{aligned} \dot{\mathbf{w}} &= \mathbf{Df}(\mathbf{x}(t)) \cdot \mathbf{w} \\ &= [\mathbf{J}_{2N} \cdot \mathbf{D}^2\mathbf{H}\ (\mathbf{x}(t))] \cdot \mathbf{w} \end{aligned} \tag{3.9}$$

with $\mathbf{D}^2\mathbf{H}(\mathbf{x}(t))$ being the Hessian matrix of the Hamiltonian function calculated on the reference orbit $\mathbf{x}(t)$, i.e.,

$$\mathbf{D}^2\mathbf{H}(\mathbf{x}(t))_{i,j} = \frac{\partial^2 \mathbf{H}}{\partial \mathbf{x}_i \partial x_j} \Phi^t(\mathbf{x}(0)), \quad {}_1, j = 1, 2, ..., 2N.$$

When dealing with Hamiltonian systems, the variational equations have to be integrated simultaneously with the Hamilton equations of motion since the x and w variables appear explicitly in it. Thus if we want to follow the time evolution of an initial deviation vector $\mathbf{w}(0)$ with respect to a reference orbit with initial condition $\mathbf{x}(0)$ we are obliged to integrate simultaneously the whole set of differential equations (eq. (3.5)) and (eq. (3.9)).

3.3 Chaos Indicators

3.3.1 The Poincaré map

A flow in the state space corresponds to a trajectory flowing around a torus with period $\frac{2\pi}{\omega}$. This naturally leads to a Poincaré mapping of a $\theta = \theta_0$ plane to itself, as depicted

in Figure 3.1. The notion of the Poincaré section was named after Henri Poincaré, who realized the first map of this type. It was M.Henon, who proposed a trick on how to compute this map.

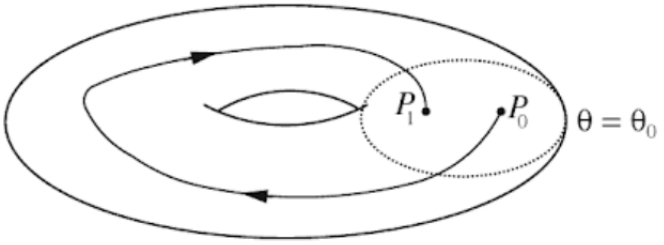

FIGURE 3.1: The first return of a point P_0 to P_1 in the plane $\theta = \theta_0$. The trajectories flow inside a torus in three-dimensional space.This figure has been reproduced from [28]

We consider an autonomous dynamical system defined by $2N$ simultaneous differential equations:

$$\frac{dx_1}{dt} = f_1(x_1, \ldots, x_{2N}) \tag{3.10}$$

$$\frac{dx_2}{dt} = f_2(x_1, \ldots, x_{2N}) \tag{3.11}$$

$$\vdots$$

$$\frac{dx_{2N}}{dt} = f_{2N}(x_1, \ldots, x_{2N}) \tag{3.12}$$

and the surface of section θ_0 defined by

$$\theta_0(x_1, \ldots, x_{2N}) = 0$$

A solution can be represented by a curve, or trajectory, in an 2N-dimensional phase space $(x_1, \ldots, x_{2N})$. The Poincaré map is a application of θ_0 on itself, generated by the points obtained as intersection of the trajectory with θ_0 which in general is an $(2N-1)$-dimesional subset of the phase space. The aim of this section is to give an efficient scheme of integration (see [28]) in order to generate the Poincare map such that the error is reduced or is comparable to the error generated by the integration of eqs. (3.10) to (3.12).

The idea is to transform such system in x_i-dependent for each $i = 1, \ldots, 2N$ such that

$$x_i - a = 0$$

and by inverting the ith eqs. (3.10) to (3.12) and dividing the $(2N-1)$- remaining equation by the ith:

$$\frac{dx_1}{dx_i} = \frac{f_1}{f_i} \tag{3.13}$$

$$\vdots$$

$$\frac{dt}{dx_i} = \frac{1}{f_i} \tag{3.14}$$

$$\vdots$$

$$\frac{dx_{2N}}{dx_i} = \frac{f_{2N}}{f_i} \tag{3.15}$$

The two system eqs. (3.10) to (3.12) and eqs. (3.13) to (3.15) can be merged into a single form. If we define $x_i = \tau$ as the current independent variable and

$$K = \frac{dt}{d\tau}$$

then eqs. (3.10) to (3.12) and eqs. (3.13) to (3.15) are two particular cases of the general form

$$\frac{dx_1}{d\tau} = K f_1 \tag{3.16}$$

$$\vdots$$

$$\frac{dx_{2N}}{d\tau} = K f_{2N} \tag{3.17}$$

$$\frac{dt}{d\tau} = K \tag{3.18}$$

obtained by taking respectively $K = 1$ and $K = 1/f_N$.

A numerical computation of Poincaré section is given by the following algorithm. The program numerically integrates the equations of a trajectory up to a given maximal integration time $t = T_{max}$, detects and computes its intersections with a surface of section of the form $x_i = x_j$

Input: 1. General form of motion equation 3.5.
2. Initial condition for the orbit $x(0)$.
3. PSS value x_i.
4. Integration time step τ.
5. Maximal integration time T_{max}.

Output: Intersections with surface of section $x_i = a$

Set the counter $k = 1$;
while $k\tau < T_{max}$ **do**
  Evolve the orbit and the deviation vector from time $t = (k-1)\tau$ *to* $t = k\tau$, *i. e. Compute* $x(k\tau)$;
  if $(x_i - x_j(k\tau))(x_i - x_j((k-1)\tau) < 0)$ *and* $x_{j+N}(k\tau) > 0$ *for some* $j \in \{1, 2, \ldots, N\}$ **then**
    Set integration step $\lambda = x_i - x_j((k-1)\tau)$;
    Set the initial conditions $y(0) = (x_1((k-1)\tau), \ldots, x_{i-1}((k-1)\tau), x_{j+1}((k-1)\tau), \ldots, x_{2N}((k-1)\tau), (k-1)\tau)$;
    Integrate eqs. (3.16) *to* (3.18) *with* $y(0)$ *for one time step using the 4th order Runge-Kutta method*;
    Store $y(\lambda)$;
  end
  Set the counter $k \leftarrow k + 1$;
end

Algorithm 1: Algorithm for the numerical computation of the (Poincaré surface of section) or PSS of a dynamical system.

3.3.2 Lyapunov Characteristic Exponent

The theory of Lyapunov Characteristic Exponents (LCEs) is crucial for chaos investigation. Lyapunov was the first person to observe the evolution of the orbits originating from an initial point near an equilibrium state formalizing this way the concept of stability. It was Henon-Heiles who introduced the notion of the divergence of two nearby orbits, going ahead in time with the quantity of the exponential divergence by Casartelli et al. [29] transforming it in an estimator of the Maximal Lyapunov Characteristic Exponent for $t \longrightarrow \infty$ by [30]. Let's start with the definition of the $LCEs$.

Let $\mathbf{A}_t$ be an $n \times n$ matrix function defined either on the whole real axis or on the set of integers, such that $\mathbf{A}_0 = \mathbf{I}_n$, for each time t the value of function $\mathbf{A}_t$ is a nonsingular matrix and $\|\mathbf{A}_t\|$ the usual 2-norm of $\mathbf{A}_t$. In particular we consider only matrices satisfying

$$\max\{\|\mathbf{A}_t\|, \|\mathbf{A}_t^{-1}\|\} \leq e^{ct}$$

with c a suitable constant.

Definition 3.4. Considering a matrix function $\mathbf{A}_t$ as above and a nonzero vector $\mathbf{w}$ of the Euclidean space $\mathbb{R}^n$ the quantity

$$\mathcal{X}(\mathbf{A}_t, \mathbf{w}) = \limsup_{t\to\infty} \frac{1}{t} \ln \|\mathbf{A}_t \mathbf{w}\ \| \tag{3.19}$$

is called the 1-dimensional Lyapunov Characteristic Exponent or the Lyapunov Characteristic Exponent of order 1 (1-LCE) of $\mathbf{A}_t$ with respect to vector $\mathbf{w}$.

For simplicity, we will usually refer to 1-LCEs as LCEs. We note that the value of LCE is independent of the norm appearing in (3.19). This can easy be seen as follows: Let us consider a second norm $\|\cdot\|'$ satisfying the inequality of equivalent norms with $\|\cdot\|$

$$\beta_1 \|\mathbf{w}\| \leq \|\mathbf{w}\|' \leq \beta_2 \|\mathbf{w}\|$$

for some positive real numbers β_1, β_2 and for all vectors $\mathbf{w}$. It is easily to see that the use of norm $\|\cdot\|'$ in (3.19) leaves unchanged the value of $\mathcal{X}(\mathbf{A}_t, \mathbf{w})$. Since all norms of finite dimensional vector spaces are equivalent, we conclude that LCEs do not depend on the chosen norm. Let $\mathbf{w}_i$, $i = 1, \ldots, p$ be a set of linearly indipendent vectors in $\mathbb{R}^n$, $\mathbf{E}_p$ be the subspace generated by all $\mathbf{w}_i$ and $vol_p(\mathbf{A}_t, \mathbf{E}^p)$ be the volume of the p-parallelogram having as edges the p vectors $\mathbf{A}_t \mathbf{w}_i$. This volume is computed as the norm of the wedge

product of this vectors

$$vol_p(\mathbf{A}_t, \mathbf{E}^p) = \|\mathbf{A}_t w_1 \wedge \cdots \wedge \ \mathbf{A}_t w_p\|.$$

Let also $vol_p(\mathbf{A}_0, \mathbf{E}^p)$ be the volume of the initial p-parallelogram defined by all $\mathbf{w}_i$, since A_0 is the identity matrix. Then the quantity

$$\lambda_t(\mathbf{E}_p) = \frac{vol_p(\mathbf{A}_t, \mathbf{E}^p)}{vol_p(\mathbf{A}_0, \mathbf{E}^p)}$$

is called the coefficient of expansion in the direction of $\mathbf{E}^p$ and it depends only on $\mathbf{E}^p$ and not of the choice of the linearly indipendent set of vectors. Obviously for an 1-dimensional subspace E_1 the coefficient of expansion is $\|\mathbf{A}_t\mathbf{w}_1\|/\|\mathbf{w}_1\|$. If the limit

$$\lim_{t\to\infty} \frac{1}{t} \log \lambda_t(\mathbf{E}_p)$$

exist it is called the characteristic exponent of order p in the direction of $\mathbf{E}^p$.

Definition 3.5. Considering the linearly indipendent set w_i, $i = 1, \ldots, p$ and the corresponding subspace $\mathbf{E}^p$ of $\mathbb{R}^n$ as above the p- dimensional Lyapunov characteristic exponent or the Lyapunov characteristic exponent of order p (p-LCE) of $\mathbf{A}_t$ with respect to subspace $\mathbf{E}^p$ is defined as

$$\mathcal{X}(A_t, E^p) = \limsup_{t\to\infty} \frac{1}{t} \log vol_p(\mathbf{A}_t, \mathbf{E}^p) \tag{3.20}$$

Similarly to the case of the 1-LCE, the value of the initial volume $vol_p(\mathbf{A}_0, \mathbf{E}^p)$ as well as the used norm, do not influence the value of $\mathcal{X}(\mathbf{A}_t, \mathbf{E}^p)$. From (3.3.2) and the Hadamard inequality, according to which the Euclidean volume of a p-parallelogram does not exceed the product of the lengths of its sides, we conclude that the LCEs of (3.19) and (3.5) are finite. From the definition of the LCE it follows that

$$\mathcal{X}(A_t, c_1 w_1 + c_2 w_2) \leq \max\{\mathcal{X}(\mathbf{A}_t, \mathbf{w}_1), \mathcal{X}(\mathbf{A}_t, \mathbf{w}_2)\}$$

for any two vectors $\mathbf{w}_1, \mathbf{w}_2 \in \mathbb{R}^n$ and $c_1, c_2 \in \mathbb{R}$ with $c_1, c_2 \neq 0$, while Hadamard inequality implies that if $\mathbf{w}_i$, $i = 1, 2, \ldots, n$ is a basis of $\mathbb{R}^n$ then

$$\sum_{i=1}^{n} \mathcal{X}(\mathbf{A}_t, \mathbf{w}_i) \geq \limsup_{t\to\infty} \frac{1}{t} \log |\det \mathbf{A}_t| \tag{3.21}$$

where $\det \mathbf{A}_t$ is the determinant of matrix $\mathbf{A}_t$.

It can be shown that for any $r \in \mathbb{R}$ the set of vectors $\{\mathbf{w} \in \mathbb{R}^n : \mathcal{X}(\mathbf{A}_t, \mathbf{w}) \leq r\}$ is a vector subspace of $\mathbb{R}^n$ and that the function $\mathcal{X}(\mathbf{A}_t, \mathbf{w})$ with $\mathbf{w} \in \mathbb{R}^n$, $\mathbf{w} \neq 0$ takes at most n different values, say

$$\nu_1 > \nu_2 > \cdots > \nu_s \text{ with } 1 \leq s \leq n. \tag{3.22}$$

For the subspaces

$$L_i = \{\mathbf{w} \in \mathbb{R}^n : \mathcal{X}(\mathbf{A}_t, \mathbf{w}) \leq \nu_i\} \tag{3.23}$$

we have

$$\mathbb{R}^n = L_1 \supset L_2 \supset \cdots \supset L_s \supset L_{s+1} = 0 \tag{3.24}$$

with $L_{i+1} \neq L_i$ and $\mathcal{X}(A_t, \mathbf{w}) = \nu_i$ if and only if $\mathbf{w} \in L_i \setminus L_{i+1}$ for $i = 1, \ldots, s$.

Definition 3.6. A basis $\mathbf{w}_i$, $i = 1, 2, \ldots, n$ of $\mathbb{R}^n$ is called normal if $\sum_{i=1}^{n} \mathcal{X}(\mathbf{A}_t, \mathbf{w}_i)$ attains a minimum at this basis. In other words, the basis $\mathbf{w}_i$, is a normal basis if

$$\sum_{i=1}^{n} \mathcal{X}(\mathbf{A}_t, \mathbf{w}_i) \leq \sum_{i=1}^{n} \mathcal{X}(\mathbf{A}_t, \mathbf{g}_i)$$

where g_i, $i = 1, 2, \ldots, n$ is any other basis of $\mathbb{R}^n$

A normal basis w_i,$i = 1, 2, \ldots, n$ is not unique but the numbers $\mathcal{X}(A_t, w_i)$ depend only on A_t and not on the particular normal basis and are called the LCEs of function A_t. By a possible permutation of the vectors of a given normal basis, which always exist, we can always assume that $\mathcal{X}(A_t, w_1) \geq \mathcal{X}(A_t, w_2) \geq \cdots \geq \mathcal{X}(A_t, w_n)$.

Definition 3.7. Let $\mathbf{w}_i$,$i = 1, 2, \ldots, n$ be a normal basis of $\mathbb{R}^n$ and $\mathcal{X}_1 \geq \cdots \geq \mathcal{X}_n$, with $\mathcal{X}_i \equiv \mathcal{X}(A_t, w_i)$, $i = 1, 2, \ldots, n$, the LCEs of these vectors. Assume that value ν_i,$i = 1, 2, \ldots, s$ appears exactly $k_i = k_i(\nu_i) > 0$ times among these numbers. Then k_i is called the multiplicity of value ν_i and the collection (ν_i, k_i) for $i = 1, 2, \ldots, s$ is called the spectrum of LCEs.

In order to clarify the used notation we stress that $\mathcal{X}_i$, $i = 1, 2, \ldots, n$ are the n (possibly nondistinct) LCEs, satisfying $\mathcal{X}_1 \geq \mathcal{X}_2 \geq \cdots \geq \mathcal{X}_n$, while ν_i, $i = 1, 2, \ldots, s$ represent the s $(1 \leq s \leq n)$, different values of the LCEs have,with $\nu_1 > \nu_2 > \cdots > \nu_s$.

Definition 3.8. The matrix function A_t is called regular as $t \to \infty$ if for each normal basis $\mathbf{w}_i$, $i = 1, 2, \ldots, n$ it holds that

$$\sum_{i=1}^{n} \mathcal{X}(A_t, w_i) = \liminf_{t\to\infty} \frac{1}{t} \log |detA_t|$$

which,due to (3.21) leads to

$$\liminf_{t\to\infty} \frac{1}{t} \log |\det A_t| = \limsup_{t\to\infty} \frac{1}{t} \log |detA_t| \tag{3.25}$$

guaranteeing that the limit

$$\lim_{t\to\infty} \frac{1}{t} \log |detA_t| \tag{3.26}$$

exists, is finite and is equal to

$$\lim_{t\to\infty} \frac{1}{t} \log |detA_t| = \sum_{i=1}^{n} \mathcal{X}(A_t, w_i) = \sum_{i=1}^{n} k_i v_i \tag{3.27}$$

We can now state a very important theorem for the LCEs:

Theorem 3.9. *If the matrix function A_t is regular then the LCEs of all orders are given by (3.19) and (3.5) where the* $\limsup_{t\to\infty}$ *is substituted by* $\lim_{t\to\infty}$

$$\mathcal{X}(A_t, w) = \lim_{t\to\infty} \frac{1}{t} \log \|A_t w\| \tag{3.28}$$

$$\mathcal{X}(A_t, E^p) = \lim_{t\to\infty} \frac{1}{t} \log vol_p(A_t, E^p) \tag{3.29}$$

In particular, for any p-dimensional subspace $E^p \subseteq \mathbb{R}^n$ we have

$$\mathcal{X}(A_t, E^p) = \sum_{j=1}^{p} \mathcal{X}_{i_j} \tag{3.30}$$

with a suitable sequence $1 \leq i_1 \leq i_2 \leq \cdots \leq i_p \leq n$.

The part of the theorem concerning equations (3.28) and (3.29) was proved in [31] and the validity of (3.30) was shown in [32].

Heretofore we have been interested in the existence and the computation of the LCEs of all orders for a general matrix function A_t. In the following, we will restrict our study to the case of multiplicative cocycles $R(t, x)$.

Definition 3.10. A cocyle is a function $R(t, x)$ which satisfies the relation

$$R(t + s, x) = R(t, \phi^s(x)) \cdot R(s, x)$$

with respect to the dynamical system ϕ^t where $R(t, x)$ is the matrix corresponding to $d_x\phi^t$.

In particular we will consider the multiplicative cocycle $d_x\phi^t$ which maps the tangent space at $x \in \mathcal{S}$ to the tangent space $\phi^t(x) \in \mathcal{S}$ for a dynamical system defined on differentiable manifold $\mathcal{S}$.

Besides the existence and finiteness of the LECs, another important property is their regularity. We will show such regularity based on a result due to Oseledec is known as Multiplicative Ergodic Theorem (MET) or shortly Oseledec Theorem [31]. MET is one of the pillars of the ergodic theory of dynamical systems because it contains important results about the dynamical structure of the multiplicative cocycle $R(t, x)$ and its asymptotic behavior when $t \to \infty$. Apart from the original version and proof proposed by Oseledec [31], which applies to continuous and discrete systems, several alternative versions and adaptions have been proposed throughout the years. For instance, Ruelle extended the results to flows and Benedettin et. al., [32] proposed an adaption for the Hamiltonian flows and symplectic maps.

The application of the Oseledec Theorem to the particular multiplicative cocycle $d_X\Phi^t$ lays the theoretical ground for the computation of LCEs for a general dynamical system. In particular MET applies to $R(t, x)$, if it satisfies the following condition

$$||R(t, x)|| \leq e^{J(x)|t|} \tag{3.31}$$

for $t \to \pm\infty$ for almost all x with respect to a measure μ, and where $J(x)$ is a μ-measurable function.For this condition it follows that $R(t, x)$, considered as a function of t for a fixed x satisfies 3.3.2. Benettin et. al., [32] considered a particular version of the original theorem [31] focused to the particular cocycle $d_X\Phi^t$ since they were interested in the regularity in the framework of continuous and discrete dynamical systems where Φ^t was a diffeomorphism of class C^1. Since here we are interested in the autonomous

Hamiltonian systems, following [31, 32], we will state the MET for the specific cocycles $d_X\Phi^t$.

Theorem 3.11. *Multiplicative Ergodic Theorem-MET. Consider a dynamical system as follows: Lets its phase space $\mathcal{S}$ be an n-dimensional compact manifold with a normalized measure ν, $\nu(\mathcal{S}) = 1$, and a smooth Riemannian metric $\|\cdot\|$. Consider also a measure-preserving diffeomorphism ϕ^t of class C^1 satisfying*

$$\phi^{t+s} = \phi^t \circ \phi^s$$

With t denoting time and having real (continuous system) or integer (discrete system) values. Then for almost all $x \in \mathcal{S}$, with respect to measure ν we have.

1. *The family of multiplicative cocycles $d_x\phi^t : \mathcal{T}_x\mathcal{S} \to \mathcal{T}_{\phi^t(x)}\mathcal{S}$, where $\mathcal{T}_x\mathcal{S}$ denotes the tangent space of $\mathcal{S}$ at point $\boldsymbol{x}$, is regular*

2. *The LCEs of all orders exist and are indipendent of the choice of the Riemannian metric of $\mathcal{S}$. In particular, for any $w \in \mathcal{T}_x\mathcal{S}$ the finite limit*

$$\mathcal{X}(\boldsymbol{x}, \boldsymbol{w}) = \lim_{t\to\infty} \frac{1}{t} \log \|d_{\boldsymbol{x}}\phi^t \boldsymbol{w}\| \tag{3.32}$$

exists and defines the LCE of order 1.There exists at least one normal basis v_i,$i = 1, 2, \ldots, n$ of $\mathcal{T}_x\mathcal{S}$ for which the corresponding (possibly nondistinct) 1-LCEs $\mathcal{X}_i(\boldsymbol{x}) = \mathcal{X}_i(\boldsymbol{x}, \boldsymbol{v}_i)$ are ordered as

$$\mathcal{X}_1(\boldsymbol{x}) \geq \mathcal{X}_2(\boldsymbol{x}) \geq \cdots \geq \mathcal{X}_n(\boldsymbol{x}) \tag{3.33}$$

Assume that the value $\nu_i(\boldsymbol{x})$,$i = 1, 2, \ldots, s$ with $s = s(\boldsymbol{x})$, $1 \leq s \leq n$ appears exactly $k_i(\boldsymbol{x}) = k_i(\boldsymbol{x}, \nu_i) > 0$ among these numbers. Then the spectrum of LCEs $(\nu_i(\boldsymbol{x}), k_i(\boldsymbol{x}))$,$i = 1, 2, \ldots, s$ is a measurable function of $\boldsymbol{x}$, and as $\boldsymbol{w} \neq 0$ varies in $\mathcal{T}_x\mathcal{S}$, $\mathcal{X}(\boldsymbol{x}, \boldsymbol{w})$ takes one of these s different values

$$\nu_1(\boldsymbol{x}) \geq \nu_2(\boldsymbol{x}) \geq \cdots \geq \nu_s(\boldsymbol{x})$$

It also holds

$$\sum_{i=1}^{s} k_i(\boldsymbol{x})\nu_i(\boldsymbol{x}) = \lim_{n\to\infty} \frac{1}{t} \log |\det\ d_x\phi^t| \tag{3.34}$$

For any p-dimensional $(1 \leq p \leq n)$ subspace $E^p \subseteq \mathcal{T}_x\mathcal{S}$, generated by a linearly indipendent set w_i, $i = 1, 2, \ldots, p$ the finite limit

$$\mathcal{X}(\boldsymbol{x}, E^p) = lim_{t\to\infty}\frac{1}{t}\log vol_p(d_x\phi^t, E^p) \tag{3.35}$$

where $vol_p(d_x\phi^t, E^p)$is the volume of the p-parallelogram having as edges the vectors $d_x\phi^t w_i$, exists, and defines the LCE of order p. The value of $\mathcal{X}(\boldsymbol{x}, E^p)$ is equal to the sum of p 1-LCE $\mathcal{X}_i(\boldsymbol{x})$, $i = 1, 2, \ldots, n$.

Let's give now the definition of maximal Lyapunov Characteristic Exponent mLCE Let $\mathbf{w}(0)$ and $\mathbf{w}(t)$ be the deviation vector at time $t = 0$ and at time $t > 0$. The equation

$$\mathbf{w}(t) = d_{\mathbf{x}}\phi^t\mathbf{w}(0)$$

represents the solution of variational equations. Then the quantity

$$\mathcal{X} = \lim_{t\to\infty}\frac{1}{t}\log\frac{\|d_{x(0)}\phi^t w(0)\|}{\|w(0)\|} = \lim_{t\to\infty}\frac{1}{t}\log\frac{\|\mathbf{w}(\mathbf{x}(t))\|}{\|\mathbf{w}(\mathbf{x}(0))\|} = \lim_{t\to\infty} X_1(t) \tag{3.36}$$

where $X_1(t) = \frac{\|w(x(t))\|}{\|w(x(0))\|}$, is called Maximal Lyapunov Characteristic Exponent $mLCE$. If $\mathcal{X} = 0$ the orbit is called regular. If $\mathcal{X} > 0$ the orbit is called chaotic. The inverse of $mLCE$

$$t_L = \frac{1}{\mathcal{X}} \tag{3.37}$$

is called Lyapunov time. Particularly, the Lyapunov time gives an estimate of the time needed for a dynamical system to become chaotic and, in practice, measures the time needed for nearby orbits of the system to diverge by e.

The existence of the limit (3.36) is guaranteed by a week version of the Oseledets theorem. The direct numerical implementation of (3.36) leads to numerical overflow of $\|\mathbf{w}(t)\|$ due to its large value that extends beyond the capacity of the memory of the computer. Fixing a small time interval τ we express time t with respect to τ as $t = k\tau$, $k = 1, 2, \ldots$.Then $X_1(t)$ can be written equivalently as:

$$\begin{aligned} X_1(k\tau) &= \frac{1}{k\tau}\sum_{n=1}^{k}\log\frac{\|\mathbf{w}(i\tau)\|}{\|\mathbf{w}((i-1)\tau)\|} \\ &\overset{cite}{=} \frac{1}{k\tau}\sum_{n=1}^{k}\log\frac{\|d_{\mathbf{x}(0)}\phi^{i\tau}\mathbf{w}(0)\|}{\|d_{\mathbf{x}(0)}\phi^{(i-1)\tau}\mathbf{w}(0)\|} \end{aligned} \tag{3.38}$$

The termination of the algorithm 2 is garanteed by Theorem 3.12 (see [27])

Theorem 3.12. *The termination of algorithm 2 is garanteed if and only if* $\| \boldsymbol{w}((i-1)\tau) \| = 1$, $i = 1, 2, \ldots, n$

Proof.

Applying composition and linearity property of $d_{\mathbf{x}}\phi^t$ one can easily prove the following equality:

$$\frac{d_{\mathbf{x}(0)}\phi^{i\tau}\mathbf{w}(0)}{\| d_{\mathbf{x}(0)}\phi^{(i-1)\tau}\mathbf{w}(0) \|} = \frac{d_{\phi^{(i-1)\tau}\mathbf{x}(0)}\phi^{i\tau}(\frac{d_{\mathbf{x}(0)}\phi^{(i-1)\tau}\mathbf{w}(0)}{\| d_{\mathbf{x}(0)}\phi^{(i-1)\tau}\mathbf{w}(0) \|}D_0)}{D_0} \tag{3.39}$$

where D_0 is the norm of the initial deviation vector $\vec{w}(0)$. Let us now denote by

$$\hat{\mathbf{w}}((i-1)\tau) = \frac{d_{\mathbf{x}(0)}\phi^{(i-1)\tau}\mathbf{w}(0)}{\| d_{\mathbf{x}(0)}\phi^{(i-1)\tau}\mathbf{w}(0) \|}D_0, \tag{3.40}$$

the deviation vector at point $\phi^{(i-1)\tau}(\mathbf{x}(0))$ having the same direction with $\mathbf{w}((i-1)\tau)$ and norm D_0, and by D_i its norm after its evolution for τ time units.

$$D_i = \| d_{\phi^{(i-1)\tau}\mathbf{x}(0)}\phi^{\tau}\hat{\mathbf{w}}((i-1)\tau) \| . \tag{3.41}$$

Using this notation we derive from (3.39)

$$\log \frac{\| d_{\mathbf{x}(0)}\phi^{i\tau}\mathbf{w}(0) \|}{\| d_{\mathbf{x}(0)}\phi^{(i-1)\tau}\mathbf{w}(0) \|} = \log \frac{D_i}{D_0} \tag{3.42}$$

From (3.36),(3.38) and (3.42) we conclude that $mLCE$ $\mathcal{X}$ can be computed as

$$\mathcal{X} = \lim_{k\to\infty} \frac{1}{k\tau} \sum_{i=1}^{k} \log \frac{D_i}{D_0}. \tag{3.43}$$

Since the initial norm D_0 can have any arbitrary value, one can usually set it to $D_0 = 1$.

Input: 1. Hamiltonian equation of motion (3.5) and variational equations (3.9).
2. Initial condition for the orbit $\mathbf{x}(0)$.
3. Initial unitary deviation vector $\mathbf{w}(0)$.
4. Renormalization time τ.
5. Maximal time T_M.
6. Minimum allowed value of $X_1(t)$: X_{1m}
7. The stopping flag SF.

Output: Report the time evolution of $X_1(t)$

```
SF ← 0;
k ← 1;
while SF = 0 do
    Evolve the orbit and the deviation vector from time t = (k − 1)τ to
     t = kτ, i. e. Compute x(kτ) and w(kτ).;
    Compute current value of α_k =‖ w(kτ) ‖;
    Compute and store current value of X_1(kτ) = (1/kτ) Σ_{i=1}^{k} log α_i;
    Renormalize deviation vector by setting w(kτ) ← w(kτ)/α_k ;
    Set the counter k ← k + 1;
    if [(kτ > T_M) or (X_1((k − 1)τ) < X_{1m})] then
        SF ← 1;
    end
end
```

Algorithm 2: The algorithm for the computation of the $mLCE$ $\mathcal{X}$ as the limit for $t \to \infty$ of $X_1(t)$ according to (3.43)

A direct numerical scheme of $mLCE$ is given by the following algorithm below. The program computes the evolution of $X_1(t)$ as a function of time t up to a given upper value of time $t = T_M$ or until $X_1(t)$ attains a very small value, smaller than a low threshold value X_{1m}.The idea of how it works is illustrated by figure 3.2.

The unitary deviation vector $\hat{\mathbf{w}}((i-1)\tau)$, $i = 1, 2, \ldots$, is evolved according to the variational equations 3.9 (continuous map) for $t = \tau$ time units. The evolved vector $\mathbf{w}(i\tau)$ is replaced by a unitary vector $\hat{\mathbf{w}}(i\tau)$ having the same direction with $\mathbf{w}(i\tau)$.

Let us turn our attention to the structure of the spectrum of $mLCE$ for N-dimensional autonomus Hamiltonian system. Such system preserve the phase space volume. So for

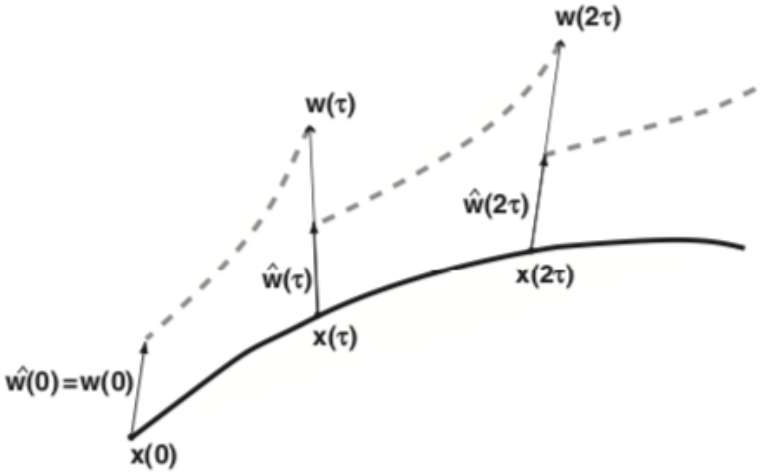

FIGURE 3.2: Numerical scheme for the computation of the $mLCE$ $\mathcal{X}_1$. This figure has been reproduced from [27].

the sum of all the $mLCE$s we have

$$\sum_{i=1}^{2N} \mathcal{X}_i(\mathbf{x}) = 0$$

It is proved in [33] that the spectrum of $mLCE$s consists of pairs of values having opposite sign.

$$\mathcal{X}_i(\mathbf{x}) = -\mathcal{X}_{2N-i+1}(\mathbf{x}), \quad i = 1, 2, \ldots, N \tag{3.44}$$

such that

$$\mathcal{X}_1(\mathbf{x}) \geq \mathcal{X}_2(\mathbf{x}) \geq \cdots \geq \mathcal{X}_N(\mathbf{x}) \geq -\mathcal{X}_N(\mathbf{x}) \geq \cdots \geq -\mathcal{X}_2(\mathbf{x}) \geq -\mathcal{X}_1(\mathbf{x}) \tag{3.45}$$

For a general differentiable flow on a compact manifold without stationary points at least one $mLCE$ must vanish then follows that at least two $mLCE$ must vanish i.e.

$$\mathcal{X}_N(\mathbf{x}) = \mathcal{X}_{N+1}(\mathbf{x}) = 0 \tag{3.46}$$

in the case of autonomous Hamiltonian flows due to the symmetry of the spectrum of $mLCE$ (see [34]).

3.3.3 SALI and GALI

$mLCE$ remains a basic method in chaos detection. New techniques are introduced by [26, 35] in the detection of chaoticity called Smaller and Generalized Alignment Index. Their ability to detect chaotic motion faster than other techniques classified them as ones of the "best" indicator of chaos, estimating here the overflow problems as a result of their faster decay of exponential growth from a numerical scheme point of view.

Definition 3.13. The quantity

$$SALI(t) = \min(\| \hat{\mathbf{w}}_1(t) + \hat{\mathbf{w}}_2(t) \|, \| \hat{\mathbf{w}}_1(t) - \hat{\mathbf{w}}_2(t) \|) \tag{3.47}$$

with $\hat{\mathbf{w}}_i(t) = \dfrac{\mathbf{w}_i(t)}{\| \mathbf{w}_i(t) \|}$, $i = 1, 2$ being unit vector is called the Smaller Alignment Index ($SALI$).If $SALI(t)$ goes to 0 the orbit is chaotic otherwise the orbit is regular.

Any two deviation vectors from a chaotic orbit with $\mathcal{X}_1 > \mathcal{X}_2$ are stretched towards the direction defined by the $mLCE$, eventually becoming aligned having the same or opposite directions. Referring to figure 3.3 easily follows when two unitary deviation vectors become aligned following the parallelogram rule.

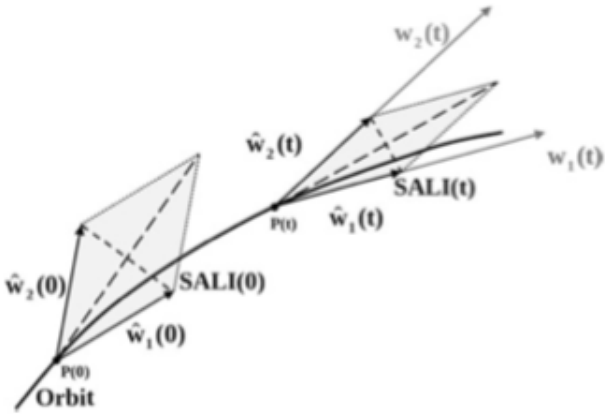

FIGURE 3.3: Schematic representation of the evolution of two deviation vectors and of the corresponding $SALI$ for a chaotic orbit.This figure have been produced by [26]

Let $\hat{\mathbf{w}}_1(t)$ and $\hat{\mathbf{w}}_2(t)$ be two initially distinct unit deviation vectors at point $P(t)$ of $\mathbf{w}_1(t)$ and $\mathbf{w}_2(t)$.They are aligned i.e they converge to the some direction when $\| \hat{\mathbf{w}}_1(t) - \hat{\mathbf{w}}_2(t) \| \to 0$ and $\| \hat{\mathbf{w}}_1(t) + \hat{\mathbf{w}}_2(t) \| \to 2$ or $\| \hat{\mathbf{w}}_1(t) - \hat{\mathbf{w}}_2(t) \| \to 2$ and $\| \hat{\mathbf{w}}_1(t) + \hat{\mathbf{w}}_2(t) \| \to 0$ if $\hat{\mathbf{w}}_1(t)$ and $\hat{\mathbf{w}}_2(t)$ change orientation. On the other hand, the regular motion is manifested when the two unitary deviation vectors are not aligned. Initially they are not neccessary on the tagent space, but as time evolves they tend to fall on the torus tagent space where their difference $\| \hat{\mathbf{w}}_1(t) - \hat{\mathbf{w}}_2(t) \|$ following the paralellogram rule remains constant.

Theorem 3.14. *If the orbit is regular or chaotic then the cost of algorithm 3 is constant or exponential, respectively obeying the law:*

$$SALI(t) \propto \begin{cases} cost \quad if \quad arg(\| \hat{\boldsymbol{w}}_1(t) \|, \| \hat{\boldsymbol{w}}_2(t) \|) \in \{0, \pi\} \\ e^{-(\lambda_1 - \lambda_2)t} otherwise \end{cases}$$

where $arg(\cdot, \cdot)$ is the angle between the two unitary deviation vectors and λ_1 , λ_2 are the first and second largest LCE.

Given two distinct orthonormal random unit deviation vectors $\mathbf{w}_1(0)$,$\mathbf{w}_2(0)$ the algorithm computes the evolution of the $SALI$ with respect to time t up to a given upper value of time $t = T_M$ or until the index becomes smaller than a low threshold value S_m. Orthonormality of $\mathbf{w}_1(t)$ and $\mathbf{w}_2(t)$ helps to avoid overflow problems meanwhile orthogonality helps to bound t he fluctuations of the $SALI$, reaching very small values around the computer's accuracy 10^{-16} in the interval $[0, \sqrt{2}]$ during the evolution of the orbits. $SALI$ is strongly connected to the area of parallelogram generated by two unit deviation vector. In other words, observing that the minimum of the two positive quantities in 3.13 is equivalent to evaluating the product

$$P(t) = \| \hat{\mathbf{w}}_1(t) + \hat{\mathbf{w}}_2(t) \| \cdot \| \hat{\mathbf{w}}_1(t) - \hat{\mathbf{w}}_2(t) \| \tag{3.48}$$

at every value of t. Indeed, if the minimum of these two quantities is zero, so will be the value of $P(t)$. On the other hand, if it is not zero $P(t)$ will be proportional to the constant about which this minimum oscillates. This suggests that, instead of computing the $SALI(t)$ from 3.13 , one might as well evaluate the exterior product of the two deviation vectors $\hat{\mathbf{w}}_1 \wedge \hat{\mathbf{w}}_2$ for which it holds

$$\| \hat{\mathbf{w}}_1 \wedge \hat{\mathbf{w}}_2 \| = \frac{\| \hat{\mathbf{w}}_1(t) + \hat{\mathbf{w}}_2(t) \| \cdot \| \hat{\mathbf{w}}_1(t) - \hat{\mathbf{w}}_2(t) \|}{2} \tag{3.49}$$

which represents the area of the parallelogram formed by the two deviation vectors.

Input: 1. Hamiltonian equation of motion 3.5 and variational equations 3.9.
2. Initial condition for the orbit $\mathbf{x}(0)$.
3. Initial orthonormal unitary deviation vector $\mathbf{w}_1(0)$,$\mathbf{w}_2(0)$.
4. Renormalization time τ.
5. Maximal time T_M.
6.Threshold value of the SALI:S_m
7.The stopping flag:SF

Output: Report the time evolution of $SALI(t)$

$SF \leftarrow 0$;
$k \leftarrow 1$;
$OC \leftarrow$ *regular*;
while $SF = 0$ **do**
  Evolve the orbit and the deviation vector from time $t = (k-1)\tau$ *to* $t = k\tau$, *i. e. Compute* $\boldsymbol{x}(k\tau)$ *and* $\boldsymbol{w}_1(k\tau)$, $\boldsymbol{w}_2(k\tau)$.;
  Normalize the two vectors, i.e.Set $\boldsymbol{w}_1(k\tau) \rightarrow \boldsymbol{w}_1(k\tau)/ \parallel \boldsymbol{w}_1(k\tau) \parallel$ *and* $\boldsymbol{w}_2(k\tau) \rightarrow \boldsymbol{w}_2(k\tau)/ \parallel \boldsymbol{w}_2(k\tau) \parallel$;
  Compute and store current value of $SALI(k\tau) = \min \parallel \hat{\boldsymbol{w}}_1(k\tau) + \hat{\boldsymbol{w}}_2(k\tau) \parallel, \parallel \hat{\boldsymbol{w}}_1(k\tau) - \hat{\boldsymbol{w}}_2(k\tau) \parallel$;
  Set the counter $k \leftarrow k+1$;
  if $SALI((k-1)\tau) < S_m$ **then**
    $SF \leftarrow 1$ *and* $OC \rightarrow$ *chaotic*;
  end
  if $(k\tau > T_M)$ **then**
    $SF \leftarrow 1$;
  end
end

Algorithm 3: The algorithm for the computation of the $SALI$ according to 3.13

Generalizing this idea we now follow the evolution of k deviation vectors, for $2 \leq k \leq 2N$ in $2N$- dimensional space by introducing a new quantity called $GALI$.

Definition 3.15. Let $\mathcal{P}_k = \{\mathbf{w} \in \mathbb{R}^k | l \leq Aw \leq u\}$ be a parallelotope where $A \in GL(n)$ and $l, u \in \mathbb{R}^k$. Then the quantity

$$GALI_k(t) = vol(\mathcal{P}) \tag{3.50}$$

where by $vol(\cdot)$ is denoted the volume of k-parallelotope, is called Generalized Alignment Index of order k, denoted by $GALI_k$.

Before explaining a numerical approach, how to define $GALI_k$ (see [36])let recall some preliminary notions. Let $V(\mathbb{R})$ be a vector space over the field of real numbers $\mathbb{R}$. Let $\Lambda(V)$ and $\Lambda^k(V)$ be the Grassman/exterior algebra and k-th exterior power of V respectively. If $e_1, \ldots, e_M$ is an orthonormal basis of V then the wedge product $\mathbf{u}_1 \wedge \mathbf{u}_2 \wedge \cdots \mathbf{u}_k$ is defined by

$$\mathbf{u}_1 \wedge \mathbf{u}_2 \wedge \cdots \mathbf{u}_k = \sum_{1 \le i_1 < i_2 < \cdots \le M} \begin{vmatrix} u_{1i_1} & u_{1i_2} & \cdots & u_{1i_k} \\ u_{2i_1} & u_{2i_2} & \cdots & u_{2i_k} \\ \vdots & \vdots & & \vdots \\ u_{ki_1} & u_{ki_2} & \cdots & u_{ki} \end{vmatrix} e_{i_1} \wedge e_{i_2} \wedge \ldots e_{i_k} \tag{3.51}$$

since $\Lambda(V)$ can be written as the direct sum of k-th exterior power of V with $i = 1, \ldots, M$ i.e.

$$\Lambda(V) = \bigoplus_{k=0}^{M} \Lambda^k(V) \tag{3.52}$$

where $\Lambda^k(V) =< e_{i_1} \wedge e_{i_2} \wedge \ldots e_{i_k} | 1 \le i_1 < i_2 < \ldots < i_k >$ and the sum in (3.52) is performed over all possible combinations of k indices out of the M total indices. So the coefficient of a particular k-vector $e_{i_1} \wedge e_{i_2} \wedge \cdots e_{i_k}$ is the determinant of the $k \times k$ submatrix of the $M \times K$ matrix of coefficients appearing (3.51) formed by $i_1, i_2, \ldots, i_k$ rows.

The inner product on V induces an inner product on each vector space $\Lambda^k(V)$ as follows: Considering two decomposable k-vectors $\mathbf{u} = \mathbf{u}_1 \wedge \ \mathbf{u}_2 \wedge \cdots \wedge \mathbf{u}_k$ and $\mathbf{v} = \mathbf{v}_1 \wedge \mathbf{v}_2 \wedge \cdots \wedge \mathbf{v}_k$ with $\mathbf{u}_i, \mathbf{v}_j \in V$, $i, j = 1, 2, \ldots, k$, the inner product of $\mathbf{u}, \mathbf{v} \in \Lambda^k(V)$ is defined by

$$< \mathbf{u}, \mathbf{v} >_k = \begin{vmatrix} u_1 \cdot v_1 & u_1 \cdot v_2 & \cdots & u_1 \cdot v_k \\ u_2 \cdot v_1 & u_2 \cdot v_2 & \cdots & u_2 \cdot v_k \\ \vdots & \vdots & & \vdots \\ u_k \cdot v_1 & u_k \cdot v_2 & \cdots & u_k \cdot v_k \end{vmatrix} \tag{3.53}$$

where U and V are matrices having as columns the coefficients of vectors u_i, v_i, $i = 1, 2, \cdots, k$ with respeskt to the orthonormal $e_1, \ldots, e_M$. Since every elementof $\Lambda^k(V)$ is a sum of a decomposable elements,this definition extends by bilinearity of any k-vector. If

$\omega_i = e_{i_1} \wedge e_{i_2} \wedge \cdot \wedge e_{i_k}$ and $\psi_i = e_{i_1} \wedge e_{i_2} \wedge \cdot \wedge e_{i_k}$ for $1 = 1, 2, \cdot, d_k$ and $1 \leq i_1 \leq i_2 \leq \cdots \leq i_k$ are two othonormal basis of $\Lambda^k(V)$ we have

$$< \omega_i, \omega_j >= \delta_{ij}, \quad i, j = 1, 2, \ldots, d_k$$

Implying that the basis is orthonormal. Inner product define a norm $\| \cdot \|$ for k vectors by

$$\| \mathbf{u} \| = \| \mathbf{u}_1 \wedge \mathbf{u}_2 \wedge \cdots \wedge \mathbf{u}_k \| = \sqrt{|U^T \cdot U|} \tag{3.54}$$

and it measures the volume $vol(P_k)$of the parallelotope having as edge the k vectors $u_1, u_2, \ldots, u_k$.

A different way of evaluation $GALI_k$ which actually proved to be more accurate, is obtained by performing the Singular Value Decomposition (SVD) of A^T. So, the $2N \times k$matrix A^T can be written as a product of a $2N \times k$ column-orthogonal matrix U, a $k \times k$ diagonal matrix Z with positive or zero elements z_i, $i = 1, \ldots, k$ (the so-called singulular values) and the transpose of a $k \times k$ orthogonal matrix V:

$$A^T = U \cdot Z \cdot V^T \tag{3.55}$$

We note that the matrices U and V are orthogonal so that:

$$U^T \cdot U = V^T \cdot V = I_k \tag{3.56}$$

with I_k being $k \times k$ unit matrix.

Using equation (3.54) for the computation of $GALI_k$ as well as equations (3.55)) and (3.56) we get:

$$GALI_k = \sqrt{det(A \cdot A^T)} \tag{3.57}$$

$$= \sqrt{\det(V \cdot Z \cdot U^T \cdot U \cdot Z \cdot V^T)} \tag{3.58}$$

$$= \sqrt{\det(V \cdot diag(z_i^2) \cdot V^T)} \tag{3.59}$$

$$= \sqrt{\det(diag(z_i^2)} \tag{3.60}$$

$$= \prod_{i=1}^{k} z_i \tag{3.61}$$

Thus, we conclude that $GALI_k$ is equal to the product of the singular values of matrix A defined by the k normalized deviation vectors. An algorithm for implementation of $GALI_k$ is given below:

Input: 1. Hamiltonian equation of motion 3.5 and variational equations 3.9.

2. Initial condition for the orbit $\mathbf{x}(0)$.

3. Initial orthonormal unitary deviation vector

$\mathbf{w}_1(0), \mathbf{w}_2(0), \ldots, \mathbf{w}_k(0)$.

4. Renormalization time τ.

5. Maximal time T_M.

6.Threshold value of the GALI:G_m

7.Order k of desired GALI

8.The stopping flag SF

Output: Report the time evolution of $GALI_k$ and the nature of the orbit

$SF \leftarrow 0$;
$k \leftarrow 1$;
$OC \leftarrow$ *regular*;
while $SF = 0$ **do**
  Evolve the orbit and the deviation vector from time $t = (k-1)\tau$ *to* $t = k\tau$, *i. e. Compute* $\boldsymbol{x}(k\tau)$ *and* $\boldsymbol{w}_1(k\tau), \boldsymbol{w}_2(k\tau), \ldots, \boldsymbol{w}_k(k\tau)$.;
  for $j = 1 \rightarrow k$ **do**
    Set $\boldsymbol{w}_j(k\tau) \rightarrow \boldsymbol{w}_j(k\tau) / \parallel \boldsymbol{w}_j(k\tau) \parallel$;
  end
  Compute and store current value of $GALI(k\tau)$
  Create matrix $A(k\tau)$ *having as rows the deviation vectors* $\boldsymbol{w}_1(k\tau), \boldsymbol{w}_2(k\tau), \ldots, \boldsymbol{w}_k(i\tau)$
  Apply SVD algorithm to compute singular values $z_1(i\tau), z_2(i\tau), \ldots, z_k(i\tau)$
  $GALI_k(i\tau) = \prod_{j=1}^{k} z_j(i\tau)$;
  Set the counter $i \leftarrow i + 1$;
  if $GALI((k-1)\tau) < G_m$ **then**
    $SF \leftarrow 1$ *and* $OC \rightarrow$ *chaotic*;
  end
  if $[(k\tau > T_M)]$ **then**
    $SF \leftarrow 1$;
  end
end

Algorithm 4: The algorithm for the computation of the $GALI$ according to 3.51

The program computes the evolution of the $GALI_k$ with respect to time t up to a given

upper value of time $t = T_m$ or until the index becomes smaller than a low threshold value G_m. For a more detailed description of the SVD method, as well as an algorithm for its implementation, the reader is referred to [37]. Referring to the accuracy of the computation of this algorithm let's state the following theorem (see [26]):

Theorem 3.16. *If the orbit is chaotic, $GALI_k$ goes to zero exponentially fast by the law:*

$$GALI_k(t) \propto e^{-\sum_{j=2}^{k}(\sigma_1-\sigma_j)t} \tag{3.62}$$

If on the other hand, the orbit lies in a N-dimensional torus $GALI_k$ display the following behaviors

$$GALI_k(t) \propto \begin{cases} constant \quad for 2 \leq k \leq N \\ \frac{1}{t^{2(k-N)-m}} if\ N \leq k \leq 2N and 0 \leq m < k-N \\ \frac{1}{t^{k-N}} if\ N \leq k \leq 2N and m \geq k-N \end{cases} \tag{3.63}$$

depending on the number m of deviation vectors which initiallly lie in the tangent space of the torus.

3.4 Applications and numerical investigation

To verify the validity of theoretical predictions, let's see the following two applications:

3.4.1 Henon Heiles model

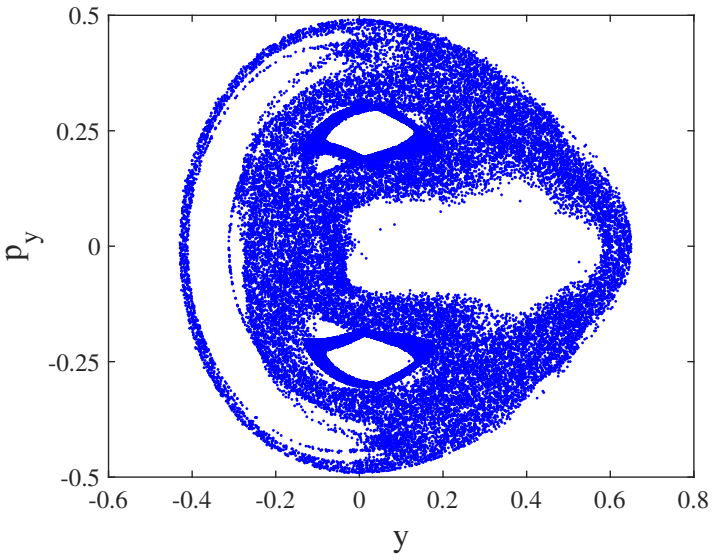

FIGURE 3.4: The Poincaré section of Henon Heiles model for $x = 0$ and $p_x \geq 0$.

Let's consider the following $2D$ continuous, conservative, autonomous Hamiltonian system

$$H(x, y, p_x, p_y) = \frac{1}{2}(p_x^2 + p_y^2) + \frac{1}{2}(x^2 + y^2) + x^2 y - \frac{1}{3}y^3 \tag{3.64}$$

known as Henon-Heiles. Such a system describes the motion of stars in a galactic center, with the motion restricted to a plane. Therefore, from the definition 3.5 and 3.9 one can easily define motion equation

$$\begin{cases} \dot{x} = p_x \\ \dot{y} = p_y \\ \dot{p_x} = -x - 2xy \\ \dot{p_y} = -y - x^2 + y^2 \end{cases} \tag{3.65}$$

and the variational equations as

$$\begin{cases} \dot{\delta x} = \delta p_x \\ \dot{\delta y} = \delta p_y \\ \dot{\delta p_x} = \delta x(-1-2y) - 2x\delta y \\ \dot{\delta p_y} = -2x\delta x + (-1+2y)\delta y \end{cases} \tag{3.66}$$

As can be seen in figure 3.4 the dimension of the system is reduced by 4 dimensional in 2 dimensional supposing $x = 0$ and $p_x \geq 0$. Poincare section helps us to visualize the dynamics of the system where chaotic orbits generate scattered dots while regular orbits create smooth curves. The bounding curve is depicted by the intersection of $H(x, y, p_x, p_y) = costant$ in 3.64 with the surface $x = 0$ using the forth order Runge-Kutta method. For these set of initial conditions, one can distinguish between "islands" of non-chaotic behavior with elliptic fixed points at their centers, where the boundary of each region meets is a hyperbolic point

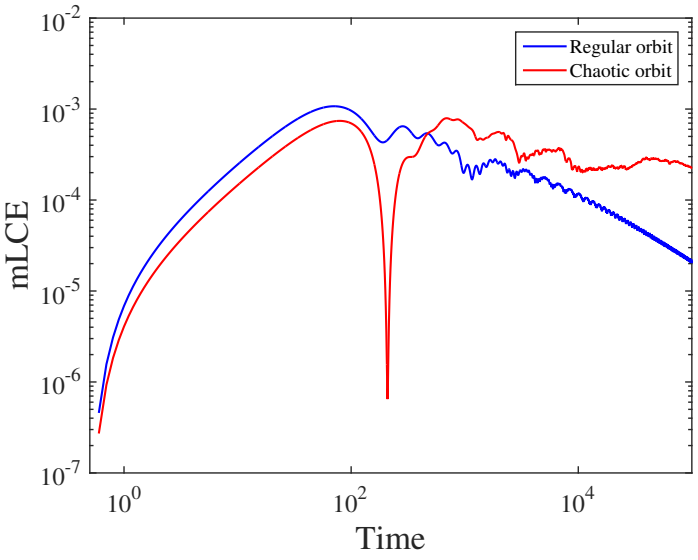

FIGURE 3.5: Plots of the time evolutionof of the mLCE $\mathcal{X}$ against time. Regular orbits with initial conditions $x = 0$, $y = -0,364855$,$p_y = -0.0278586$ and $p_x = 0.24$ is dysplaid with red colour and chaotic orbits with initial conditions $x = 0$, $y = -0,25$,$p_y = 0$ and $p_x = 0.42$ is dysplaid with blue colour . The axes are in logarithmic scale.

from chaotic regions. Increasing the value of energy, the regions between these islands will be filled with a completely random set of points. These confined areas of chaos are a cross-section of a strange attractor. The existence of this strange attractor guarantee as to apply the definition of mLCE. In the figure 3.5 is depicted as a quantitative analysis of the chaotic and regular nature of orbits of the system using the computation of the mLCE. In this analysis the time evolution of the deviation vector using the variational equation is used as a method of computation since in literature co-exist another method

known as the time evolution of nearby orbits. Furthermore as predicted theoretically, depending on the spectrum of mLCE i.e. $\mathcal{X}_1 = -\mathcal{X}_3$ and $\mathcal{X}_2 = -\mathcal{X}_4 = 0$ chaotic orbits have a positive mLCE i.e., $\mathcal{X} > 0$ (the red curve)while for regular orbits $\mathcal{X}$ tends to zero(the blue curve).

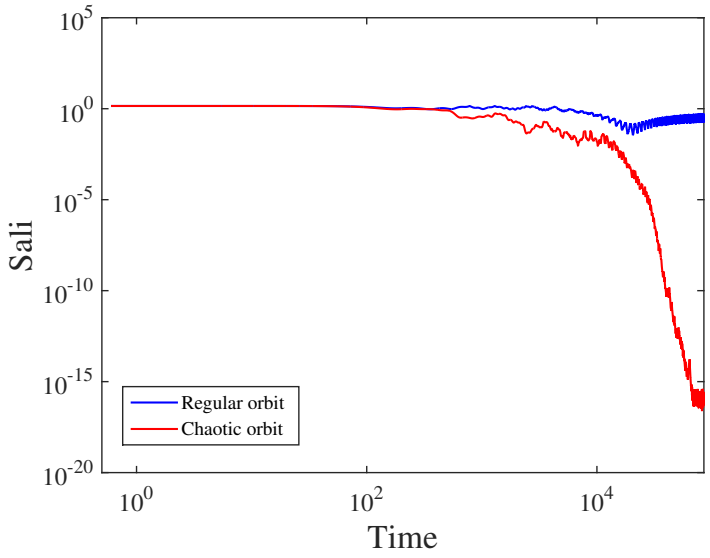

FIGURE 3.6: Plots in log-log scale of $SALI$ as a function of time t for a chaotic and a regular orbits.Regular orbits with initial conditions $x = 0$, $y = -0,364855$,$p_y = -0.0278586$ and $p_x = 0.24$ is dysplaid with blue colour and chaotic orbits with initial conditions $x = 0$, $y = -0,25$,$p_y = 0$ and $p_x = 0.42$ is dysplaid with red colour .

Another easy and efficient method to detect chaotic and regular orbits from a qualitative facet is given by the $SALI$ method. Contrary, from the $mLCE$,if the $SALI \to 0$ the orbit behaves chaotic, while when the value of $SALI$ fluctuate around non zero values the orbit is individualized regular. Refering to the figure 3.6 this result are obtained for this set of initial conditions: $x = 0$, $y = -0,364855$,$p_y = -0.0278586$, $p_x = 0.24$ (blue curve) and $x = 0$, $y = -0,25$,$p_y = 0$, $p_x = 0.42$(red curve) respectively. So the theoretical results are numerically validated for an orthonormal set of initial variational vectors. Moreover, it can be seen that the exponential decay of the chaotic orbit corresponds to a function proportional to $e^{-\mathcal{X}_1 t}$.

Remain to trait the $GALI$ method as the last test of chaos indicator. The $GALI$ is a set of $GALI_k$ curve with $2 < k < 2N$ for an N-degree of freedom Hamiltonian system. ùsuch methods give an accurate estimation of the nature of orbits. Depending on the evolution of k-orthonormal deviation vector, such a method is classified according to [26] as the best estimator of chaos. More precisely, since our system is four-dimensional, we have to study the time evolution of $GALI_2$, $GALI_3$, and $GALI_4$. As shown inf figure 3.7 of chaotic orbits $GALI_2$, $GALI_3$ and $GALI_4$ tends to zero exponentially following the lows $e^{-\mathcal{X}_1 t}$, $e^{-3\mathcal{X}_1 t}$, $e^{-4\mathcal{X}_1 t}$, respectively in accordance with theoretical prediction of theorem

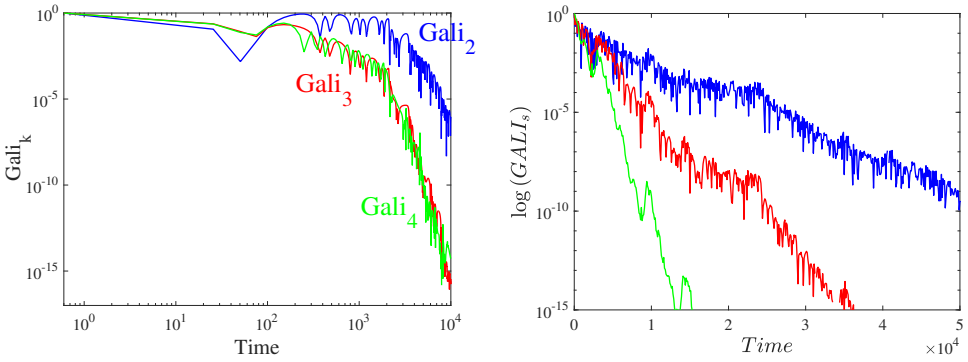

FIGURE 3.7: (a) Plots in log-log scale of time evolution of $GALI_2$, $GALI_3$ and $GALI_4$,for a regular orbits with initial conditions $x = 0$, $y = -0,364855$,$p_y = -0.0278586$ and $p_x = 0.24$. (b) Plots of evolution of time of $GALI_2$, $GALI_3$ and $GALI_4$,for a chaotic orbit with initial conditions $x = 0$, $y = -0,25$,$p_y = 0.42$ and $p_x = 0$. Note that the t-axis is linear

3.16. In the case of 4-dimensional phase space of a 2-degree of freedom Hamiltonian flow, the tangent space is one dimensional since the only possible torus is one dimensional ($s = 1$) invariant curve. So the time evolution of $GALI_3$ and $GALI_4$ obey the lows t^{-2}, t^{-4} respectively.

Concluding, evaluating the rate of divergence to 0, $GALI_4$ remains the fastest indicator of chaos followed by $GALI_3$, $GALI_2$, and $SALI$ ending with $mLCE$ as the least indicator. This classification depends on the number of the time evolution of the deviation vector. So growing the number of deviation vector, we increase the rate of divergence of chaos. For example, for $t > 10$ $GALI_4$ starts to decay exponentially faster than $GALI_3$ and $GALI_2$.

3.4.2 Tokamak model

The description of the dynamical behavior of single or multiple particles under the influence of a magnetic field inside a tokamak, we will follow the Hamiltonian formalism introduced earlier by Vittot and coworkers in Ref. [3]. They have shown that the conservative dynamics for a particle with mass m and charge q in the case without plasma is given by the following effective Hamiltonian function:

$$H(r,\dot{r}) = \frac{\dot{r}^2}{2} + \frac{C^2}{2r^2} + \frac{\left(\frac{B_0 R q}{m}\log(r)\right)^2}{2} + \frac{B_0 R q}{m} C' \log(r) \tag{3.67}$$

where r is the polar coordinate, R is the radius of the tube and torus of the tokamak, B_0 the magnetic field and the constants C, C' as given in Ref. [3]. In order to tackle the problem from the analytical and numerical point of view, Skokos *et. al.* [38] have

proposed to use for the case of the system with two particles the coupling term $\Omega(xp_y - yp_x)$ for the independent equations of each particle. This makes the Hamiltonian self-consistent and integrable:

$$H(x,y,p_x,p_y) = \frac{p_x^2}{2} + \frac{p_y^2}{2} + K^2\left(\frac{C_1}{2x^2} + \frac{C_2}{2y^2} + \frac{\log^2 x}{2} + \frac{\log^2 y}{2}\right) - \Omega(xp_y - yp_x) \quad (3.68)$$

where we have used the constant $K = \dfrac{B_0 Rq}{m} > 0$ and let C_1,C_2 are $T-$periodic functions greater than 1. Also notice that in order to ease the calculation, we have considered the constant $C' = 0$. From this we can now obtain the equations of the motion:

$$\begin{cases} \dot{x} = p_x + \Omega y \\ \dot{y} = p_y - \Omega x \\ \dot{p_x} = K^2\left(\dfrac{C_1}{2x^3} - \dfrac{\log x}{x}\right) + \Omega p_y \\ \dot{p_y} = K^2\left(\dfrac{C_1}{2y^3} - \dfrac{\log y}{y}\right) - \Omega p_x \end{cases} \quad (3.69)$$

and the corresponding variational equations are

$$\begin{cases} \dot{\delta x} = \Omega\delta y + \delta p_x \\ \dot{\delta y} = -\Omega\delta x + \delta p_y \\ \dot{\delta p_x} = -K^2\left(\dfrac{3C_1}{x^4} + \dfrac{1}{x^2} - \dfrac{\log x}{x^2}\right)\delta x + \Omega\delta p_y \\ \dot{\delta p_y} = -K^2\left(\dfrac{3C_2}{y^4} + \dfrac{1}{y^2} - \dfrac{\log y}{y^2}\right)\delta y - \Omega\delta p_x \ . \end{cases} \quad (3.70)$$

In Chapter 4 it will be analytically shown by means of topological methods that the aformentioned system (3.67) behaves chaotically in a particular regime of parameters. In the following we will verify such results by using the numerical techniques of chaos detection, the *SALI* and *GALI* methods.

3.4.2.1 Detection chaotic behaviour of charged particles in the tokomak: numerical approach

After a thorough reviewing of the numerical measures for detecting the presence of chaotic motions in conservative systems, we are now ready to apply such methods to the problem of stability of charged particles under the influence of the magnetic field inside the tokamak. We will start by solving numerically the variational Hamilton eqs. (3.70) to obtain the orbits of the particles involved. At this point, we are

able to measure the values of $SALI$ and $GALI$ by correspondingly computing formulas (3.13) and (3.61). For our model (3.68) we have fixed the energy at $H = 1.8$ and we have chosen the parameters $K = 1.7$, $C_1 = (1 + 0.2\cos(18\omega t))\log(1 + 0.2\cos(18\omega t))$, $C_2 = (1.1 + 0.2\cos(18\omega t))\log(1.1 + 0.2\cos(18\omega t))$[1] where by varying the value of Ω is possible to study the behavior of the system under different coupling strengths. At variance with the works [3] and Chapter 4 where only one particle is considered, here we study a $4-$dimensional version of the system (3.68), but the results can easily be extended to higher dimensions. Let us note that such results can only be obtained using numerical methods. For illustration purpose, we will first consider two well-known classical methods for chaos detection and we will later compare them to the $SALI$ and $GALI$ ones. In Fig. 3.8 *a*) we have plotted the Poincare map obtained from the orbits of the system under scrutiny. Although in this case no regular curves appear at all, in general, the Poincaré map is not an exhaustive method meaning that not always is possible to have a mathematical certainty about the presence of chaos. This is mostly due to the fact of being the procedure itself of a qualitative nature. This is the case, for example, when for a given number of numerical iterations, we notice only regular orbits in the Poincaré section and the chaotic islands in between will appear only when we increase the number of iterations. Another standard technique which constitutes a quantitative measure of chaos, is the $mLCE$ [32]. It has been considered in Fig. 3.8 *b*) where we have plotted the dependence of $mLCE$ as a function of time and although the curve seems to have a decaying trend, there is not a clear evidence of convergence, sometimes yielding to misleading conclusions.

To solve the problem of the finite time integration and the speed of the convergence of the algorithms, we will restore to the $SALI$ and $GALI$ measures. In Fig. 3.9 we plot the results obtained by both aforementioned methods. Obviously, in both cases, the methods give very satisfactory results regarding the chaoticity of the system we study in this work. In fact, the major advantages of these methods are their convergence in a relatively short time, making the estimation regarding the stability of the behavior of our system with considerable higher accuracy than previous methods. Furthermore, the $GALI$ method, compared to the $SALI$ one, can be optimized even more in terms of convergence time once the number of the vectors on which the measure is based is further increased. This way, we can conclude that with these new methods we have more confidence that our system is chaotic or not. Moreover, by means of numerical techniques, we are able to evaluate the chaoticity for higher dimensions.

[1]The reason for such particular expressions for the constants C_1 and C_2 can be found in section 3.3 of Chapter 4.

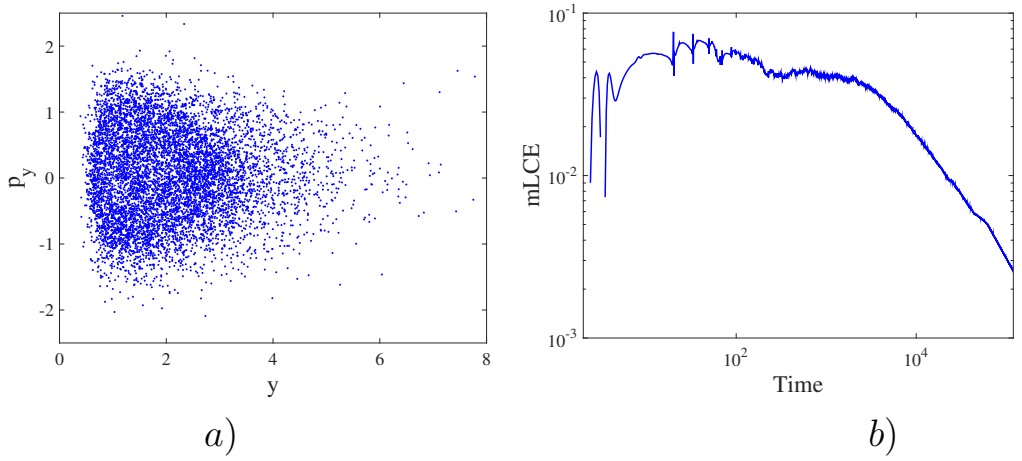

FIGURE 3.8: *a*) We plot the Poincare section of the model (3.68) obtained for $x = 0.5$, $p_x > 0$ and $\Omega = 0.1$. The system in this state represent a total sea of chaoticity, however a large number of points is required in general to have a overall evaluation of where the system behaves chaotically. *b*) Plots in log-log scale of time evolutions of $mLCE$ versus time for a chaotic orbit with initial conditions $x = 0.5$, $y = 0.92$, $p_x = 1.85$ and $p_y = 0.62$. As it can be noticed although the long simulation the $mLCE$ is not yet converging making the detection of the chaos difficult.

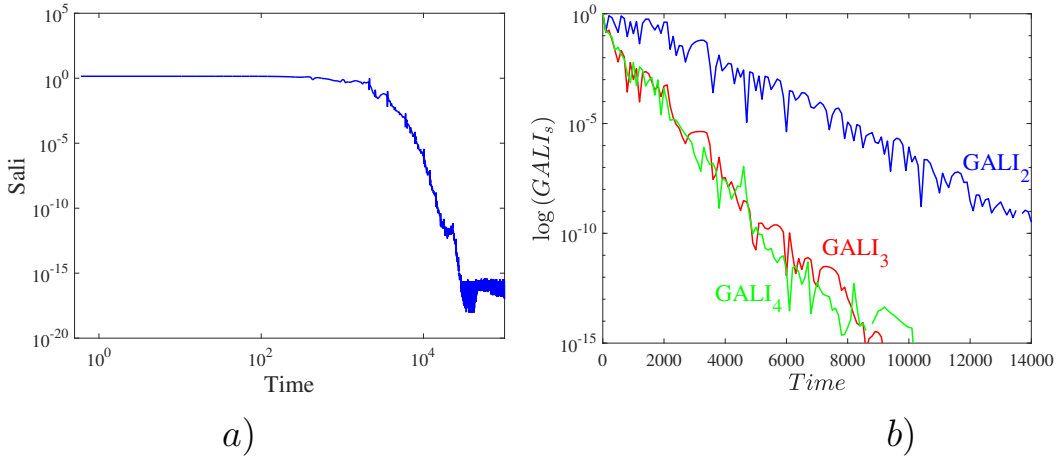

FIGURE 3.9: *a*) We plot the evolution of the $SALI$ measure in the log-log scale. The finite time convergence of the method allows to conclude for certain that our system is chaotic. *b*) Similar results are also obtained from the $GALI$ method where we plot the evolution of the curves for different number of vectors considered . In this case it is easy to conclude in a shorter time about the chaoticity of the system once more vectors are taken in consideration.

3.4.2.2 Conclusions

In this work, we study by means of numerical methods the stability of the dynamics of a Hamiltonian system of charged particles under the effect of the magnetic field inside a tokamak in the absence of plasma. In fact, it has been previously shown from the qualitative perspective using analytical approaches based on topological methods that the 2−dimenstional version of this system is highly chaotic. Here our goal has been

two-fold, first to verify these results by alternative tools such as the numerical ones and second to extend them to higher dimensions by means of numerical chaos indicators we chose to apply to our problem. To this aim, we have used the well-known Small Alignment Index ($SALI$) and Generalised Alignment Index ($GALI$) methods to the question of stability of the system under study. These methods are known of having quite reasonable convergence time with a very high accuracy making them quite favorable compared to more classical ones, such as the Poincare map or the maximal Lyapunov Characteristic Exponent. The disadvantages in the former are due to the large number of points needed for the estimation of the chaoticity which translated to long integration time and the latter is usually known for its long algorithmic convergence time. This makes the results obtained in particularly complicated systems for a finite time from both previous methods misleading. On the contrary, the $SALI$ and $GALI$ algorithms are renowned for their fast exponential convergence time. In addition, $GALI$ can be further optimized in order to decrease the waiting time. We have used both methods to the problem of stability of charged particles in the tokamak verifying once more, this time by numerical means, that such a system is highly chaotic. In addition, we have extended our results to systems of a higher number dimensions (i.e. the number of charged particles), that cannot be explained in terms of the theoretical approach that will be used in Chapter 4.

Chapter 4

A topological approach to chaos for the Duffing equation

In this chapter we present two applications of the topological approach introduced in the Chapter 2, in order to prove the presence of chaotic dynamics in a model of charged particles in a toroidal magnetic field previously studied by Cambon et al. [8] from the numerical point of view.

Before introducing these two main applications, we describe the general structure of the Duffing equations and present also an alternative technique which is usually applied to prove analytically the presence of chaotic dynamics, the so-called Melnikov method.

4.1 A brief introduction to the Duffing equation

One of the simplest but more widely studied examples of a planar conservative systems is given by the two-dimensional system

$$\begin{cases} \dot{x} = y \\ \dot{y} = -g(x) \end{cases} \tag{4.1}$$

which corresponds to the scalar equation

$$\ddot{x} + g(x) = 0 \tag{4.2}$$

in the phase-plane.

Throughout the section we will suppose that $g : J \to \mathbb{R}$ is a locally Lipschitz continuous function defined on an open interval $J \subseteq \mathbb{R}$ where g vanishes at least in a point. Without

loss of generality (using, if necessary, a simple change of variables) we can suppose that $0 \in J$ and $g(0) = 0$, so that the origin is an equilibrium point of (4.1). In general, a point $P = (x_0, y_0)$ is an equilibrium point for (4.1) if and only if $y_0 = 0$ and $g(x_0) = 0$.

System (4.1) is a planar Hamiltonian system with associated Hamiltonian (energy function)

$$H(x, y) = \frac{1}{2}y^2 + G(x), \qquad G(x) = \int_0^x g(s)\, ds.$$

As a consequence, the orbits of (4.1) are contained in the level sets of H. In fact, if $(x(t), y(t))$ is any solution of (4.1) then $(x(t), y(t)) \in \Gamma^c$ for all t, where

$$\Gamma^c := \{(x, y) \in \mathbb{R}^2 : H(x, y) = c\}, \quad \text{for } c = H(x(0), y(0)).$$

Equation (4.2) is the *autonomous* Duffing equation, named after Georg Duffing (1861–1944). A large literature, still growing up, has been devoted to the investigation of the perturbations of (4.2) by periodic forcing terms, as well as by damping terms, leading to

$$\ddot{x} + g(t, x) = 0 \tag{4.3}$$

and to

$$\ddot{x} + c\dot{x} + g(t, x) = 0, \tag{4.4}$$

respectively. Usually, in (4.3) and (4.4) the nonlinear restoring force $g : \mathbb{R} \times J \to \mathbb{R}$ is a continuous function, locally Lipschitzian in the x-variable and periodic in the t-variable of a fixed period $T > 0$. The domain J for the x-variable in an open interval of the real line. The most common case is given by $J = \mathbb{R}$, however research has been devoted also to the case when $J \neq \mathbb{R}$, in order to describe some physical models where the points at the boundary of J represent possible singularities of the vector field.

Classical results on the Duffing equation can be found in the books of J.K. Hale [39] and Guckenheimer and Holmes [40]. In [41] the study of harmonic and subharmonic solutions for (4.3) was performed in the case $J = \mathbb{R}$, while in [42, 43] the cases $J =]0, +\infty[$ and $J =]a, b[$ where considered as well.

Concerning the presence of chaotic-like solutions in [40, Section 4.5] the Melnikov method is applied to the perturbed equation

$$\ddot{x} + \varepsilon c\dot{x} + g(x) = \varepsilon p(\omega t), \tag{4.5}$$

where $c, \varepsilon, \omega > 0$ and $p(\cdot)$ is a non-constant periodic forcing term. According to [40], the functions $g(x)$ and $p(t)$ should be sufficiently smooth (of class C^r with $r \geq 2$).

The main assumption in [40] is the presence of a homoclinic solution $\gamma_0(t) = (q_0(t), v_0(t))$ at the origin for the autonomous system (4.1). Associated with $\gamma(t)$, the Melnikov function

$$M(\alpha) := \int_{-\infty}^{+\infty} \left(v_0(t)p(\omega(t+\alpha)) - cv_0(t)^2\right) dt$$

is introduced. Melnikov's theory (cf. [40, Theorem 4.5.3]) guarantees that, if $M(\alpha)$ has a simple zero for some $\alpha = \alpha_0$, then, for $\varepsilon > 0$ sufficiently small, there exists an hyperbolic equilibrium point $P_\varepsilon^{\alpha_0}$ near the origin for system

$$\begin{cases} \dot{x} = y \\ \dot{y} = -g(x) - \varepsilon p(\omega t) - \varepsilon c y \end{cases} \tag{4.6}$$

such that its stable and unstable manifolds $W^s(P_\varepsilon^{\alpha_0})$ and $W^u(P_\varepsilon^{\alpha_0})$ intersect transversely. This property, in turn, via the Smale-Birkhoff theorem, implies that some N-th iterate of the Poincaré map Φ_ε associated with system (4.6), has a Smale horseshoe and therefore it has an invariant set where it is conjugate to the Bernoulli shift on a set of symbols. As a consequence, Φ_ε^N presents chaotic dynamics in the sense of Devaney. Further relevant results in this directions can be found in [44] for the equation

$$\ddot{x} + \lambda a(t) g(x) = 0$$

and in [45] for

$$\ddot{x} + g(x) = \varepsilon p(t).$$

The Melnikov method, although very powerful and relevant from the point of view of the applications is typically applied in situations where the unperturbed Duffing system (4.1) possesses homoclinic or heteroclinic solutions. Moreover, the analysis of the Melnikov function $M(\alpha)$ or its variants can be extremely difficult when an explicit analytic form of the homoclinic solution $\gamma(t)$ is unknown. Finally, the result allows to make conclusions for small perturbations, namely for $\varepsilon > 0$ sufficiently small.

A classical application of the Melnikov method to the periodically perturbed Duffing equation (4.5) deals with the case

$$g(x) = -x + x^3. \tag{4.7}$$

In this situation, for the associated autonomous system (4.1), the origin is a saddle point and the energy level line $H(x, y) = 0$, that is

$$\frac{1}{2}y^2 - \frac{1}{2}x^2 + \frac{1}{4}x^4 = 0$$

is composed by two homoclinic orbits

$$\Gamma_+^0 := \{(x,y) : x > 0, H(x,y) = 0\}, \quad \Gamma_-^0 := \{(x,y) : x < 0, H(x,y) = 0\}$$

and the origin. Each of the orbits $\Gamma_\pm^0$ is the locus of a homoclinic solution solution $\gamma_0^\pm(t) = (q_0^\pm(t), v_0^\pm(t))$, for which an explicit analytical expression is known, namely:

$$q_0^+(t) = \sqrt{2}\text{sech}t, \quad v_0^+(t) = -\sqrt{2}\text{sech}t\tanh t$$

and $\gamma_0^-(t) = -\gamma_0^+(t)$.

Then, in case of (4.6) with $g(x)$ as in (4.7), we can explicitly compute the Melnikov function as

$$\begin{aligned} M(\alpha) &= \int_{-\infty}^{+\infty} \left(v_0(t)p(\omega(t+\alpha)) - cv_0(t)^2\right) dt \\ &= -\sqrt{2}\int_{-\infty}^{+\infty} \text{sech}t\tanh t p(\omega(t+\alpha))\, dt - 2c\int_{-\infty}^{+\infty} \text{sech}^2 t\tanh^2 t\, dt \end{aligned}$$

Using the fact that

$$\int_{-\infty}^{+\infty} \text{sech}^2 t\tanh^2 t\, dt = \frac{2}{3},$$

we obtain the explicit formula

$$M(\alpha) = -\frac{4}{3}c - \sqrt{2}\int_{-\infty}^{+\infty} \text{sech}t\tanh t p(\omega(t+\alpha))\, dt.$$

This latter expression can be evaluated whenever a specific analytical expression of $p(t)$ is known. For instance, following [40], for

$$p(t) := E\cos(\omega t),$$

the following form of $M(\alpha)$ is obtained.

$$\begin{aligned} M(\alpha) &= -\frac{4}{3}c - \sqrt{2}E\int_{-\infty}^{+\infty} \text{sech}t\tanh t\cos(\omega(t+\alpha))\, dt \\ &= -\frac{4}{3}c - \sqrt{2}E\cos(\omega\alpha)\int_{-\infty}^{+\infty} \text{sech}t\tanh t\cos(\omega t)\, dt \\ &\quad +\sqrt{2}E\sin(\omega\alpha)\int_{-\infty}^{+\infty} \text{sech}t\tanh t\sin(\omega t)\, dt \end{aligned}$$

Since the function $t \mapsto \text{sech}t\tanh t$ is odd (see Figure 4.1), the first integral vanishes.

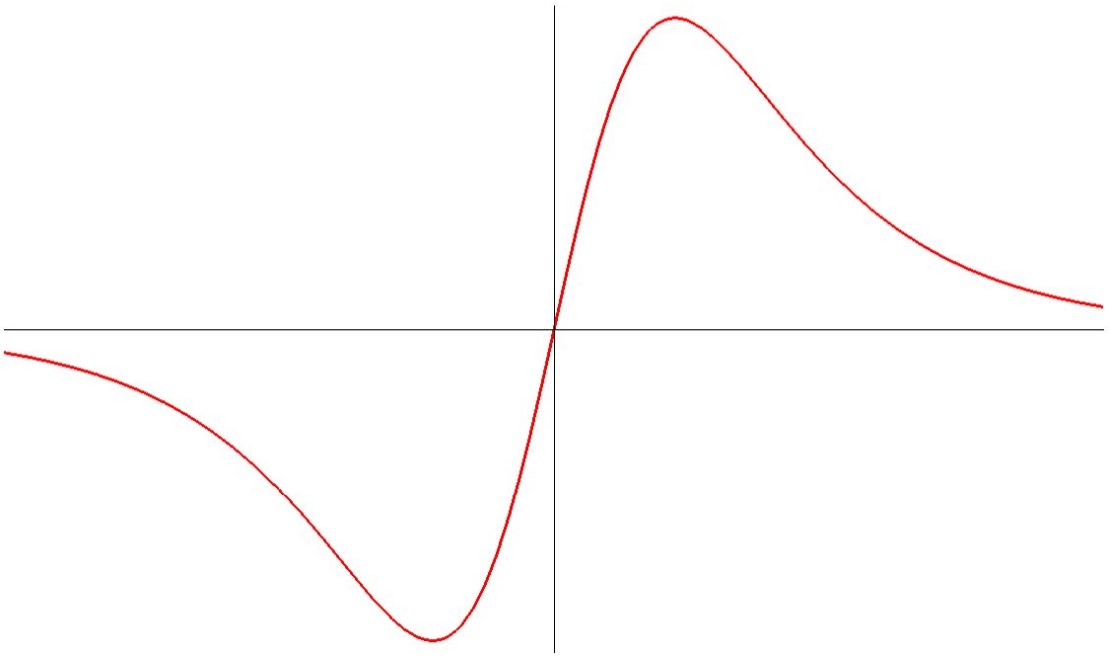

FIGURE 4.1: Graph associated with the function $t \mapsto \mathrm{sech}t \tanh t$.

Concerning the second integral, we observe that the function $t \mapsto \mathrm{sech}t \tanh t \sin(\omega t)$ is even, so that

$$\int_{-\infty}^{+\infty} \mathrm{sech}t \tanh t \sin(\omega t)\, dt = 2 \int_{0}^{+\infty} \mathrm{sech}t \tanh t \sin(\omega t)\, dt := K(\omega).$$

The analytical expression of $K(\omega)$ can be found using the method of the residues (cf. [40]) and is given by

$$K(\omega) = \pi\omega \mathrm{sech}\left(\frac{\pi\omega}{2}\right).$$

In conclusion, for (4.6) with $g(x)$ as in (4.7) and in the special case of $p(t) = E\cos(t)$, we obtain

$$M(\alpha) = \sqrt{2}EK(\omega)\sin(\omega\alpha) - \frac{4}{3}c.$$

This function has simple zeros in the variable α and therefore the Melnikov method guarantees the presence of chaotic dynamics for a N-th iterate of the Poincaré map associated with system (4.6) for $\varepsilon > 0$ sufficiently small, if an only if

$$\frac{E}{c} > \frac{4}{3\sqrt{2}K(\omega)}.$$

As one can see from this example taken from [40], the Melnikov method in principle can be applied to a wide class of equations; on the other other hand, it may be very difficult to prove the result about the existence of simple zeros for the function $M(\alpha)$ without knowing the specific analytical expression of the homocinic solution. In [45], Battelli and Palmer found a general result for the Duffing equation

$$\ddot{x} + a^2 g(x) = p(t), \tag{4.8}$$

where $p(t)$ is a T-periodic and both $g(x)$ and $p(t)$ are sufficiently smooth (at least of class C^{r+3} for $r \geq 5$). Assuming the existence of homoclinic or heteroclinic points $z^{\pm}$ with

$$g(z^{\pm}) = 0, \quad g'(z^{\pm}) < 0$$

for the autonomous equation

$$\ddot{x} + g(x) = 0,$$

the Authors in [45] proved the existence of transversal intersection (as in Melnikov theorem) for the Poincaré map associated with (4.8), provided that $a > 0$ is sufficiently large and one of the following conditions holds:

- $z^+ \neq z^-$ and there exists t_0 such that $p(t_0) = 0 \neq p'(t_0)$; *The case of heteroclinic points*;
- $z^+ = z^-$ and there exists t_0 such that $p'(t_0) = 0 \neq p''(t_0)$ *The case of homoclinic points.*

The advantage of this result with respect to the classical Melnikov formulation (as presented in [40]) depends on the fact that an explicit analytic expression for the homoclinic/heteroclinic solutions is not needed. There are still, however, some assumptions on the forcing term which require simple zeros or simple zeros for the derivative.

4.2 An application of the Melnikov method

In this section, we show a new application of the Melnikov method, described in the preceding section, to a second-order Duffing equation previously considered in [46]. More precisely, in [46] the Authors consider the piecewise linear oscillator

$$\ddot{x} + x = \sin(\sqrt{2}t) + s(x),$$

where

$$s(x) := \begin{cases} -1, & \text{for } x \leq -\frac{1}{5} \\ 5x, & \text{for } -\frac{1}{5} \leq x \leq +\frac{1}{5} \\ 1, & \text{for } x \geq \frac{1}{5} \end{cases}$$

(see Figure 4.2).

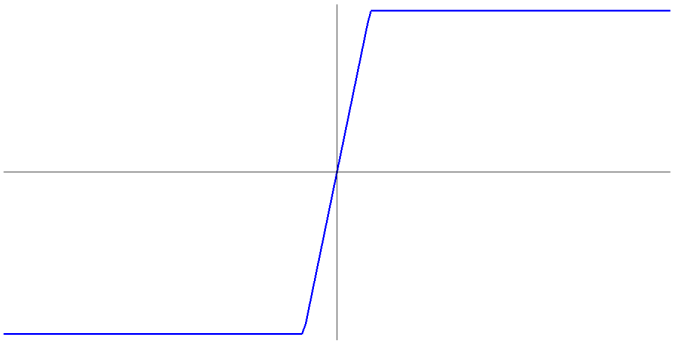

FIGURE 4.2: Graph associated with the function $s(x)$.

The proofs in [46] apply a method based on topological degree theory, for which some geometric conditions must be satisfied. In order to check these geometric assumptions, computer assisted proof are used to verify the inequalities required in the application of the topological techniques. Here we propose a different approach based on recent variants of the Melnikov method to non-smooth (possibly discontinuous) systems which have been developed in [47, 48].

We study the periodically perturbed Duffing equation

$$\ddot{x} + \psi(x) = p(t), \tag{4.9}$$

where $p : \mathbb{R} \to \mathbb{R}$ is a T-periodic function and and

$$\psi(x) := x - s(x),$$

for $s(x)$ the piecewise linear function defined as above, so that

$$\psi(x) := \begin{cases} x + 1, & \text{for } x \leq -\frac{1}{5} \\ -4x, & \text{for } -\frac{1}{5} \leq x \leq +\frac{1}{5} \\ x - 1, & \text{for } x \geq \frac{1}{5} \end{cases}$$

(see Figure 4.3).

By definition, the function ψ has exactly three zeros, namely, $-1, 0, 1$.

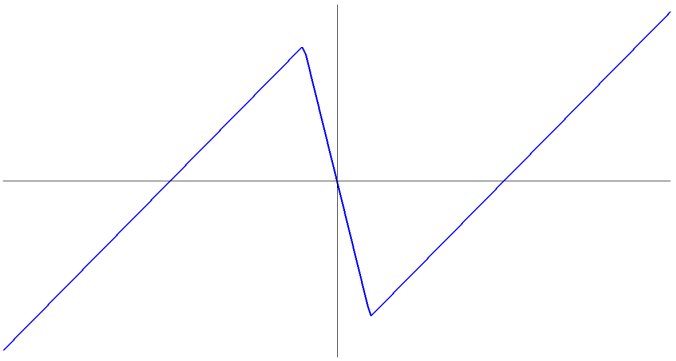

FIGURE 4.3: Graph associated with the function $psi(x)$.

Passing to the phase-plane, equation (4.9) writes as

$$\begin{cases} \dot{x} = y \\ \dot{y} = -\psi(x) - p(t) \end{cases} \tag{4.10}$$

which is a periodic perturbation of the autonomous Hamiltonian system

$$\begin{cases} \dot{x} = y \\ \dot{y} = -\psi(x) \end{cases} \tag{4.11}$$

with Hamiltonian (energy function)

$$H(x,y) = \frac{1}{2}y^2 + \Psi(x), \qquad \Psi(x) = \int_0^x \psi(s)\, ds.$$

An explicit computation shows that

$$\Psi(x) := \begin{cases} \frac{1}{2}x^2 + x + \frac{1}{10}, & \text{for } x \leq -\frac{1}{5} \\ -2x^2, & \text{for } -\frac{1}{5} \leq x \leq +\frac{1}{5} \\ \frac{1}{2}x^2 - x + \frac{1}{10}, & \text{for } x \geq \frac{1}{5} \end{cases}$$

(see Figure 4.4).

The phase-portrait associated with system (4.11) shows that there are three equilibrium points $-P = (-1,0)$, $0 = (0,0)$ and $P = (1,0)$. The points $-P$ and P are two centers surrounded by two orbits $\mathcal{O}^-$ and $\mathcal{O}^+$ (respectively) which are homoclinic trajectories to the origin, which is a saddle point.

In the sequel, we focus our attention on the homoclinic orbit contained in the right-half plane, which is described as the zero-level line of Ψ with $x > 0$, namely

$$\mathcal{O}^+ = \{(x,y) : x > 0, H(x,y) = 0\}.$$

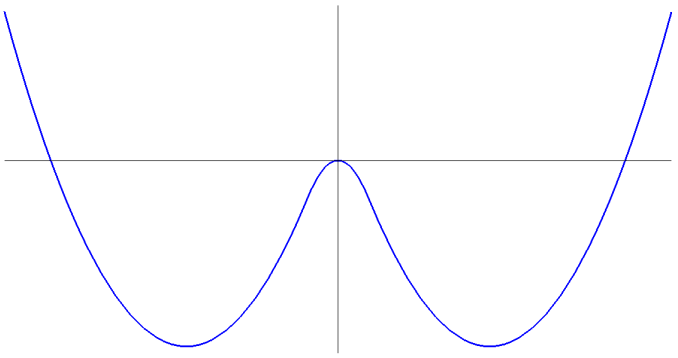

FIGURE 4.4: Graph associated with the function $\Psi(x)$.

The line $\mathcal{O}^+$ intersects the positive x-axis at the point

$$Q = (1 + \frac{2}{\sqrt{5}}, 0) \tag{4.12}$$

and can be expressed as the union of the graphs of the functions

$$y = \sqrt{-2\Psi(x)}, \quad y = -\sqrt{-2\Psi(x)}$$

(see Figure 4.5).

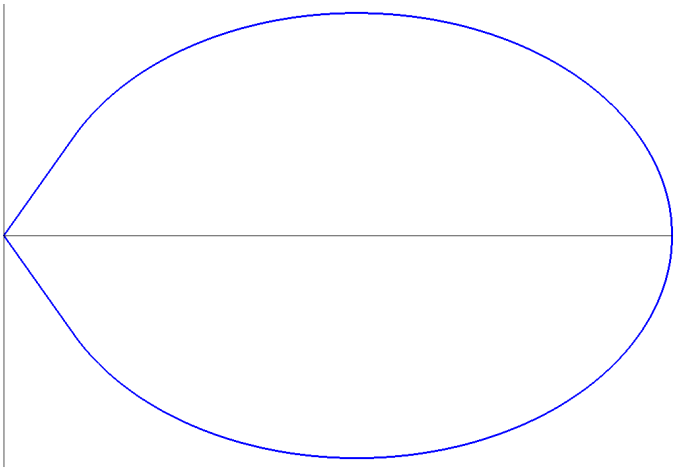

FIGURE 4.5: Graphs associated with the functions $y = \pm\sqrt{-2\Psi(x)}$ which define the homoclinic orbit $\mathcal{O}^+$. In the picture, for typographical reasons, the aspect-ratio has been modified, using a different scale for the x and the y axes.

By symmetry, we restrict for a moment our analysis to the upper graph, that is the part of the homoclinic orbit contained in the first quadrant. A direct computation shows that the homoclinic is described by

$$y = 2x, \quad \text{for } \ 0 < x \leq \frac{1}{5} \tag{4.13}$$

and

$$y = \sqrt{2x - x^2 - \frac{1}{5}}, \quad \text{for } \frac{1}{5} \leq x \leq 1 + \frac{2}{\sqrt{5}}\,. \tag{4.14}$$

Similarly, for $y \leq 0$ we have

$$y = -2x, \quad \text{for } 0 < x \leq \frac{1}{5} \tag{4.15}$$

and

$$y = -\sqrt{2x - x^2 - \frac{1}{5}}, \quad \text{for } \frac{1}{5} \leq x \leq 1 + \frac{2}{\sqrt{5}}\,. \tag{4.16}$$

In this manner, we see that the homoclinic orbit $\mathcal{O}^+$ can be described as follows:

- The local unstable manifold of the origin, contained in the half-line $y = 2x$, for $x > 0$;
- The circumference $\mathcal{C}$ of equation

  $$5x^2 + 5y^2 - 10x + 1 = 5((x-1)^2 + y^2) - 4 = 0$$

  with center at $(1, 0)$ and radius $2/\sqrt{5}$;
- The local stable manifold of the origin, contained in the half-line $y = -2x$.

Observe that the lines $y = \pm 2x$ and the circumference $\mathcal{C}$ intersect transversally the vertical line $x = \frac{1}{5}$, which is the manifold where the planar vector field $(y, -\psi(x))$ is not smooth (see Figure (see Figure 4.6). In this manner we can enter in the setting of the Melnikov theory for non-smooth systems developed in [47].

As a next step, we define analytically the Melnikov function. To this end, we need to find an explicit parametric expression of the homoclinic orbit $\mathcal{O}^+$ by means of a solution of the autonomous Duffing equation (4.11). This task is solved by considering separately the differential equations

$$\ddot{x} - 4x = 0, \quad 0 < x(t) \leq \frac{1}{5} \tag{4.17}$$

and

$$\ddot{x} + x - 1 = 0, \quad \frac{1}{5} \leq x(t) \leq 1 + \frac{2}{\sqrt{5}}\,. \tag{4.18}$$

The first equation corresponds to the system

$$\begin{cases} \dot{x} = y \\ \dot{y} = 4x \end{cases} \qquad \text{in the strip } \;]0, \frac{1}{5}] \times \mathbb{R}, \tag{4.19}$$

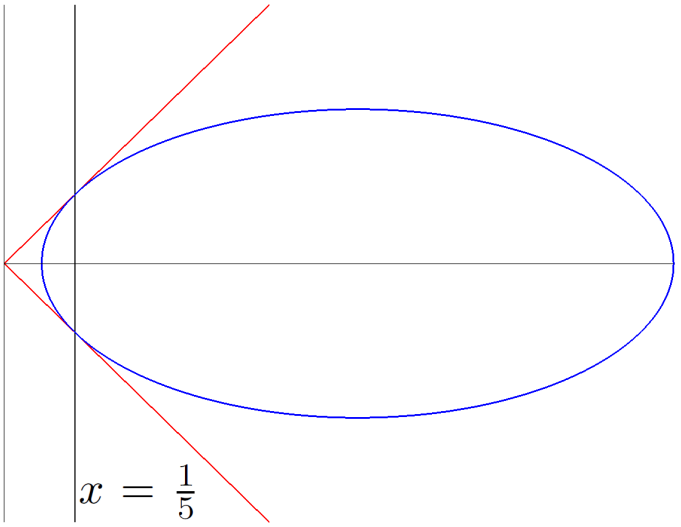

FIGURE 4.6: Graphs associated with the lines $y = \pm 2x$ and with the circumference $\mathcal{C}$. All these lines/curves intersect transversally the line $x = \frac{1}{5}$ where the vector field is not smooth. In the picture, for typographical reasons, the aspect-ratio has been modified, using a different scale for the x and the y axes.

while, for the second one, we have

$$\begin{cases} \dot{x} = y \\ \dot{y} = 1 - x \end{cases} \qquad \text{in the strip } [\frac{1}{5}, 1 + \frac{2}{\sqrt{5}}] \times \mathbb{R}, \tag{4.20}$$

as equivalent system.

In order to find the homoclinic solution, we have to find the solution of system (4.20) passing through the point Q defined in (4.12) and to glue it with the solutions corresponding to the local unstable and stable manifolds of the origin, which are obtained, solving (4.19).

The local unstable manifold at the origin. We solve the system (4.19), looking for solutions $(x(t), y(t))$ with $x(t) > 0$, $y(t) > 0$, which tend to the origin as $t \to -\infty$. The corresponding solutions have the form

$$\begin{cases} x(t) = L \exp(2(t - t_1)) \\ y(t) = 2L \exp(2(t - t_1)) \end{cases} \qquad L > 0,\ t_1 \in \mathbb{R}. \tag{4.21}$$

Parameterizing the arc of circumference. We solve the system (4.20) looking for solutions $(x(t), y(t))$ with $x(t) > 0$ and such that the trajectory passes through the point Q. The

corresponding solutions have the form

$$\begin{cases} x(t) = 1 + r\sin(t - t_2) \\ y(t) = r\cos(t - t_2) \end{cases} \qquad r > 0,\ t_2 \in \mathbb{R}. \tag{4.22}$$

Taking

$$r := \frac{2}{\sqrt{5}},$$

we have that the trajectory passes through the point Q at the time

$$\hat{t} := \frac{\pi}{2} + t_2 \approx 2.677945045.$$

The local stable manifold at the origin. We solve the system (4.19), looking for solutions $(x(t), y(t))$ with $x(t) > 0$, $y(t) < 0$, which tend to the origin as $t \to +\infty$. The corresponding solutions have the form

$$\begin{cases} x(t) = L\exp(-2(t - t_3)) \\ y(t) = -2L\exp(-2(t - t_3)) \end{cases} \qquad L > 0,\ t_3 \in \mathbb{R}. \tag{4.23}$$

We can take the same coefficient $L > 0$ in both (4.21) and (4.23), modifying (if necessary) t_1, t_3 .

Now we are in position to fix the missing parameters $L > 0$ and $t_1 < t_2 < t_3$ in order to obtain the parametrization of the homoclinic solution.

We initiate conventionally assuming that at the time $t = 0$ the solution starts at the point

$$P_0 := (\frac{1}{5}, \frac{2}{5}),$$

which is the point of tangency of the local unstable manifold $y = 2x$ with the circumference $\mathcal{C}$. In this case, from equation (4.21), we obtain $t_1 = 0$ and

$$L := \frac{1}{5}\,.$$

Next, from equation (4.22) and having $r > 0$ already fixed as above, we determine the precise value of the time t_2 so that at the initial time $t = 0$, the solution of (4.22) starts at the point P_0 . In this manner we obtain the system

$$\begin{cases} 1 + \frac{2}{\sqrt{5}}\sin(0 - t_2) = \frac{1}{5} \\ \frac{2}{\sqrt{5}}\cos(0 - t_2) = \frac{2}{5} \end{cases}$$

and hence

$$t_2 := \arcsin(2/\sqrt{5}).$$

As already observed the solution achieves its maximum in the x-component at the time

$$\hat{t} = \frac{\pi}{2} + \arcsin(2/\sqrt{5}).$$

Thus the analytic expression of the homoclinic solution $(x(t), y(t))$ is

$$x(t) := \begin{cases} \frac{1}{5}\exp(2t), & \text{for } t \leq 0 \\ 1 + \frac{2}{\sqrt{5}}\sin(t - \arcsin(2/\sqrt{5})), & \text{for } 0 \leq t \leq \hat{t} \end{cases}$$

and

$$y(t) := \begin{cases} \frac{2}{5}\exp(2t), & \text{for } t \leq 0 \\ \frac{2}{\sqrt{5}}\cos(t - \arcsin(2/\sqrt{5})), & \text{for } 0 \leq t \leq \hat{t}. \end{cases}$$

We do not need to study further the equations in order to glue the solutions of (4.22) with (4.23), because, by the symmetry of the system, we know that the homoclinic solution has symmetry with respect to $\hat{t}$, with $q_0(t)$ even and $v_0(t)$ odd with respect to the origin of the time-axis shifted at $\hat{t}$. Hence, the homoclinic solution, defined on the whole real line takes the form

$$x(t) := \begin{cases} \frac{1}{5}\exp(2t), & \text{for } t \leq 0 \\ 1 + \frac{2}{\sqrt{5}}\sin(t - \arcsin(2/\sqrt{5})), & \text{for } 0 \leq t \leq 2\hat{t} \\ \frac{1}{5}\exp(-2(t - 2\hat{t})), & \text{for } t \geq 2\hat{t}. \end{cases} \tag{4.24}$$

and

$$y(t) = x'(t) := \begin{cases} \frac{2}{5}\exp(2t), & \text{for } t \leq 0 \\ \frac{2}{\sqrt{5}}\cos(t - \arcsin(2/\sqrt{5})), & \text{for } 0 \leq t \leq 2\hat{t} \\ -\frac{2}{5}\exp(-2(t - 2\hat{t})), & \text{for } t \geq 2\hat{t} \end{cases} \tag{4.25}$$

Introduction of the Melnikov function. From equations (4.24) and (4.25), we have obtained the precise analytical expression of the homoclinic solution $\gamma_0(t) = (q_0(t), v_0(t))$, that we write as

$$q_0(t) := \begin{cases} \frac{1}{5}\exp(2(t + \hat{t})), & \text{for } t \leq -\hat{t} \\ 1 + \frac{2}{\sqrt{5}}\cos(t), & \text{for } -\hat{t} \leq t \leq \hat{t} \\ \frac{1}{5}\exp(-2(t - \hat{t})), & \text{for } t \geq \hat{t}. \end{cases} \tag{4.26}$$

and

$$v_0(t) = q_0'(t) := \begin{cases} \frac{2}{5}\exp(2(t+\hat{t})), & \text{for } t \leq -\hat{t} \\ -\frac{2}{\sqrt{5}}\sin(t), & \text{for } -\hat{t} \leq t \leq \hat{t} \\ -\frac{2}{5}\exp(-2(t-\hat{t})), & \text{for } t \geq \hat{t} \end{cases} \tag{4.27}$$

in order to make evident the symmetry with respect to $t = 0$.

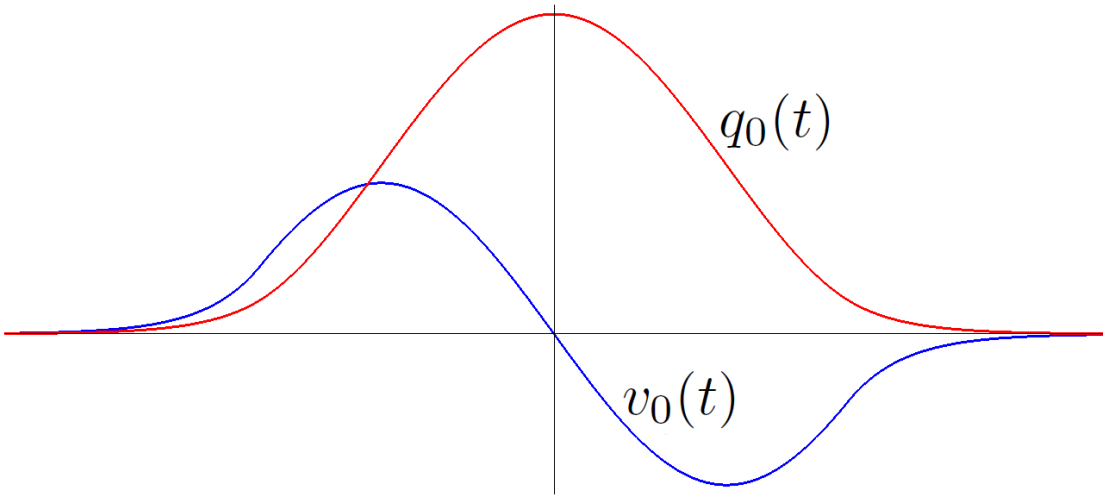

FIGURE 4.7: Graph associated with the function $v_0(t)$ and $q_0(t)$.

We consider now the Melnikov function associated with equation (4.28)

$$\ddot{x} + \varepsilon c\dot{x} + \psi(x) = \varepsilon p(\omega t), \tag{4.28}$$

which is defined as

$$M(\alpha) := \int_{-\infty}^{+\infty} \left(v_0(t)p(\omega(t+\alpha)) - cv_0(t)^2\right) dt \tag{4.29}$$

To start with a simpler situation, we consider the case

$$p(t) = \sin(t).$$

Putting

$$p(\omega(t+\alpha)) = \sin(\omega t)\cos(\omega\alpha) + \cos(\omega t)\sin(\omega\alpha)$$

in (4.29) and using the fact that v_0 is odd, we have that $\int_{-\infty}^{+\infty} v_0(t)\cos(\omega t)\,dt = 0$ and hence

$$M(\alpha) = \cos(\omega\alpha)\int_{-\infty}^{\infty} v_0(t)\sin(\omega t)\,dt - c\int_{-\infty}^{\infty} v_0(t)^2\,dt.$$

Next, using the fact that $v_0(t)\sin(\omega t)$ and $v_0(t)^2$ are even functions, we obtain

$$M(\alpha) = 2\cos(\omega\alpha)\int_{-\infty}^{0} v_0(t)\sin(\omega t)\,dt - 2c\int_{-\infty}^{0} v_0(t)^2\,dt.$$

Hence, for any $\omega > 0$ such that the auxiliary function

$$N(\omega) := \int_{-\infty}^{0} v_0(t)\sin(\omega t)\,dt = \int_{0}^{+\infty} v_0(t)\sin(\omega t)\,dt$$

does not vanish, we can find a suitable c (sufficiently small) such that $M(\alpha)$ has simple zeros located near the simples zeros of $\cos(\omega\alpha)$ and hence the Melnikov method applies.

In [46], the Authors prove the presence of chaotic dynamics for the case $\omega := \sqrt{2}$. With our method, computing $N(\sqrt{2}) \cong -4.508948445$, we obtain chaos according to Melnikov theorem for (4.28), provided that $|c|$ and $\varepsilon > 0$ are sufficiently small. Moreover, from the numerical study of the function $N(\omega)$, we can extend the result to all the values of ω such that $N(\omega) \neq 0$. A simple analysis of this function shows that the following result holds.

Lemma 4.1. *There exists* $\omega^* \gtrapprox 2.36707$ *such that* $N(\omega) < 0$ *for each* $0 < \omega < \omega^*$.

Proof. We observe that, for $N(\omega)$ defined as

$$N(\omega) = \int_{0}^{+\infty} v_0(t)\sin(\omega t)\,dt,$$

we have $N(\omega) \to 0$ for $\omega \to 0^+$ and

$$N'(\omega) = \int_{0}^{+\infty} t v_0(t)\cos(\omega t)\,dt$$

with

$$\lim_{\omega\to 0^+} N'(\omega) = \int_{0}^{+\infty} t v_0(t)\,dt \cong -8.870707261 < 0.$$

On the other hand, a direct calculations shows that $N(\pi) \cong 2.331126686 > 0$. This implies that there is a maximal interval $]0, \omega^*[$ such that $N(\omega) < 0$ for each $0 < \omega < \omega^*$. Using Maple software an approximate lower estimate for ω^* is given by $\omega^* \gtrapprox 2.36707$. □

Figure 4.8 shows the behavior of $N(\omega)$ for ω in a right-neighborhood of the origin.

In any case, the analysis of the function shows that $N(\omega) \neq 0$ except for a discrete set of points.

In the next sections, we propose a different topological approach which although provides a weaker conclusion than the Melnikov method (namely the semi-conjugacy, instead

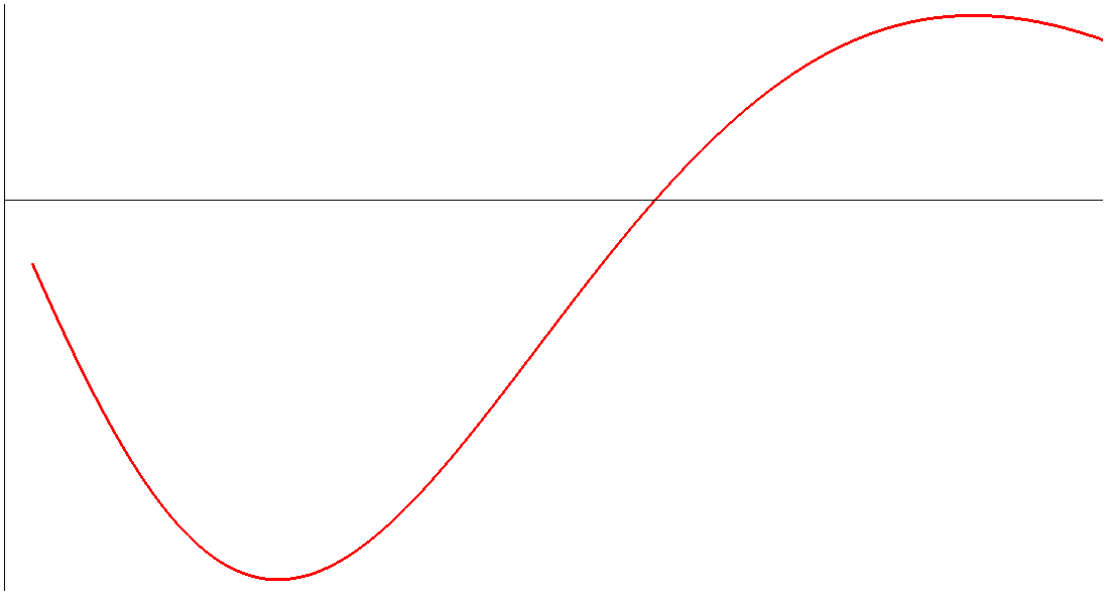

FIGURE 4.8: Graph associated with the function $N(\omega)$ for $\omega \in [0.1, 4]$

of conjugacy with the Bernoulli shift), nevertheless it applies to a broader variety of situations. In particular, we give applications to the case of perturbations of centers and, moreover, we allow larger perturbations, namely the parameter ε is not assumed to be small [1].

4.3 An example of chaotic dynamics for the motion of a charged particle in a magnetic field

4.3.1 Mathematical model

In this section we will provide the mathematical description of a physical problem, following the approach considered in [8] and motivated by a model for the confinement of charged particles inside a toroidal geometric configuration, like in the case of tokamaks.

In [8, Appendix A] the Authors consider the motion of a single particle of charge q and mass m inside a tokamak in absence of the plasma. Hence, they suppose that the magnetic field has only a component in the θ-direction, due to the effect of the external coils around the tokamak chamber. In this context, the magnetic vector field is assumed to have the special form

$$\mathbf{B} = \frac{B_0 R}{\rho} \hat{\mathbf{e}}_\theta \,,$$

where $\rho > 0$ is the distance of the point from the z-axis and $\hat{\mathbf{e}}_\theta$ is the unit vector associated with the θ-direction. The (large) constant $R > 0$ represents the distance of the center of the torus from the z-axis (see [8, Fig. 1]) [1].

Now we apply the Newton second law to the particle moving in this magnetic field, using also the fact that the force acting on the charged particle is given by $\mathbf{F} = q\vec{v} \wedge \mathbf{B}$ (where $\vec{v}$ is the velocity of the particle). Passing to the cylindrical coordinates (ρ, θ, z) and recalling also the expressions of the velocity and the acceleration in cylindrical coordinates, namely

$$\vec{v} = \dot{\rho}\hat{\mathbf{e}}_\rho + \rho\dot{\theta}\hat{\mathbf{e}}_\theta + \dot{z}\hat{\mathbf{e}}_z$$

and

$$\vec{a} = (\ddot{\rho} - \rho\dot{\theta}^2)\hat{\mathbf{e}}_\rho + (\rho\ddot{\theta} + 2\dot{\rho}\dot{\theta})\hat{\mathbf{e}}_\theta + \ddot{z}\hat{\mathbf{e}}_z,$$

we obtain

$$\begin{cases} \ddot{\rho} - \rho\dot{\theta}^2 = -\frac{B_0 Rq}{m\rho}\dot{z} \\ \rho\ddot{\theta} + 2\dot{\rho}\dot{\theta} = 0 \\ \ddot{z} = \frac{B_0 Rq}{m\rho}\dot{\rho}, \end{cases} \tag{4.30}$$

where B_0 is the magnitude of the magnetic field.

Integrating the last two equations we obtain:

$$\rho^2\dot{\theta} = C \tag{4.31}$$

$$\dot{z} = \frac{B_0 Rq}{m}\log\rho + C' \tag{4.32}$$

where C and C' are two constants. Then we can use expressions (4.31) and (4.32) in equation (4.30), to get

$$\ddot{\rho} - \rho\Big(\frac{C}{\rho^2}\Big)^2 = -\frac{B_0 Rq}{m\rho}\Big(\frac{B_0 Rq}{m}\log\rho + C'\Big).$$

We multiply it by $\dot{\rho}$ and obtain

$$\dot{\rho}\ddot{\rho} - \rho\dot{\rho}\Big(\frac{C}{\rho^2}\Big)^2 = -\frac{B_0 Rq}{m\rho}\dot{\rho}\Big(\frac{B_0 Rq}{m}\log\rho + C'\Big).$$

An integration gives

$$\frac{\dot{\rho}^2}{2} - C^2\int\frac{1}{\rho^3}\,d\rho = -\Big(\frac{B_0 Rq}{m}\Big)^2\int_{\xi=\log\rho}\xi\,d\xi - \frac{B_0 RqC'}{m}\int\frac{1}{\rho}\,d\rho.$$

[1] We adopt a slight change of notation with respect to [8, II. Model], in the sense that our variable ρ is denoted in [8, Appndix A] at first as ξ and then as r and, in the same Appendix, our variable θ is at first denoted as ϕ but at the end it is called θ. For this reason, we prefer to denote it as θ, from the beginning.

This latter expression defines the following *effective Hamiltonian* $H_{\text{eff}} = H_{\text{eff}}(x, y)$ with $x = \rho > 0$ and $y = \dot{\rho}$:

$$H_{\text{eff}}(x, y) = \frac{y^2}{2} + \frac{C^2}{2x^2} + \frac{1}{2}\left(\frac{B_0 Rq}{m}\log x\right)^2 + \frac{B_0 Rq}{m} C' \log x$$

(cf. [8, (A7)]). This also shows that the equation describing the particle trajectory in the magnetic field defined above, is integrable (for a constant magnetic field). Recall that C and C' are two real constants.

To simplify our analysis, from now on we consider the special case

$$C' = 0, \quad C \neq 0$$

(as in [8, p.4]) and get the Hamiltonian

$$H(x, y) := \frac{y^2}{2} + \frac{C^2}{2x^2} + \frac{(B_0 Rq \log x)^2}{2m^2},$$

which is the typical energy function associated with a planar conservative system of the form of (4.2) with

$$g(x) = G'(x), \forall\, x > 0 \quad \text{and} \quad G(x) = \frac{C^2}{2x^2} + \frac{1}{2}(K \log x)^2,$$

for

$$K := \frac{B_0 Rq}{m}.$$

4.3.2 The monotonicity of the the period map

As observed in the previous section, we are led to consider the Hamiltonian

$$H(x, y) := \frac{y^2}{2} + \frac{C^2}{2x^2} + \frac{(K \log x)^2}{2},$$

where $C, K > 0$ are suitable constants. The Hamiltonian H is the energy associated to an autonomous planar differential system of the form (4.2) that now we prefer to write as

$$\dot{u} = v, \quad \dot{v} = -K^2 g(u), \tag{4.33}$$

for $u(t) := x(t) = \rho(t) > 0$ for all t and

$$g(x) := -\frac{(C/K)^2}{x^3} + \frac{\log(x)}{x}, \quad x > 0. \tag{4.34}$$

The planar differential system (4.33) is studied in the phase-plane $\Omega = \mathbb{R}_0^+ \times \mathbb{R}$. The analysis of the trajectories of (4.33) shows the presence of a unique equilibrium point $P_0 := (x_0, 0)$ which is a global center (see Figure 4.9). Using the condition $g(x_0) = 0$ we can write equivalently (4.34) as

$$g(x) := -\frac{x_0^2 \log(x_0)}{x^3} + \frac{\log(x)}{x}, \quad \text{for } x_0 > 1. \tag{4.35}$$

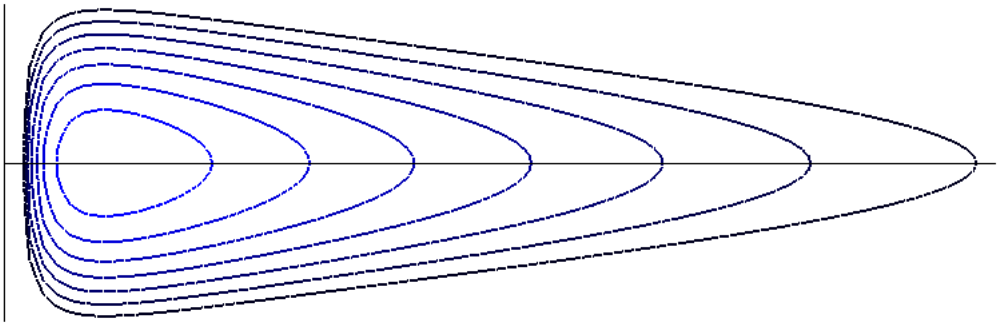

FIGURE 4.9: Some level lines of the Hamiltonian function $H(x, y) = \dfrac{y^2}{2} + G(x)$, for $G(x) = \dfrac{(C/K)^2}{2x^2} + \dfrac{(\log x)^2}{2}$ in the phase-plane $\Omega = \mathbb{R}_0^+ \times \mathbb{R}$. Note that the level lines $H = \text{constant} > H(x_0, 0)$ are the periodic orbits of system (4.33).

Observe that any solution $u(t)$ of the equation

$$\ddot{u} + K^2 g(u) = 0,$$

which is equivalent to the planar system (4.33), can be written as $u(t) = x(Kt)$, where $x(t)$ is a solution of

$$\ddot{x} + g(x) = 0.$$

This proves that we can confine ourselves to the study of the orbits of system

$$\dot{x} = y, \quad \dot{y} = -g(x) \tag{4.36}$$

(for g defined as in (4.35)), which, as already observed above, describes a global center at $P_0 = (x_0, 0)$ in the phase-plane Ω.

We introduce now the potential function

$$V(x) := \frac{1}{2}\left(\frac{x_0^2\log(x_0)}{x^2} + \log^2(x) - \log(x_0) - \log^2(x_0)\right), \tag{4.37}$$

which has has a non-degenerate strict absolute minimum at the point x_0 . Indeed, observe that

$$V'(x) = g(x), \quad V(x) > V(x_0) = 0, \quad \forall x > 0$$

and, moreover,

$$V''(x_0) = g'(x_0) = 2\frac{\log(x_0)}{x_0^2} + \frac{1}{x_0^2} > 0,$$

For any value $E > 0$, we denote by $\Gamma(E)$ the level line of energy E, in the domain Ω, defined by

$$\frac{y^2}{2} + V(x) = E. \tag{4.38}$$

Note that, for any $E > 0$, $\Gamma(E)$ is a strictly star-shaped curve (around P_0) which is also a periodic orbit of (4.36). We denote by $\tau(E)$ the (minimal) period of $\Gamma(E)$, for each $E > 0$.

Now we are in position to prove the following result.

Theorem 4.2. *The period-mapping $\tau : \mathbb{R}_0^+ \to \mathbb{R}_0^+$ associated with* (4.36) *is a strictly monotone increasing function such that*

$$\lim_{E\to 0^+} \tau(E) = \frac{2\pi}{\sqrt{g'(x_0)}}, \quad \lim_{E\to+\infty} \tau(E) = +\infty. \tag{4.39}$$

Proof. We preliminarily observe that potential function $V : \mathbb{R}_0^+ \to \mathbb{R}^+$ is strictly decreasing on $]0, x_0]$ and strictly increasing on $[x_0, +\infty[$ with

$$\lim_{x\to 0^+} V(x) = \lim_{x\to+\infty} V(x) = +\infty.$$

Recalling also that $V(x_0) = 0$, we find that, for every $E > 0$, the equation $V(x) = E$, has exactly two solutions that we denote by $d^{\mp}(E)$ and we choose such that

$$0 < d^-(E) < x_0 < d^+(E).$$

We set

$$\tau^+(E) := 2\int_{x_0}^{d^+(E)} \frac{dx}{\sqrt{2(E - V(x))}} = 2\int_{x_0}^{d^+(E)} \frac{dx}{\sqrt{2(V(d^+(E)) - V(x))}}$$

and

$$\tau^-(E) := 2\int_{d^-(E)}^{x_0} \frac{dx}{\sqrt{2(E-V(x))}} = 2\int_{d^-(E)}^{x_0} \frac{dx}{\sqrt{2(V(d^-(E))-V(x))}}\,.$$

Recalling that $\Gamma(E)$ the level energy curve in (4.38) (with $E>0$), we have that $\Gamma(E)$ intersects the line $x=x_0$ the points $P^{\pm}(E) := (x_0, \pm\sqrt{2E})$. Then $\tau^+(E)$ is the time needed to run from $P^+(E)$ to $P^-(E)$ along $\Gamma(E)$ in the half-plane $x \geq x_0$. Similarly, $\tau^-(E)$ is the time needed to run from $P^-(E)$ to $P^+(E)$ along $\Gamma(E)$ in the strip $0 < x \leq x_0$. In this manner, we have that

$$\tau(E) = \tau^+(E) + \tau^-(E).$$

As a consequence of $g(x)/x \to 0$ as $x \to +\infty$, we have that $\tau^+(E) \to +\infty$ as $E \to +\infty$ (cf. [49]). This in turns implies that $\tau(E) \to +\infty$ as $E \to +\infty$. On the other hand, using the fact that $g(x_0)=0$ and $g(x) = g'(x_0)(x-x_0)$, we easily obtain that $\lim_{E\to 0^+} \tau(E) = 2\pi/\sqrt{g'(x_0)}$. Thus (4.39) is verified.

Proving the monotonicity of the period map $\tau(E)$ is a more difficult task. In fact, even if we could prove the monotonicity of $\tau^+(E)$, using Opial's results [49], nevertheless we have to take into account that $\tau^-(E) \to 0$ as $E \to +\infty$. In fact, due to the presence of a singularity at $x=0^+$ satisfying the strong force condition $V(0^+) = -V'(0^+) = +\infty$, we know that the solutions move faster and faster near the singularity as $d^-(E) \to 0^+$ (cf. [43]); thus the monotonicity "balance" for $\tau(E)$ does not follows from the analysis of $\tau^+(E)$ and $\tau^-(E)$, separately.

To our aim, we then apply a theorem by Chicone [50] which, in our situation, reads as follows.

Let us set

$$N(x) := 6V(x)V''(x)^2 - 3V'(x)^2V''(x) - 2V(x)V'(x)V'''(x).$$

Then $\tau(E)$ is strictly monotone increasing on $\mathbb{R}_0^+$, if $N(x) > 0$ for all $x \neq x_0$.

For $V(x)$ defined as in (4.37), we find explicitly $N(x)$ and then we introduce the function

$$N_1(x) := x^{10}N(x), \quad \text{for } x > 0,$$

which takes the following form

$$\begin{aligned}
N_1(x) \;=\;& -3(\log(x_0))x^6 + (\log(x))^4x^6 + 3(\log(x_0))(\log(x))x^6 \\
& -(\log(x_0))(\log(x))^2x^6 - 3(\log(x_0))^2x^6 + 3(\log(x_0))^2(\log(x))x^6 \\
& -(\log(x_0))^2(\log(x))^2x^6 - 15(\log(x_0))^3x_0^2x^4 + 4(\log(x_0))^3(\log(x))x_0^2x^4 \\
& +3(\log(x_0))x_0^2x^4 + 4(\log(x_0))^2(\log(x))x_0^2x^4 - 15(\log(x_0))^2x_0^2x^4 \\
& -4(\log(x))^3(\log(x_0))x_0^2x^4 + (\log(x_0))(\log(x))^2x_0^2x^4 + 3(\log(x_0))(\log(x))x_0^2x^4 \\
& +15(\log(x))^2(\log(x_0))^2x_0^4x^2 + 17(\log(x_0))^2(\log(x))x_0^4x^2 + 12(\log(x_0))^2x_0^4x^2 \\
& -15(\log(x_0))^3x_0^4x^2 - 15(\log(x_0))^4x_0^4x^2 + 6(\log(x_0))^3x_0^6
\end{aligned}$$

(the computation has been verified using symbolic manipulations with Maple software). In order to simplify the analysis of the function $N_1(x)$, we introduce the auxiliary function

$$N_2(\theta) := \frac{N_1(\theta x_0)}{x_0^6}, \quad \text{for } \theta > 0$$

and obtain

$$\begin{aligned}
N_2(\theta) \;=\;& (\log(\theta))^4\theta^6 + 3(\log(x_0))(\log(\theta))\theta^6 - 3(\log(x_0))\theta^6 + 2(\log(x_0))^3\theta^6 \\
& +5(\log(\theta))^2(\log(x_0))^2\theta^6 - (\log(x_0))(\log(\theta))^2\theta^6 + (\log(x_0))^2(\log(\theta))\theta^6 \\
& +4(\log(\theta))^3(\log(x_0))\theta^6 + 2(\log(\theta))(\log(x_0))^3\theta^6 - 12(\log(x_0))^2(\log(\theta))^2\theta^4 \\
& -12(\log(x_0))^2\theta^4 + 6(\log(x_0))^2(\log(\theta))\theta^4 - 4(\log(x_0))(\log(\theta))^3\theta^4 \\
& +3(\log(x_0))(\log(\theta))\theta^4 - 10(\log(x_0))^3\theta^4 - 8(\log(x_0))^3(\log(\theta))\theta^4 \\
& +(\log(x_0))(\log(\theta))^2\theta^4 + 3(\log(x_0))\theta^4 + 15(\log(x_0))^2(\log(\theta))^2\theta^2 \\
& +17(\log(x_0))^2(\log(\theta))\theta^2 + 30(\log(x_0))^3(\log(\theta))\theta^2 + 12(\log(x_0))^2\theta^2 \\
& +2(\log(x_0))^3\theta^2 + 6(\log(x_0))^3.
\end{aligned}$$

As a final change of variables, we set

$$x_0 := \exp(u_0), \quad \theta := \exp(t)$$

and consider the function

$$N_3(t) := N_2(\exp(t)), \quad \text{for } t \in \mathbb{R}.$$

After some simplifications, one can see that $N_3(t)$ can be represented as

$$N_3(t) = M_3(t)u_0^3 + M_2(t)u_0^2 + M_1(t)u_0 + M_0(t), \tag{4.40}$$

where

$$\begin{aligned}
M_3(t) &:= 30te^{2t} + 2te^{6t} - 8te^{4t} + 6 + 2e^{2t} + 2e^{6t} - 10e^{4t},\\
M_2(t) &:= 15t^2e^{2t} - 12t^2e^{4t} + 5t^2e^{6t} + 17te^{2t} + te^{6t} + 6te^{4t} - 12e^{4t} + 12e^{2t},\\
M_1(t) &:= 4t^3e^{6t} - 4t^3e^{4t} + t^2e^{4t} - t^2e^{6t} + 3te^{6t} + 3te^{4t} - 3e^{6t} + 3e^{4t},\\
M_0(t) &:= t^4e^{6t}.
\end{aligned}$$

Observe that the sign of $N(x)$ for $x > 0$ and with $x_0 > 1$ is the same as that of $N_3(t)$ for $t \in \mathbb{R}$ and $u_0 > 0$. One can also easily check that

$$N(x_0) = N_1(x_0) = N_2(1) = N_3(0) = 0.$$

Our goal is to prove that $N_3(t) > 0$ for all $t \neq 0$, which is equivalent to prove that $N(x) > 0$ for all $x \neq x_0$. By the expression of $N_3(t)$ and recalling that $u_0 > 0$, we are led to study separately the functions $M_i(t)$ for $i = 0, 1, 2, 3$.

With this respect we have the following

$$\textit{Claim. For all } i = 0, 1, 2, 3 : \ M_i(0) = 0 \textit{ and } M_i(t) > 0 \textit{ for all } t \neq 0.$$

It trivially follows that $M_i(0) = 0$ for all $i = 0, 1, 2, 3$ and $M_0(t) > 0$ for all $t \neq 0$.

Let us check now the other cases of the claim:

Case 1: $M_3(t) > 0$ for all $t \neq 0$. To check this assertion, we introduce the auxiliary function

$$P_3(t) := M_3(t)e^{-4t}$$

and prove that P_3 has a minimum for $t = 0$ and is convex. Indeed, one can easily prove that $P_3'(0) = P_3''(0) = 0$ and, moreover,

$$P_3''(t) = -112e^{-2t} + 16e^{2t} + 96e^{-4t} + 120te^{-2t} + 8te^{2t}.$$

Next we introduce the function

$$S_3(t) := P_3''(t)e^{2t}$$

and prove that $S_3'(0) = 0$, with

$$S_3''(t) = (320 + 384e^{-6t} + 128t)e^{4t}$$

It is easy to see that the function

$$K_3(t) := 320 + 384e^{-6t} + 128t$$

achieves its minimum positive value $(1024 + 64\log(18))/3$ in $t = \frac{\log 18}{6}$ and, moreover, $K_3''(t) = 13824e^{-6t} > 0$ for all t. From the information on the function K_3, we have that $S_3''(t) > 0$ for all t and therefore, $S_3(t) > 0$ for all $t \neq 0$. Finally, having proved that $P_3'(0) = 0$ and $P_3''(t) > 0$ for all $t \neq 0$, we can conclude that $M_3(t) > 0$ for all $t \neq 0$.

The verification of the inequalities for $M_2(t)$ and $M_1(t)$ follows a similar argument. We give below only the main steps in the proofs.

Case 2: $M_2(t) > 0$ for all $t \neq 0$. To check this assertion, we introduce the following auxiliary function

$$M_2(t)e^{-4t}$$

and prove that $P_2(t)$ has a minimum for $t = 0$ and is convex. Indeed, one can easily prove that $P_2'(0) = P_2''(0) = P_2'''(0) = 0$. To prove the convexity, one can check that $P_2'''(t) = e^{-2t}(f(t) - g(t))$ where $f(t) = e^{4t}(40t^2 + 128t + 72)$ e $g(t) = 120t^2 - 224t + 72$. Since for $t > 0$, $f(t) > g(t)$ it follows that $P_2'''(t) > 0$ for all $t > 0$. In similar way we can prove that $W''(t) \geq 0$ for $t < 0$ and then the conclusion easily follows.

Case 3: $M_3(t) > 0$ for all $t \neq 0$. To check this assertion, we follow again a similar argument as above and introduce the auxiliary function

$$P_1(t) := M_1(t)e^{-4t}.$$

We have that $P_1'(0) = P_1''(0) = P_1'''(0) = 0$ with

$$P_1''(t) = e^{2t}(16t^3 + 44t^2 + 28t - 2) - 24t + 2.$$

A direct computation shows that $P_1''''(t) > 0$ for all $t > 0$. This in turns implies that $P_1''(t) > 0$ for all $t > 0$. In order to study the sign on $]-\infty, 0]$, we consider $S_1(t) := P_1''(-t)e^{2t}$ for $t \geq 0$. Then we obtain $S_1(0) = S_1'(0) = 0$ and

$$S_1''(t) = -96t + 88 + 104e^{2t} + 96te^{2t},$$

which is positive for every $t > 0$. From this we obtain that $P_1''(t) > 0$ for all $t \neq 0$ and then the conclusion follows from the same argument as in Case 1. □

4.3.3 Subharmonic solutions and chaotic dynamics

In [8] the authors give numerical evidence of the presence of chaotic motions, by introducing a perturbation into the magnetic field. In particular, the magnetic moment $\mu = \frac{mv_\perp}{2B}$ is considered to vary (slowly) as a function $\mu(t)$.

Since the unperturbed equation (after rescaling and change of variables) reduces to system (4.36) with $g(x)$ defined as in (4.35), we can suppose to perturb our system by varying the constant x_0. Namely, we can treat x_0 as a parameter $\nu > 1$ and assume that such parameter can change with the time t in a periodic manner. This leads us to consider an equation of the form

$$\ddot{x} + g(t, x) = 0, \tag{4.41}$$

with

$$g(t, x) := -\frac{\nu(t)^2 \log(\nu(t))}{x^3} + \frac{\log(x)}{x}, \tag{4.42}$$

with $\nu : \mathbb{R} \to \mathbb{R}$ a bounded, measurable and T-periodic function such that $\nu(t) > 1$ for all $t \in \mathbb{R}$. Equivalently, we consider the planar system

$$\dot{x} = y, \quad \dot{y} = -g(t, x) \tag{4.43}$$

in the phase-plane $\Omega = \mathbb{R}_0^+ \times \mathbb{R}$. Solutions are considered in the Carathéodory sense (cf. [51]) and are intended in the classical sense when ν is continuous (or piecewise continuous).

Periodically perturbed scalar differential equations with singularities at the origin have been the focus of several investigations after the seminal work of Lazer and Solimini [52] who considered the case

$$g(t, x) = \delta \frac{1}{x^\alpha} - e(t), \quad \delta = \pm 1.$$

A general study of different kind of ODEs with singularities can be found in [53]; we also refer to [54] for several interesting models and problems in this area. The kind of nonlinearity $g(t, x)$ considered in our model example presents some similarities with the one analyzed in the work of Margheri and Torres [55] where, motivated by a problem of celestial mechanics,

$$g(t, x) = \frac{h(t)}{x^2} - \frac{\mu^2}{x^3}\,.$$

As a first result concerning equation (4.41) we discuss the existence and multiplicity of subharmonic solutions, namely periodic solutions of minimal period mT with $m \geq 2$.

To this aim, the following consequence of [43] holds.

Theorem 4.3. *Assume that there are two constants ν_-, ν_+ such that*

$$1 < \nu_- \leq \nu(t) \leq \nu_+, \quad \forall\, t \in \mathbb{R}. \tag{4.44}$$

Then (4.41) *has a sequence $(x_k)_k$ of positive kT-periodic solutions with minimal period tending to infinity.*

Proof. From (4.44), we have

$$-\frac{\nu_+^2 \log \nu_+}{x^3} + \frac{\log(x)}{x} \leq g(t,x) \leq f(x) := -\frac{\nu_-^2 \log \nu_-}{x^3} + \frac{\log(x)}{x}\,.$$

Now we introduce the function

$$F(x) := \frac{1}{2}\left(\frac{\nu_-^2 \log \nu_-}{x^2} + \log^2(x)\right), \quad \text{with } \; F'(x) = f(x), \text{ for } \; x > 0$$

and observe that $F(0^+) = +\infty$ and $F(x)/x^2 \to 0$ as $x \to +\infty$. Moreover, we have $g(t,x)\mathrm{sgn}(x-1) > 0$ for $0 < x < 1/d$ and $x > d$, with $d > 1$ and sufficiently large. Then we can apply a result from [43] concerning the equation $\ddot{x} + g(t,x) = e(t)$ (in our case, we take $e = 0$). More precisely, we enter in the setting of [43, Theorem 2.1 & Remark 2.1], according to which (4.41) has a sequence $(x_k)_k$ of positive kT-periodic solutions with minimal period tending to infinity. □

Condition (4.44) is always satisfied if $\nu : \mathbb{R} \to]1, +\infty[$ is a continuous and T-periodic function.

As a next step, we show how to provide more precise information on the dynamics of the solutions of (4.41). To this purpose, associated with (4.43) we introduce the Poincaré map Φ_0^T where, for $t_1 < t_2$ we set

$$\Phi_{t_1}^{t_2}(z) := \zeta(t_2, t_1, z),$$

where $\zeta(\cdot, t_1, z)$ is the solution $\zeta(t) = (x(t), y(t))$ of system (4.43) satisfying the initial condition $\zeta(t_1) = z \in \Omega$.

As a consequence of the fundamental theory of ODEs, the domain of the Poincaré map Φ_0^T is an open subset of Ω. In the next result we prove that Φ_0^T is defined on the whole right half-plane.

Theorem 4.4. *Suppose that $\nu : \mathbb{R} \to]1, +\infty[$ is a continuously differentiable T-periodic function. Then, for any initial point $z_0 \in \Omega = \mathbb{R}_0^+ \times \mathbb{R}$ the solution of* (4.43) *with*

$(x(0), y(0)) = z_0$ *is defined for all* $t \in \mathbb{R}$. *As a consequence,* Φ_0^T *is a homeomorphism of* Ω *onto itself.*

Proof. We introduce the energy function

$$E(t,x,y) := \frac{1}{2}\left(y^2 + \frac{a(t)}{x^2} + \log^2(x)\right), \quad \text{for } a(t) := \nu(t)^2 \log(\nu(t)),$$

which is motivated by (4.37) and by the fact that $\frac{\partial E}{\partial x} = g(t,x)$. Notice that

$$E(t,x,y) \to +\infty, \text{ uniformly in } t \in [0,T], \text{ as } (x,y) \to \partial\Omega, \tag{4.45}$$

for $\Omega = \mathbb{R}_0^+ \times \mathbb{R}$. Let $(x(t), y(t))$ be the solution of (4.43) with $(x(0), y(0)) = z_0 \in \Omega$ and let $]\alpha, \beta[$ the maximal interval of existence for the solution. We set $v(t) := E(t, x(t), y(t))$ and observe that $v(t) > 0$ for all $t \in]\alpha, \beta[$. Differentiating, we obtain

$$\begin{aligned} |v'(t)| &= \left|\frac{\partial E}{\partial t}(t, x(t), y(t))\right| = \frac{a'(t)}{x(t)^2} \le 2\frac{\|a'\|_\infty}{a_{\min}}\frac{1}{2}\frac{a(t)}{x(t)^2} \\ &\le 2\frac{\|a'\|_\infty}{a_{\min}} E(t, x(t), y(t)) = 2\frac{\|a'\|_\infty}{a_{\min}} v(t). \end{aligned}$$

Hence, Gronwall inequality implies that

$$E(t, x(t), y(t)) = v(t) \le K_0 e^{K_1|t|}, \quad \forall\, t \in]\alpha, \beta[\,,$$

where we have set

$$K_0 := v(0) = E(0, z_0), \quad K_1 := 2\frac{\|a'\|_\infty}{a_{\min}}\,.$$

The upper bound on the energy function and (4.45) imply that $]\alpha, \beta[= \mathbb{R}$, namely the solution is globally defined. □

Remark 4.5. The proof can be easily modified in order to include the case of a periodic function $\nu(t)$ which is piecewise smooth, that is we suppose that there are at most a finite number of points $0 \le t_0 < t_1 < t_2 < \cdots < t_m < T \le t_{m+1} = t_0 + T$ such that on each open interval $]t_i, t_{i+1}[$ $(i = 0, \dots, m)$ ν is the restriction of a continuously differentiable function defined on $[t_i, t_{i+1}]$ and such that $\nu(t) > 1$ for all t.

Our aim is to prove the presence of chaotic dynamics for the map

$$\Phi := \Phi_0^T.$$

To this end, we consider a simplified form for the function $\nu(t)$, namely, we take a stepwise map for the form

$$\nu_{x_1,x_2}(t) := \begin{cases} x_1, & \text{for } 0 \le t < T_1 \\ x_2, & \text{for } T_1 \le t < T_1 + T_2 = T \end{cases} \tag{4.46}$$

where $x_1\,, x_2 > 1$ and $T_1\,, T_2 > 0$ are given constants with $x_1 \neq x_2$. In the special case in which $\nu(t) = \nu_{x_1,x_2}(t)$, the associated Poincaré map can be decomposed as

$$\Phi_0^T = \Phi_2 \circ \Phi_1$$

where Φ_i is the Poincaré map for the time-interval $[0, T_i]$ associated with the autonomous Hamiltonian system

$$(\mathfrak{S}_i): \quad \dot{x} = y, \quad \dot{y} = -g_i(x),$$

with

$$g_i(x) := -\frac{x_i^2 \log(x_i)}{x^3} + \frac{\log(x)}{x},$$

$i = 1, 2$. The corresponding Hamiltonian functions (which are the energies of the two conservative systems) are defined as

$$E_i(x, y) := \frac{1}{2}\left(y^2 + \frac{x_i^2 \log(x_i)}{x^2} + \log^2(x)\right).$$

In this setting, the following result holds.

Theorem 4.6. *Suppose that $\nu : \mathbb{R} \to]1, +\infty[$ is T-periodic function with $\nu(t) = \nu_{x_1,x_2}(t)$ for some $x_1 \neq x_2$. Then there exist $T_1^*\,, T_2^* > 0$ such that for each $T_1 > T_1^*$ and $T_2 > T_2^*$, the Poincaré map exhibits chaotic dynamics.*

The precise concept of "chaos" that we obtain in Theorem 4.8 corresponds to the so-called chaotic dynamics in the coin-tossing sense [56, 57] and is recalled in the Chapter 2. In any case, as a consequence of our definition, the existence of subharmonic solutions of any order for the equation (4.41) is guaranteed, together with the existence of an uncountable set of bounded and non-periodic solutions which can be coded according to any prescribed sequence of symbols.

Before exhibiting the technical details of the proof, we describe informally, with the aid of Figure 4.10 and Figure 4.11 below, how to show the presence of a horseshoe-type geometry for the perturbed system.

Just to fix the ideas, from now on we suppose that

$$1 < x_1 < x_2$$

(the other case, being treated in a completely symmetric manner). First of all, we observe that system (4.43) for $\nu(t)$ as in (4.46) is a *nonlinear switched system* [58] in the sense that we have two autonomous systems

$$(\mathfrak{S}_1): \quad \begin{cases} \dot{x} = y \\ \dot{y} = \frac{x_1^2 \log(x_1)}{x^3} - \frac{\log(x)}{x} \end{cases}$$

and

$$(\mathfrak{S}_2): \quad \begin{cases} \dot{x} = y \\ \dot{y} = \frac{x_2^2 \log(x_2)}{x^3} - \frac{\log(x)}{x}, \end{cases}$$

which alternate in a periodic fashion, with $(\mathfrak{S}_1)$ acting on a time-interval of length T_1, followed by $(\mathfrak{S}_2)$ acting on a time-interval of length T_2 and with $T_1 + T_2 = T$.

As already observed, both systems determine a global center on the domain Ω having $P := (x_1, 0)$ and, respectively, $Q := (x_2, 0)$ as equilibrium points. Typical trajectories of $(\mathfrak{S}_1)$ or $(\mathfrak{S}_2)$ are shown in 4.9 and the periodic orbits surrounding P and Q are the level lines of the first integrals E_1 and E_2.

Now, as in Figure 4.10 below, we construct two closed annuli $\mathcal{A}_P$ and $\mathcal{A}_Q$ around the equilibrium points P and Q. These closed annuli are made by (and filled with) the periodic orbits/level lines of the corresponding autonomous systems and are of the form

$$\mathcal{A}_P := \{(x, y) \in \Omega \, : \, c_1 \leq E_1(x, y) \leq d_1\},$$

$$\mathcal{A}_Q := \{(x, y) \in \Omega \, : \, c_2 \leq E_2(x, y) \leq d_2\},$$

with $d_i > c_i > E_i(x_i, 0)$ for $i = 1, 2$.

Choosing suitably the energy levels c_i and d_i we can produce two annular domains $\mathcal{A}_P$ and $\mathcal{A}_Q$ which intersect into two compact disjoint rectangular regions $\mathcal{R}_1$ and $\mathcal{R}_2$ which are symmetric with respect to the x-axis and with $\mathcal{R}_1 \subset \mathbb{R}_0^+ \times \mathbb{R}_0^+$ and $\mathcal{R}_2 = \Lambda(\mathcal{R}_1)$, where $\Lambda : (x, y) \mapsto (x, -y)$. Whenever this situation occurs, we say that the two annuli $\mathcal{A}_P$ and $\mathcal{A}_Q$ are *linked* together. We denote by

$$\Gamma_P^\ell := \{(x, y) \in \Omega : E_1(x, y) = \ell > E_1(x_1, 0)\}$$

and

$$\Gamma_Q^\ell := \{(x, y) \in \Omega : E_2(x, y) = \ell > E_2(x_2, 0)\}$$

the closed level lines of energy ℓ associated with systems $(\mathfrak{S}_1)$ and $(\mathfrak{S}_2)$ around the points P and Q, respectively.

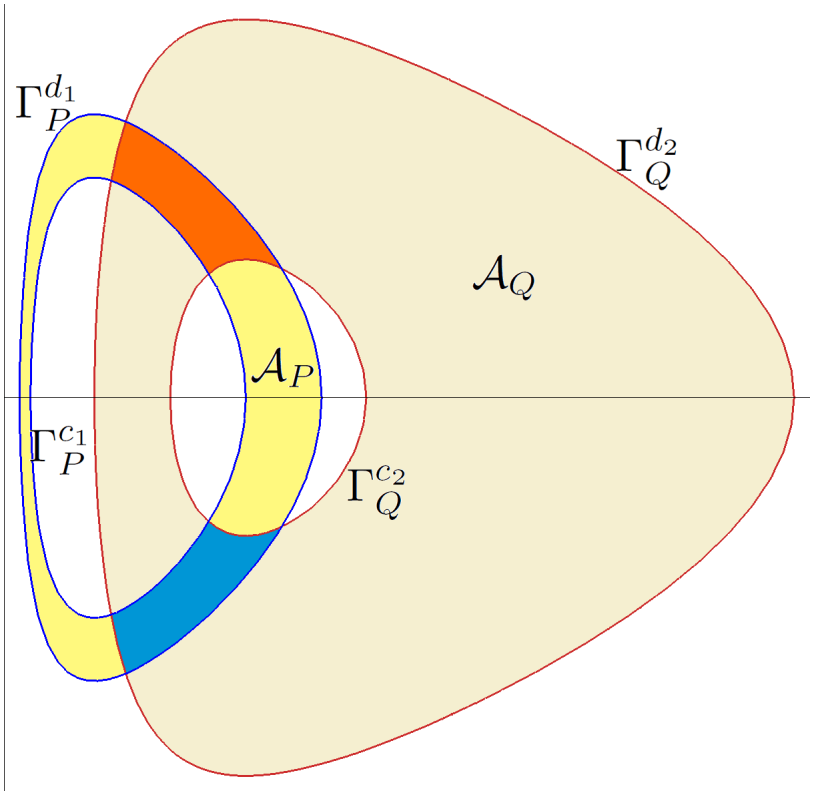

FIGURE 4.10: Example of two linked annuli $\mathcal{A}_P$ and $\mathcal{A}_Q$ with their boundary orbits $\Gamma_P^{c_1}$, $\Gamma_P^{d_1}$, and $\Gamma_Q^{c_2}$, $\Gamma_Q^{d_2}$, respectively.

At this point, we can enter in the setting of the theory of *Linked Twist Maps* [59] (see also [55, 60–64] for related references including applications to situations similar to the one considered in the present article) and, in particular, we can apply the results in [65] to have guaranteed the presence of chaotic-like dynamics for the switched system (4.43) provided that the switching times T_1 and T_2 are sufficiently large. Indeed, if we denote by $\tau_P(\ell)$ and $\tau_Q(\ell)$ the periods of the orbits Γ_P^ℓ and Γ_Q^ℓ, respectively, by Theorem 4.2 we have that

$$\tau_P(c_1) < \tau_P(d_1), \quad \text{and} \quad \tau_Q(c_2) < \tau_Q(d_2). \tag{4.47}$$

These conditions, in turn, imply that, if T_1 and T_2 are large enough, then the Poincaré maps Φ_1 (associated with system $(\mathfrak{S}_1)$) and Φ_2 (associated with system $(\mathfrak{S}_2)$) satisfy a twist condition at the boundaries of $\mathcal{A}_P$ and $\mathcal{A}_Q$, with a sufficiently large gap in the rotation numbers and therefore [65, Theorem 3.1] can be applied.

In order to describe more in detail our approach, we anticipate a few geometrical features about the "Stretching Along the Paths" (SAP-technique) which is presented in the Chapter 2

First of all, we provide an "orientation" to the rectangular regions $\mathcal{R}_1$ and $\mathcal{R}_2$, by selecting, for each of these regions, a pair of opposite edges which are conventionally called the "left" and the "right" sides. In our specific example of Figure 4.10, we orientate $\mathcal{R}_1$ and $\mathcal{R}_2$ as follows. Let $\mathcal{R}_1^-$ (respectively $\mathcal{R}_2^-$) be the intersection of $\mathcal{R}_1$ (respectively $\mathcal{R}_2$) with the inner and outer boundaries of $\mathcal{A}_P$ (respectively $\mathcal{A}_Q$). In other terms,

$$\mathcal{R}_i^- = \mathcal{R}_{i,l}^- \cup \mathcal{R}_{i,r}^-$$

for $i = 1, 2$ and we name as "left" the component of $\mathcal{R}_1^-$ which is closer to the equilibrium point P as well as the component of $\mathcal{R}_2^-$ which is closer to the equilibrium point Q (so that the "right" components will be the other ones). Thus we set

$$\mathcal{R}_{1,l}^- := \mathcal{R}_1 \cap \Gamma_P^{c_1}, \quad \mathcal{R}_{1,r}^- := \mathcal{R}_1 \cap \Gamma_P^{d_1}$$

and

$$\mathcal{R}_{2,l}^- := \mathcal{R}_2 \cap \Gamma_Q^{c_2}, \quad \mathcal{R}_{2,r}^- := \mathcal{R}_2 \cap \Gamma_Q^{d_2}$$

(see Figure 4.11).

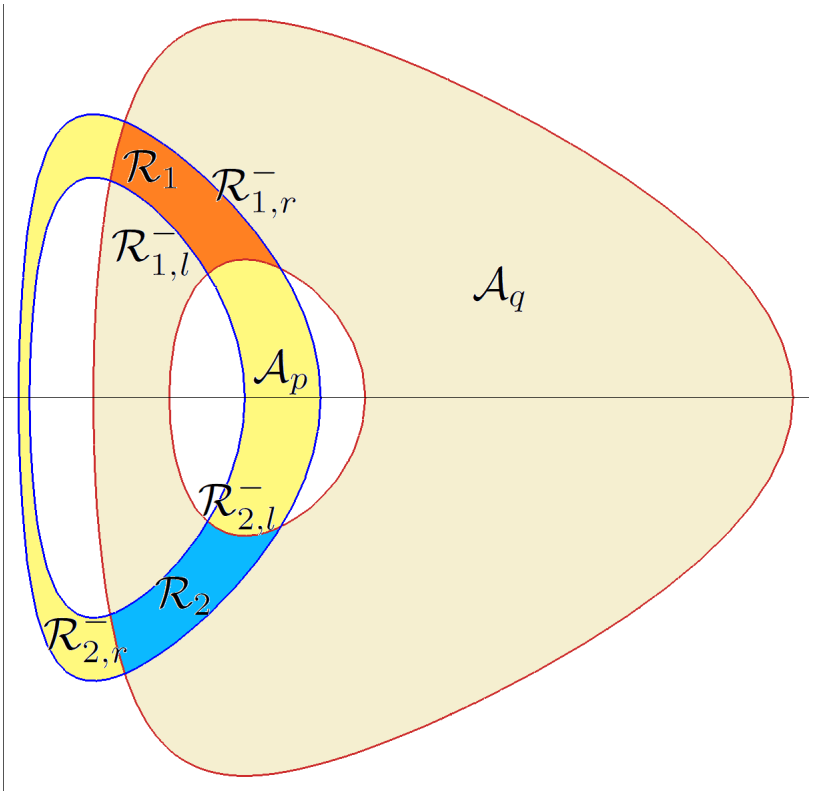

FIGURE 4.11: Example of two linked annuli $\mathcal{A}_P$ and $\mathcal{A}_Q$ and the rectangular regions $\mathcal{R}_1$ and $\mathcal{R}_2$ with their orientations.

We take any arbitrary (continuous) path $\gamma : [0, 1] \to \mathcal{R}_1$ with $\gamma(0) \in \mathcal{R}_{1,l}^-$ and $\gamma(1) \in \mathcal{R}_{1,r}^-$ and describe its deformation in the phase-plane under the action of the Poincaré map

Φ_0^T.

Recall that $\Phi_0^T = \Phi_2 \circ \Phi_1$, where Φ_1 the Poincaré map associated with the system $(\mathfrak{S}_1)$ for the time interval $[0, T_1]$ and Φ_2 the Poincaré map associated with the system $(\mathfrak{S}_2)$ for the time interval $[T_1, T]$ which, due to the fact that the system is autonomous, is the same as the Poincaré map of $(\mathfrak{S}_2)$ for the time interval $[0, T_2]$.

From $\tau_P(c_1) < \tau_P(d_1)$ it follows that the points of $\mathcal{R}_{1,l}^-$ move faster than those belonging to $\mathcal{R}_{1,r}^-$ under the action of $(\mathfrak{S}_1)$. Hence, if we choose the first switching time T_1 large enough, the resulting image of γ through Φ_1 is that of spiral crossing a certain number of times, say m_1, the rectangular region $\mathcal{R}_2$ from $\mathcal{R}_{2,r}^-$ to $\mathcal{R}_{2,l}^-$. Thus we can select m_1 subintervals of $[0, 1]$ such that $\Phi_1 \circ \gamma$ restricted to each of these intervals is a path which lies in $\mathcal{R}_2$ and connects the two components of $\mathcal{R}_2^-$. Figure 4.12 illustrates this situation.

We can then repeat the same argument as above for the map Φ_2, observing that, as a consequence of $\tau_Q(c_2) < \tau_Q(d_2)$, the points of $\mathcal{R}_{2,l}^-$ move faster than those belonging to $\mathcal{R}_{2,r}^-$ under the action of $(\mathfrak{S}_2)$. Hence, if we choose the second switching time T_2 large enough, the resulting image of each of the m_1 sub-paths of $\Phi_1 \circ \gamma$ contained in $\mathcal{R}_2$, is a spiral crossing a certain number of times, say m_2, the rectangular region $\mathcal{R}_1$ from $\mathcal{R}_{1,r}^-$ to $\mathcal{R}_{1,l}^-$.

As a conclusion, we obtain that any path γ contained in $\mathcal{R}_1$ and joining the two components of $\mathcal{R}_1^-$ has at least $m_1 \times m_2$ sub-paths whose image, under the action of the Poincaré map Φ_0^T, cross again the rectangle $\mathcal{R}_1$. This a typical horseshoe situation for the symbolic dynamics on $m_1 \times m_2$ symbols.

Therefore our main result can be reformulated as follows:

Theorem 4.7. *For every pair of positive integers (m_1, m_2) with $m := m_1 \times m_2 \geq 2$, there exist two positive constants $T_1^*(m_1)$ and $T_2^*(m_2)$ such that for all*

$$T_1 > T_1^*(m_1) \quad \text{and } T_2 > T_2^*(m_2),$$

the Poincaré map Φ_0^T induces chaotic dynamics on m symbols in $\mathcal{R}_1$.

Clearly, a completely symmetric argument can be applied in order to guarantee the existence of chaotic dynamics for Φ_0^T on $\mathcal{R}_2$.

The idea and the main steps of the proof are already described above. In the next section we just provide a few technical details which were missing in the above discussion and we also give a precise estimate for the numbers $T_1^*(m_1)$ and $T_2^*(m_2)$ (see (4.48) and (4.49)).

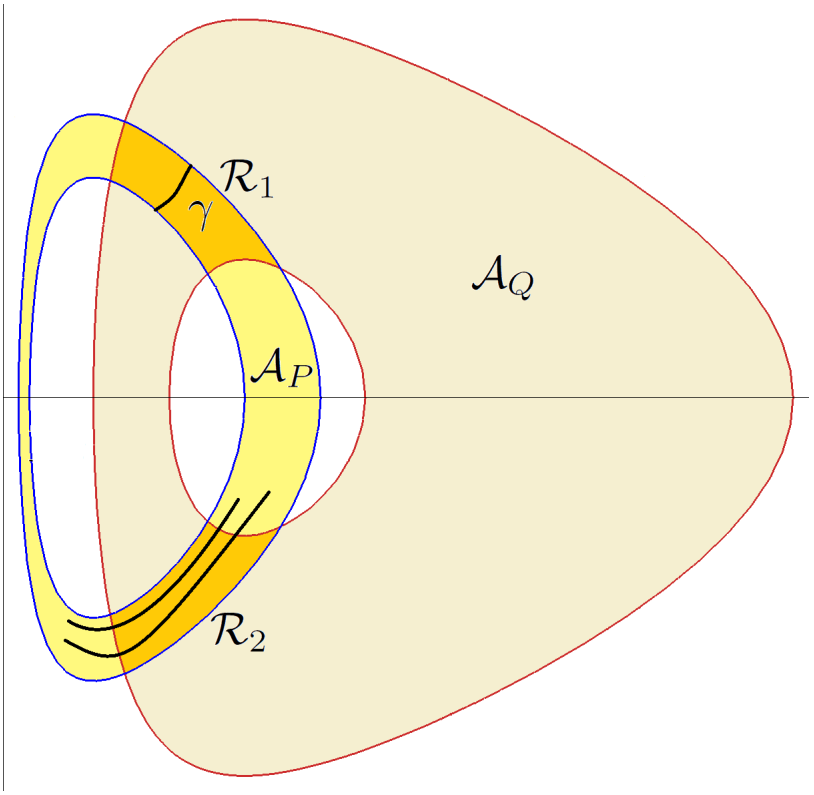

FIGURE 4.12: Example of a path γ in $\mathcal{R}_1$ and joining the opposite sides $\mathcal{R}_1^-$. In this picture we suppose that the image of γ through Φ_1 is a spiral crossing at least $m_1 = 2$ times the rectangle $\mathcal{R}_2$ coherently with the orientation chosen for $\mathcal{R}_2$ Each of the m_1 sub-paths crossing $\mathcal{R}_2$ will be then transformed by Φ_2 to spiral-like curves crossing $\mathcal{R}_1$ a certain number of times (say m_2). So, at the end, we find that there are at least $m_1 \times m_2$ sub-paths σ_i of γ such that $\Phi_0^T = \Phi_2 \circ \Phi_1$ stretches each of the σ_i to a path crossing again $\mathcal{R}_1$ in the same direction as γ. The crucial steps to make this argument working are: 1) the invariance of $\mathcal{A}_P$ under Φ_1 and $\mathcal{A}_Q$ under Φ_2 and 2) the twist property at the boundary of the two annuli (this last one coming from the gap between the periods expressed by (4.47)).

The result is stable with respect to small perturbations. In particular, it holds for a $g(t, x)$ as in (4.42), defined by a smooth T-periodic function $\nu(t)$, provided that $|\nu(t) - \nu_{x_1,x_2}(t)|$ is small in the L^1-norm on $[0, T]$.

4.3.4 Technical estimates and proof of the main result

Our proof follows the argument in [66] when a similar problem was investigated for the Lotka-Volterra prey-predator planar system. Indeed, the dynamical features of the present model and those in [66] present strong analogies due to the fact that the period map is strictly monotone increasing, according to the results in Section 4.4.2 and those in [67, 68].

We start by studying the effect of the Poincaré map Φ_1 on the points of $\mathcal{R}_1$.

For any point $z \in \mathcal{R}_1$, we consider the evolution in time along the solutions of the system $(\mathfrak{S}_1)$. So, $\Phi_0^t(z)$ is the solution of $(\mathfrak{S}_1)$ starting at the initial point $\Phi_0^0(z) = z$ and evaluated at the time t, for $0 \leq t \leq T_1$. Consistently with the definitions in Section 4.4.3, we have $\Phi_1 := \Phi_0^{T_1}$. Let us also consider a system of polar coordinates with center in $P = (x_1, 0)$, taking the clockwise direction for the positive orientation of the angles and denote by $\vartheta_1(t, z)$ the angle associated to $\Phi_0^t(z)$. We use the convention that for the initial points $z \in \mathcal{R}_1$ we have that $-\pi < \vartheta_1(0, z) < 0$.

Using the fact that the annulus $\mathcal{A}_P$ is made by level lines of the energy of system $(\mathfrak{S}_1)$ (which are strictly star-sped curves around P), we have that for any non-negative integer k, it holds that

$$\vartheta_1(t, z) \gtreqless \vartheta_1(0, z) + 2k\pi \iff t \gtreqless \tau_P(\ell_z),$$

for

$$\ell_z := E_1(z),$$

where we recall that $\tau_P(\ell)$ is the fundamental period of the level line of energy $E_1(x, y) = \ell$ and, in our case, $c_1 \leq \ell \leq d_1$. Observe also that for any fixed z, the map $t \mapsto \vartheta_1(t, z)$ is strictly monotone increasing; this follows from

$$\frac{d}{dt}\vartheta(t) = \frac{y(t)^2 + g_1(x(t))(x(t) - x_1)}{y(t)^2 + (x(t) - x_1)^2} > 0.$$

Let $\gamma : [0, 1] \to \mathcal{R}_1$ be a continuous path with with $\gamma(0) \in \mathcal{R}_{1,l}^-$ and $\gamma(1) \in \mathcal{R}_{1,r}^-$. We want to describe its deformation in the phase-plane under the action of the Poincaré map Φ_0^t. To this end we consider the angular function

$$\varphi_1(t, s) := \vartheta_1(t, \gamma(s)), \quad \text{for } 0 \leq t \leq T_1\,,\ s \in [0, 1],$$

which is continuous on the pair (t, s).

Let ℓ the energy level line of the point $z = \gamma(s)$ for some $s \in [0, 1]$. For any $t > 0$, the following estimate holds:

$$\varphi_1(t, s) > \pi + 2\pi \left(\left\lfloor \frac{t}{\tau_P(\ell)} \right\rfloor - 1 \right),$$

$$\varphi_1(t, s) < 2\pi + 2\pi \left(\left\lceil \frac{t}{\tau_P(\ell)} \right\rceil - 1 \right),$$

where, for any real number r, by $\lfloor r \rfloor$ and $\lceil r \rceil$ we denote, respectively, the greatest integer less than or equal to r and the least integer greater than or equal to r.

Hence we find that

$$\varphi_1(t,0) > \pi + 2\pi N_1^+(t), \quad \text{for } N_1^+(t) := \left\lfloor \frac{t}{\tau_P(c_1)} \right\rfloor - 1$$

(because $E_1(\gamma(0)) = c_1$) and

$$\varphi_1(t,1) < 2\pi + 2\pi N_1^-(t), \quad \text{for } N_1^-(t) := \left\lceil \frac{t}{\tau_P(d_1)} \right\rceil - 1$$

(due to the fact that $E_1(\gamma(1)) = d_1$).

Clearly, if $\pi + 2\pi N_1^+(t) > 2\pi + 2\pi N_1^-(t)$, then the interval $[\varphi_1(t,1), \varphi_1(t,0)]$ covers at least one interval of the form $[2k\pi + \pi, 2k\pi]$ and therefore the path $s \mapsto \Phi_0^t(\gamma(s))$ crosses at least once the set $\mathcal{R}_2$. By the same argument, we obtain that, in order to have at least m_1 crossings, we may impose that

$$\left\lfloor \frac{t}{\tau_P(c_1)} \right\rfloor - \left\lceil \frac{t}{\tau_P(d_1)} \right\rceil > m_1 \,,$$

which is satisfied provided that

$$\frac{t}{\tau_P(c_1)} - \frac{t}{\tau_P(d_1)} > m_1 + 2.$$

As a consequence we can determine the number

$$T_1^*(m_1) := \frac{\tau_P(d_1) - \tau_P(c_1)}{\tau_P(c_1)\tau_P(d_1)}(m_1 + 2) \tag{4.48}$$

such that, for any $t > T_1^*(m_1)$, the image of γ through Φ_0^t is a spiral-like path which crosses at least m_1 times the rectangle $\mathcal{R}_2$.

To complete the argument, let us fix now a time $T_1 > T_1^*(m_1)$ and define

$$\alpha_1 := \max\{\vartheta_1(T_1, w) : w \in \mathcal{R}_{1,r}^-\}, \quad \beta_1 := \min\{\vartheta_1(T_1, z) : z \in \mathcal{R}_{1,l}^-\}.$$

By the previous estimates on the angular function, we know that the interval $[\alpha_1, \beta_1]$ contains at least m_1 consecutive and disjoint compact intervals of the form $[2j\pi, (2j+1)\pi]$ for $j = k_1^*, k_1^* + 1, \ldots, k_1^* + m_1 - 1$, where k_1^* is a suitable positive integer depending on T_1. Then, for each $i = 1, \ldots, m_1$ we define the compact set

$$\mathcal{K}_i := \{u \in \mathcal{R}_1 \,;\, \Phi_1(u) \in \mathcal{R}_2 \,, \vartheta_1(T_1, u) \in [2(k_1^* + i - 1)\pi, (2(k_1^* + i - 1) + 1)\pi]\}$$

and where $\Phi_1 = \Phi_0^T$ and, by the previous discussion on the path γ, we find that the following property holds: *for every path* $\gamma : [0,1] \to \mathcal{R}_1$ *such that* $\gamma(0) \in \mathcal{R}_{1,l}^-$ *and* $\gamma(1) \in \mathcal{R}_{1,r}^-$ *there exists a subinterval* $[t_i', t_i''] \subset [0,1]$ *such that* $\gamma(s) \in \mathcal{K}_i$ *and* $\Phi_1(\gamma(s)) \in \mathcal{R}_2$ *for*

all $t \in [t_i', t_i'']$ *and, moreover,* $\Phi_1(\gamma(t_i'))$ *and* $\Phi_1(\gamma(t_i''))$ *belong to different components of* $\mathcal{R}_2^-$. This in turns implies that

$$(\mathcal{K}_i, \Phi_1) : (\mathcal{R}_1, \mathcal{R}_1^-) \twoheadrightarrow (\mathcal{R}_2, \mathcal{R}_2^-), \quad \forall i := 1, \dots, m_1 \,,$$

with $\mathcal{K}_1, \dots \mathcal{K}_{m_1}$ pairwise disjoint compact subsets of $\mathcal{R}_1$.

Repeating verbatim the same argument for the map Φ_2 relatively to the rectangle $\mathcal{R}_2$ we can determine the number

$$T_2^*(m_2) := \frac{\tau_Q(d_2) - \tau_Q(c_2)}{\tau_Q(c_2)\tau_Q(d_2)}(m_2 + 2) \tag{4.49}$$

such that for every $T_2 > T_2^*(m_2)$ there are m_2 pairwise disjoint compact subsets $\mathcal{K}_1', \dots \mathcal{K}_{m_2}'$ of $\mathcal{R}_2$ such that

$$(\mathcal{K}_i', \Phi_2) : (\mathcal{R}_2, \mathcal{R}_2^-) \twoheadrightarrow (\mathcal{R}_1, \mathcal{R}_1^-), \quad \forall i := 1, \dots, m_2 \,.$$

Then the conclusion follows from the main Theorem. This completes the proof of Theorem 4.7. □

4.4 Complicated dynamics in a model of charged particles

4.4.1 Mathematical model

We follow the calculations in [8, Appendix B], in order to introduce the mathematical model that we are going to study. In [8] the Authors introduce a cylindrical magnetic geometry, which is considered as the limit, when R tends to infinity, of the toroidal system. The approximation to new geometric configuration leads to a magnetic field rewritten as

$$\mathbb{B} = B_0 \vec{\mathbf{e}}_z + f(r)\vec{\mathbf{e}}_\theta.$$

This is derived in [8] from (**??**) as a limit for $R \to \infty$ and considering the z-direction identified with the axes along with $\vec{\mathbf{e}}_\phi$, which is considered now as a constant. In order to avoid misunderstanding, it is important to notice (cf. [8, Appendix B]) that the z-direction here is not the one considered originally in [8, Fig. 1]. Moreover, with respect to [8], now the function f already incorporates the effect of B_0 .

In order to find the differential system describing the dynamics of the particle of mass m and charge q moving in this magnetic field, we use the fact that the force acting on the charged particle is given by $\mathbf{F} = q\vec{v} \wedge \mathbf{B}$ (where $\vec{v}$ is the velocity of the particle). Next we

recall also the expressions of the velocity and the acceleration in cylindrical coordinates, namely

$$\vec{v} = \dot{r}\hat{\mathbf{e}}_r + r\dot{\theta}\hat{\mathbf{e}}_\theta + \dot{z}\hat{\mathbf{e}}_z$$

and

$$\vec{a} = (\ddot{r} - r\dot{\theta}^2)\hat{\mathbf{e}}_r + (r\ddot{\theta} + 2\dot{r}\dot{\theta})\hat{\mathbf{e}}_\theta + \ddot{z}\hat{\mathbf{e}}_z.$$

Then, an application of the Newton second law, yields to

$$\begin{cases} \ddot{r} - r\dot{\theta}^2 = \frac{q}{m}(B_0 r\dot{\theta} - f(r)\dot{z}) \\ r\ddot{\theta} + 2\dot{r}\dot{\theta} = -\frac{qB_0}{m}\dot{r} \\ \ddot{z} = \frac{q}{m}\dot{r}f(r) \end{cases} \tag{4.50}$$

Multiplying by r the second equation and then integrating the second and the third equations, we obtain

$$\begin{cases} \dot{\theta} = \frac{A}{r^2} - \frac{qB_0}{2m} \\ \dot{z} = \frac{q}{m}F(r) \end{cases} \tag{4.51}$$

where A is a constant and $F(r) = \int^r f(x)dx$. Substituting the two equations of (4.51) into the first equation of (4.50), we obtain this second-order ODE

$$\ddot{r} - \frac{A^2}{r^3} + \left(\frac{qB_0}{2m}\right)^2 r + \frac{q^2}{m^2}f(r)F(r) = 0. \tag{4.52}$$

Multiplying equation (4.52) by $\dot{r}$ and then integrating we finally obtain

$$\int \dot{r}\ddot{r}dt - \int_{r=r(t)} \frac{A^2}{r^3}dr + \left(\frac{qB_0}{2m}\right)^2 \int_{r=r(t)} rdr + \frac{q^2}{m^2}\int_{r=r(t)} F(r)F'(r)dr = \text{constant}.$$

Thus we end up with an effective Hamiltonian,

$$H_{eff} := \frac{m\dot{r}^2}{2} + \frac{mA^2}{2r^2} + \frac{(qB_0)^2}{8m}r^2 + \frac{q^2}{2m}F^2(r).$$

4.4.2 Geometric configurations

Following [8] we consider the effective Hamiltonian

$$H_{\text{eff}} := \frac{\dot{r}^2}{2} + \frac{A^2}{2r^2} + \frac{B_0^2}{8}r^2 + F^2(r) \tag{4.53}$$

for

$$F(r) := ar^2 \exp\left(-\frac{r^2}{c^2}\right), \tag{4.54}$$

where A, a, c are suitable positive constants and B_0 is the intensity (magnitude) of the magnetic field. Without loss of generality, we have considered in (4.53) a unitary mass m and a unitary charge q (cf. formula $(B7)$ in [8]). According to the formula of H_{eff}, the term depending on $f(r)$ should be of the form $F^2(r)/2$, but clearly there is no mistake in replacing it with $F^2(r)$ (just rename the original function f or replace a with $a\sqrt{2}$ in (4.54)). As in [8] we assume that the constants in the function F are adjusted in order to generate a double well potential in the effective Hamiltonian. We split H_{eff} as

$$H_{\text{eff}} = E_c + V_0(r) + F^2(r),$$

where E_c, is the kinetic energy and V_0 is the potential in absence of the component of the magnetic field given by $f(r)$. To explain the details, the potential $V_0(r)$ tends to infinity for $r \to 0^+$ and $r \to +\infty$ and it has a unique point of minimum at $r_0 > 0$, where $r_0^2 := 2A/B_0$. In [8], the Authors propose to fix the parameters a and c for the function F in order to produce a maximum point near r_0, so that the new potential $V_0(r) + F^2(r)$ assumes a double-well shape as in Figure 4.13 below. This is obtained by choosing c^2 close to r_0^2 and $a > 0$ sufficiently large.

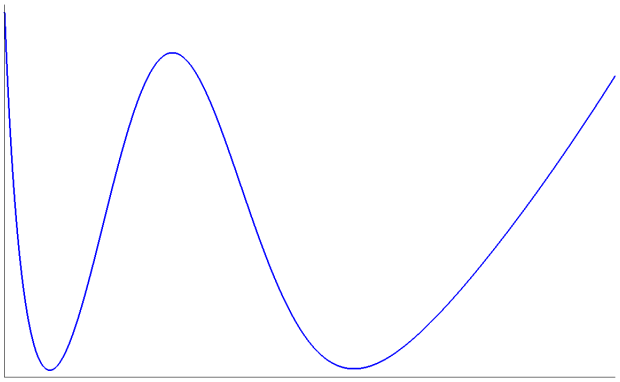

FIGURE 4.13: A possible profile of the modified potential $V_0(r) + F^2(r)$ for $r > 0$. The coefficients are tuned-up with a choice of $c^2 > r_0^2$.

The level lines of the effective Hamiltonian function in the right half-plane $\mathbb{R}_0^+ \times \mathbb{R}$ describe a phase-portrait with two centers separated by homoclinic orbits emanated from an intermediate saddle point. The typical portrait is like in Figure 4.14.

The level lines of H_{eff} are associated with the orbits of the second-order Duffing equation

$$\ddot{x} + g(x) = 0, \tag{4.55}$$

or, equivalently, the planar conservative system

$$\begin{cases} \dot{x} = y \\ \dot{y} = -g(x), \end{cases} \tag{4.56}$$

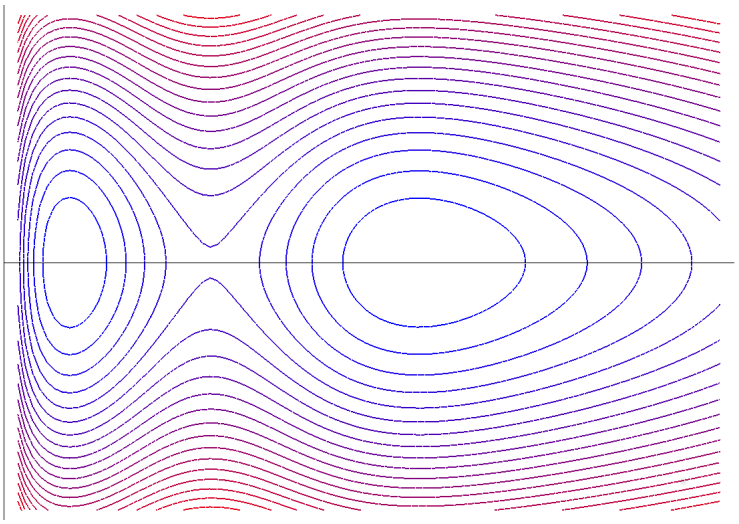

FIGURE 4.14: Some level lines associated with the Hamiltonian H_{eff} in the plane $(r, \dot{r})$ for $r > 0$.

for $x := r > 0$, $y = \dot{r}$ and

$$g(x) := \frac{d}{dx}\left(V_0(x) + F(x)^2\right) = -\frac{A^2}{x^3} + \frac{{B_0}^2}{4}x + 2F(x)f(x), \tag{4.57}$$

where we have set

$$f(x) := F'(x). \tag{4.58}$$

If we choose F in order to produce a potential as described in [8, Section IV] and in Figure 4.13, we find that the map g has precisely three simple zeros for $x > 0$ that we denote and order as

$$a < x_s < b.$$

In the phase-plane $\mathbb{R}_0^+ \times \mathbb{R}$, the points $(a, 0)$ and $(b, 0)$ are local centers, while $(x_s, 0)$ is a saddle point.
The level line

$$H(x, y) := \frac{y^2}{2} + V_0(x) + F^2(x) = c_s := V_0(x_s) + F^2(x_s)$$

is a double homoclinic loop, namely, it splits as

$$\mathcal{O}_l \cup \{(x_s, 0)\} \cup \mathcal{O}_r\,,$$

where $\mathcal{O}_l$ and $\mathcal{O}_r$ two homoclinic orbits at the saddle point $\{(x_s, 0)\}$. By convention, we suppose that $\mathcal{O}_l$ is contained in the strip $0 < x < x_s$ and surrounds $(a, 0)$, while $\mathcal{O}_r$ is contained in the half-plane strip $x > x_s$ and surrounds $(b, 0)$. We denote by $(\underline{a}, 0)$ and the $(\underline{b}, 0)$ the intersection points of $\mathcal{O}_l$ and, respectively, $\mathcal{O}_r$ with the x-axis. By

definition, we have

$$0 < \underline{a} < a < x_s < b < \underline{b},$$

with $\underline{a}, x_s, \underline{b}$ the three solutions of $V_0(x) + F^2(x) = c_s$ (see Figure 4.13).
We also introduce the open regions

$$\mathcal{W}_l := \{(x, y) : 0 < x < x_s\,,\ H(x, y) < c_s\}$$

and

$$\mathcal{W}_r := \{(x, y) : x > x_s\,,\ H(x, y) < c_s\}.$$

By construction, we have

$$\partial\mathcal{W}_l = \mathcal{O}_l \cup \{(x_s, 0)\} \quad \text{and} \quad \partial\mathcal{W}_r = \mathcal{O}_r \cup \{(x_s, 0)\}$$

(see Figure 4.15).

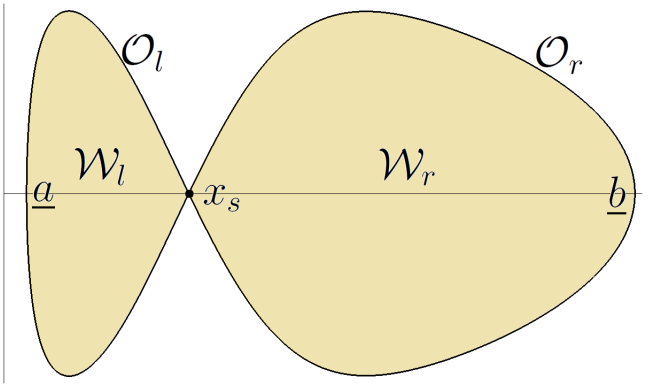

FIGURE 4.15: The saddle point $(x_s, 0)$ with the homoclinic orbits $\mathcal{O}_l, \mathcal{O}_l$ and the resulting regions $\mathcal{W}_l, \mathcal{W}_l$.

As a next step, we suppose that the modulus of the magnetic field B_0 is affected by a small change so that the three equilibrium points $(a, 0), (x_s, 0)$ and $(b, 0)$ are shifted along the x-axis. We suppose that the effect is small enough so that the new point $(x_s, 0)$ will belong to the region surrounded by $\mathcal{O}_l$ or the one surrounded by $\mathcal{O}_r$. More precisely, if we denote by $B_0^{(1)}$ and $B_0^{(2)}$ two different values of the magnetic field and associated the index $i = 1, 2$ to the corresponding equilibrium points and homoclinic orbits, we will assume that

$$H^{(1)}(x_s^{(2)}, 0) < H^{(1)}(x_s^{(1)}, 0) \quad \text{and} \quad H^{(2)}(x_s^{(1)}, 0) < H^{(2)}(x_s^{(1)}, 0). \tag{4.59}$$

We tacitly use the convention the apex $i = 1, 2$ is associated to the points, orbits and regions of the phase-plane associated with the differential systems having Hamiltonians $H^{(1)}$ and $H^{(2)}$ for the magnetic fields $B_0^{(1)}$ and $B_0^{(2)}$. Under the assumption (4.59) the homoclinic loops associated with the two Hamiltonian systems, overlap as in Figure 4.16.

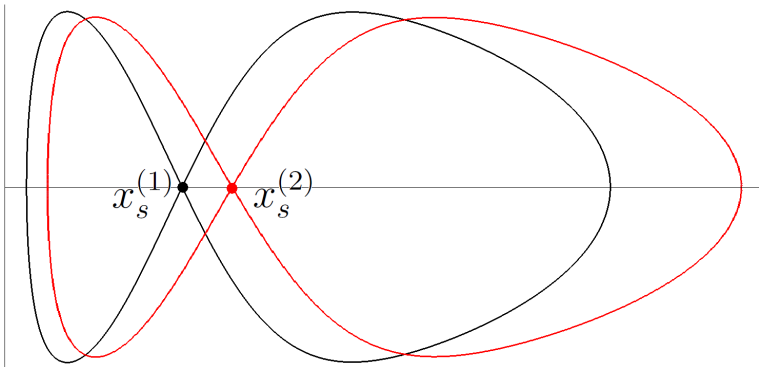

FIGURE 4.16: An example of the double homoclinic loops overlapping. The effect is obtained by moving the saddle point x_s. This occurs via a change of parameters in the equation. The aspect/ratio has been slightly modified in order to make the overlapping more evident.

Our plan is to construct some regions homeomorphic to rectangles which are obtained as intersections of suitable narrow bands around the homoclinics.

Let us consider the level line $H^{(1)}(x,y) = c^{(1)}$ with $c^{(1)} < H^{(1)}(x_s^{(1)}, 0)$ and $H^{(1)}(x_s^{(1)}, 0) - c^{(1)}$ small enough. This level line splits into two components, which are contained in the open regions $\mathcal{W}_l^{(1)}$ and $\mathcal{W}_r^{(1)}$, respectively. Now the equation $V_0(x) + F^2(x) = c^{(1)}$ has four solutions that we will denote $a_\pm^{(1)}$ and $b_\pm^{(1)}$, so that

$$\underline{a}^{(1)} < a_-^{(1)} < a^{(1)} < a_+^{(1)} < x_s^{(1)} < b_-^{(1)} < b^{(1)} < b_+^{(1)} < \underline{b}^{(1)}\,.$$

For the system associated with $B_0^{(2)}$, we can similarly determine some corresponding points with

$$\underline{a}^{(2)} < a_-^{(2)} < a^{(2)} < a_+^{(2)} < x_s^{(2)} < b_-^{(2)} < b^{(2)} < b_+^{(2)} < \underline{b}^{(2)}\,.$$

By suitably selecting the energy levels, it is always possible to enter in a setting such that the *crossing condition*

$$(CC) \qquad \begin{array}{lll} a_-^{(1)} < & \underline{a}^{(2)} < a_-^{(2)} < a_+^{(1)} \\ & b_-^{(1)} < a_+^{(2)} \\ b_-^{(2)} < & b_+^{(1)} < \underline{b}^{(1)} < b_+^{(2)} \end{array}$$

holds.

Let us consider now the ∞-shaped regions

$$\mathcal{A}^i := \{(x,y) : x > 0\,,\ c^{(i)} \le H^{(i)}(x,y) \le c_s^{(i)}\}, \qquad \text{for } \ i = 1, 2,$$

which are bounded by the homoclinics $\mathcal{O}_l^{(i)}$ and $\mathcal{O}_l^{(i)}$.

The level line $\leq H^{(i)}(x,y) = c^{(i)}$ has two components which are closed orbits contained in the regions $\mathcal{W}_l^{(i)}$ and $\mathcal{W}_r^{(i)}$, respectively. We set, for $i = 1, 2$,

$$\Gamma_l^{(i)} := \{(x,y) : 0 < x < x_s^{(i)}\,,\ H^{(i)}(x,y) = c^{(i)}\} \subseteq \mathcal{W}_l^{(i)},$$

$$\Gamma_r^{(i)} := \{(x,y) : x > x_s^{(i)}\,,\ H^{(i)}(x,y) = c^{(i)}\} \subseteq \mathcal{W}_r^{(i)}$$

and denote by $\tau_l^{(i)}$ and $\tau_r^{(i)}$ the fundamental periods of the orbits $\Gamma_l^{(i)}$ and $\Gamma_r^{(i)}$, respectively.

The sets $\mathcal{A}^1$ and $\mathcal{A}^2$ intersects into six rectangular regions that we denote by $\mathfrak{a}_\pm, \mathfrak{b}_\pm, \mathfrak{c}_\pm$, respectively, labelling from left to right and using the sign $+$ or $-$ according to the fact that the region is contained in the upper or lower half-plane (see Figure 4.17).

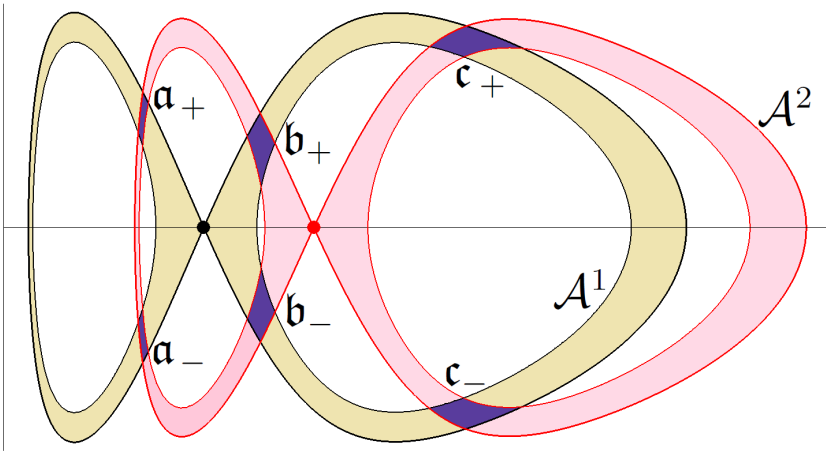

FIGURE 4.17: An example of intersection of $\mathcal{A}^1$ with $\mathcal{A}^2$ producing the six rectangular regions $\mathfrak{a}_\pm, \mathfrak{b}_\pm, \mathfrak{c}_\pm$.

Each one of the six regions introduced above can be oriented in two different manners. By an orientation of a topological rectangle $\mathcal{R}$, we mean the selection of two opposite sides whose union is denoted by $\mathcal{R}^-$. The two components of $\mathcal{R}^-$ are conventionally called the left and the right side (the order according to which we select to associate the terms "right" or "left" with the two sides of $\mathcal{R}^-$ is not relevant). The pair $(\mathcal{R}, \mathcal{R}^-)$ is called an *oriented rectangle*.

Now, let $\mathcal{R}$ be any of the $\mathfrak{a}_\pm, \mathfrak{b}_\pm, \mathfrak{c}_\pm$. We observe that $\mathcal{R}$ can be orientated in two different manners, by choosing as $\mathcal{R}^-$ the two intersection of $\mathcal{R}$ with $H^{(1)} = c^{(1)}$ and with $H^{(1)} = c_s^{(1)}$ or the two intersection of $\mathcal{R}$ with $H^{(2)} = c^{(2)}$ and with $H^{(2)} = c_s^{(2)}$. The corresponding oriented rectangle $(\mathcal{R}, \mathcal{R}^-)$ will be denoted as $\breve{\mathcal{R}}$ in the former case and as $\widehat{\mathcal{R}}$ in the latter one. For example and with reference to Figure 4.17, the oriented rectangle $\widehat{\mathfrak{b}}_-$ is the region $\mathfrak{b}_-$ (center-below) in which we have selected as a couple of opposite sides forming $\mathfrak{b}_-^-$ the intersections of $\mathfrak{b}_-$ with the level lines $H^{(2)} = c^{(2)}$ and $H^{(2)} = c_s^{(2)}$. Analogously, the oriented rectangle $\breve{\mathfrak{c}}_+$ is the region $\mathfrak{c}_+$ (upper-right) in

which we have selected as a couple of opposite sides forming $\mathfrak{c}_+^-$ the intersections of $\mathfrak{c}_+$ with the level lines $H^{(1)} = c^{(1)}$ and $H^{(1)} = c_s^{(1)}$.

At this point we are ready to introduce a dynamical aspect, by supposing that we switch periodically between the two systems associated with the Hamiltonians $H^{(1)}$ and $H^{(2)}$. More in detail, we consider the non-autonomous second-order scalar equation

$$\ddot{x} + g(t, x) = 0 \tag{4.60}$$

and also the associated first order system

$$\begin{cases} \dot{x} = y \\ \dot{y} = -g(t, x) \end{cases} \tag{4.61}$$

in the right-half plane $x > 0$, where $g : \mathbb{R} \times \mathbb{R}_0^+ \to \mathbb{R}$ is T-periodic in the t-variable and such that

$$g(t, x) := \begin{cases} g_1(x), & \text{for } 0 \leq t < T_1 \\ g_2(x), & \text{for } T_1 \leq t < T_1 + T_2 = T, \end{cases} \tag{4.62}$$

where

$$g_i(x) := \frac{\partial H^{(i)}}{\partial x}(x, y), \quad \text{for } i = 1, 2.$$

Equation (4.61) is a switched system (see [69] and the references therein) and its associated Poincaré map Φ can be decomposed as

$$\Phi = \Phi_2 \circ \Phi_1$$

where Φ_i is the Poincaré map on the time-interval $[0, T_i]$ associated with the system

$$\begin{cases} \dot{x} = y \\ \dot{y} = -g_i(x) \end{cases} \tag{4.63}$$

for $i = 1, 2$.

Notice that, by the particular nature of the switched system (4.61), we can equivalently study the Poincaré map

$$\Phi = \Phi_1 \circ \Phi_2.$$

Indeed, in this latter case, we consider just a shift in time of the solutions.

4.4.3 Main result

After this preliminary discussion, we are now in position to state our main result which reads as follows.

Theorem 4.8. *For any integer $m \geq 2$, there are T_1^* and $T_2^* > 0$ such that for each $T_1 > T_1^*$ and $T_2 > T_2^*$, the Poincaré map Φ induces chaotic dynamics on m symbols in each of the sets $\mathfrak{a}_\pm$, $\mathfrak{b}_\pm$ and $\mathfrak{c}_\pm$. Moreover, the result is robust in the sense that it is stable for small perturbations of system* (4.61).

Our definition of chaotic dynamics is linked to the concept of chaos according to Block and Coppel [70, 71], with a special emphasis to the presence of periodic points. More precisely, we say that a continuous and one-to-one map ψ induces chaotic dynamics on m symbols in a set $\mathcal{R}$ if there exists m pairwise disjoint compact subsets $H_1, \ldots, H_m$ of $\mathcal{R}$ such that for each two-sides sequence $(s_i)_{i\in\mathbb{Z}}$ of m symbols there exists a trajectory $x_{i+1} = \psi(x_i)$ of ψ such that $x_i \in H_{s_i}$ for each $i \in \mathbb{Z}$. Moreover, if the sequence of symbols $(s_i)_{i\in\mathbb{Z}}$ is a k-periodic sequence, then also the sequence of points $(x_i)_{i\in\mathbb{Z}}$ is k-periodic. As a consequence of this definition, we have also that there exists a compact invariant set $\Lambda \subseteq \mathcal{R}$ having the set of periodic points of ψ as dense subset such that $\psi|_\Lambda$ is topologically semiconjugate (by a continuous and surjective map h) to the full shift automorphism on m-symbols $\sigma : \Sigma_m \to \Sigma_m := \{1, \ldots, m\}^{\mathbb{Z}}$. Moreover, for each k-periodic two-sided sequence $\mathtt{s} := (s_i)_{i\in\mathbb{Z}}$, the set $h^{-1}(\mathtt{s})$ contains a k-periodic point of ψ (see [72–74]).

4.4.4 Technical estimates and proof of the main result

Let $\widehat{\mathcal{M}} := (\mathcal{M}, \mathcal{M}^-)$ and $\widehat{\mathcal{N}} := (\mathcal{N}, \mathcal{N}^-)$ be oriented rectangles and let ψ be a continuous map. Let also m be a positive integer. We say that the triplet $(\widehat{\mathcal{M}}, \widehat{\mathcal{N}}, \psi)$ has the SAP (stretching along the paths) property with crossing number m, if there exist $H_1, \ldots, H_m$ pairwise disjoint compact subsets of $\mathcal{M}$ such that any path γ in $\mathcal{M}$ connecting the two components of $\mathcal{M}^-$ possesses m sub-paths $\gamma_1, \ldots \gamma_m$ with γ_i in H_i such that $\psi \circ \gamma_i$ is a path in $\mathcal{N}$ connecting the two components of $\mathcal{N}^-$. When this situation occurs, we write

$$\psi : \widehat{\mathcal{M}} \overset{\circ}{\Rightarrow}^m \widehat{\mathcal{N}}.$$

We avoid mentioning the apex m when $m = 1$.

The above property is compatible with composition of maps, indeed we have that:

$$\phi : \widehat{\mathcal{L}} \overset{\circ}{\Rightarrow}^k \widehat{\mathcal{M}},\ \psi : \widehat{\mathcal{M}} \overset{\circ}{\Rightarrow}^m \widehat{\mathcal{N}} \implies \psi \circ \phi : \widehat{\mathcal{L}} \overset{\circ}{\Rightarrow}^{km} \widehat{\mathcal{N}}.$$

The SAP property will be applied to prove the existence of complex dynamics for the Poincaré map, using the following result.

Lemma 4.9. *Let* $\widehat{\mathcal{R}} := (\mathcal{R}, \mathcal{R}^-)$ *be an oriented rectangle and* $\psi : \mathcal{R} \to \mathbb{R}^2$ *be a continuous and one-to-one map. Suppose that*

$$\psi : \widehat{\mathcal{R}} \Leftrightarrow\!\!\!\rightarrow^m \widehat{\mathcal{R}},$$

for some $m \geq 2$. *Then* ψ *induces chaotic dynamics on* m *symbols on the set* $\mathcal{R}$.

Remark 4.10. A byproduct of Lemma 4.9 implies the existence of at least m fixed points for ψ in $\mathcal{R}$. More precisely, each of the pairwise disjoint compact sets $H_1 \dots, H_m$, involved in the definition of $\psi : \widehat{\mathcal{R}} \Leftrightarrow\!\!\!\rightarrow^m \widehat{\mathcal{R}}$, contains at least one fixed point of ψ. $\lhd$

See [72–75] for the general theory.

Now we are going to describe the crossing relationships involving the sets $\breve{\mathfrak{a}}_\pm$, $\breve{\mathfrak{b}}_\pm$, $\breve{\mathfrak{c}}_\pm$ and the dual ones $\widehat{\mathfrak{a}}_\pm$, $\widehat{\mathfrak{b}}_\pm$, $\widehat{\mathfrak{c}}_\pm$ by the maps Φ_i.

Lemma 4.11. *Given any positive integer* ℓ_1, *it holds that*

$$\Phi_1 : \breve{\mathfrak{a}}_+ \Leftrightarrow\!\!\!\rightarrow^{\ell_1} \widehat{\mathfrak{a}}_-,$$

provided that $T_1 > \ell_1 \tau_l^{(1)}$.

Proof. Let $\gamma : [0,1] \to \mathfrak{a}_+$ be a (continuous) map such that $\gamma(0) \in \Gamma_l^{(1)}$ and $\gamma(1) \in \mathcal{O}_l^{(1)}$. Equivalently, $H^{(1)}(\gamma(0)) = c^{(1)}$ and $H^{(1)}(\gamma(1)) = c_s^{(1)}$. We examine the evolution of the set $\bar{\gamma} := \gamma([0,1])$ along the Poincaré map Φ_1. Observe that Φ_1 is associated with the system

$$\dot{x} = y, \quad \dot{y} = -g_1(x) \tag{4.64}$$

on the time-interval $[0, T_1]$.
Along the proof, we denote by $\zeta(t, z_0) = (x(t, z_0), y(t, z_0))$ the solution of (4.64) satisfying the initial condition $\zeta(0) = z_0$. By definition, $\Phi_1(z_0) = \zeta(T_1, z_0)$, for any $z_0 \in \mathbb{R}_0^+ \times \mathbb{R}$.

The point $\gamma(1)$ belongs to the homoclinic trajectory and therefore it remains on $\mathcal{O}_l^{(1)}$ for all the forward time, moving in the phase-plane from left to right but never meeting the saddle point $x_s^{(1)}$. As a consequence, $x(t, \gamma(1)) < x_s^{(1)}$ and $y(t, \gamma(1)) > 0$ for all $t \in [0, T_1]$. On the other hand, the point $\gamma(0)$ belongs to the periodic orbit $\Gamma_l^{(1)}$ of period $\tau_l^{(1)}$ and therefore, if $T_1 > \tau_l^{(1)}$, it makes at least ℓ_1 complete turns (in the clockwise sense) around the center $(a^{(1)}, 0)$ in the interval $[0, T_1]$.

If we introduce a polar coordinate system (θ, ρ), starting from the half-line $\{(x,0) : x < a^{(1)}\}$ and counting positive rotations in the clockwise sense, we have that $0 < \theta(\gamma(s)) < \pi$ for all $s \in [0,1]$ and then we define the sets

$$H_j := \{z \in \mathfrak{a}_+ \,:\, (2j-1)\pi < \theta(\Phi^{(1)}(z)) < 2j\pi\}, \quad \text{for } j = 1, \dots, \ell_1.$$

By the previous observation about the movement of the points $\gamma(1)$ and $\gamma(0)$ under the influence of the dynamical system of (4.64), we know that $\theta(\Phi_1(\gamma(1))) < \pi$, while $\theta(\Phi_1(\gamma(0))) > 2j\pi$. A simple continuity argument on the map $[0,1] \ni s \mapsto \theta(\Phi_1(\gamma(s)))$, implies the existence of ℓ_1 pairwise disjoint intervals $[\alpha_j, \beta_j] \subseteq [0, T_1]$ such that $(2j-1)\pi \le \theta(\Phi_1(\gamma(s))) \le 2j\pi$ for all $s \in [\alpha_j, \beta_j]$ with $\theta(\Phi_1(\gamma(\alpha_j)) = 2j\pi$ and $\theta(\Phi_1(\gamma(\beta_j)) = (2j-1)\pi$.
By definition, the path $\Phi_1 \circ \gamma$ restricted to the interval $[\alpha_j, \beta_j]$ is contained in the half-annulus

$$\mathcal{A}^i \cap \{(x,y) : 0 < x < x_s^{(1)}\,,\ y \le 0\}$$

and therefore, it crosses the rectangle $\mathfrak{a}_-$ intersecting both components of $\mathfrak{a}_-^-$. Using again an elementary continuity argument of the map $s \mapsto \Phi_1(\gamma(s))$, for each $j = 1, \dots, \ell_1$, we determine a sub-interval $[\alpha_j', \beta_j'] \subseteq [\alpha_j, \beta_j]$ such that, $\Phi_1(\gamma(s)) \in \mathfrak{a}_-$ for all $s \in [\alpha_j', \beta_j']$. Moreover, $\Phi_1(\gamma(\alpha_j'))$ and $\Phi_1(\gamma(\beta_j'))$ belong to different components of $\mathfrak{a}_-$. Note also that, by construction, $\gamma(s) \in H_j$ for all $s \in [\alpha_j', \beta_j']$. We have thus verified the SAP property for $(\breve{\mathfrak{a}}_+, \hat{\mathfrak{a}}_-, \Phi_1)$ with crossing number ℓ_1, provided that $T_1 > \ell_1 \tau_l^{(1)}$ and the proof is complete. □

At this point, we can repeat the same argument of the proof of Lemma 4.11 and consider all the possible combinations between the oriented rectangles and the maps Φ_i. We can summarize these conclusions by the following lemmas where the times $\tau *_i$ can be easily determined from the periods of the closed orbits $\Gamma_l^{(i)}$ and $\Gamma_s^{(i)}$.

Lemma 4.12. *There exist times τ_1^* and τ_2^*, such that, for any positive integers ℓ_1, ℓ_2 it holds that:*

$\Phi_1 : \breve{\mathfrak{a}}_\pm \overset{\ell_1}{\Rightarrow} \hat{\mathfrak{a}}_\pm\,, \quad \breve{\mathfrak{b}}_\pm \overset{\ell_1}{\Rightarrow} \hat{\mathfrak{b}}_\pm\,,\ \hat{\mathfrak{c}}_\pm\,, \quad \breve{\mathfrak{c}}_\pm \overset{\ell_1}{\Rightarrow} \hat{\mathfrak{b}}_\pm\,,\ \hat{\mathfrak{c}}_\pm\,,$
provided that $T_1 > \ell_1 \tau_1^*$.

$\Phi_2 : \hat{\mathfrak{a}}_\pm \overset{\ell_2}{\Rightarrow} \breve{\mathfrak{a}}_\pm\,,\ \breve{\mathfrak{b}}_\pm\,, \quad \hat{\mathfrak{b}}_\pm \overset{\ell_2}{\Rightarrow} \breve{\mathfrak{a}}_\pm\,,\ \breve{\mathfrak{b}}_\pm\,, \quad \hat{\mathfrak{c}}_\pm \overset{\ell_2}{\Rightarrow} \breve{\mathfrak{c}}_\pm\,,$
provided that $T_2 > \ell_2 \tau_2^*$.

In the above lemma, when we write a condition such as $\breve{\mathfrak{a}}_\pm \overset{\ell}{\Rightarrow} \hat{\mathfrak{a}}_\pm$, we mean that all the four possibilities in the choice of $\pm$ for the domain and codomain are possible.

The content of Lemma 4.12 is explained by means of Figure 4.18 and Figure 4.19.

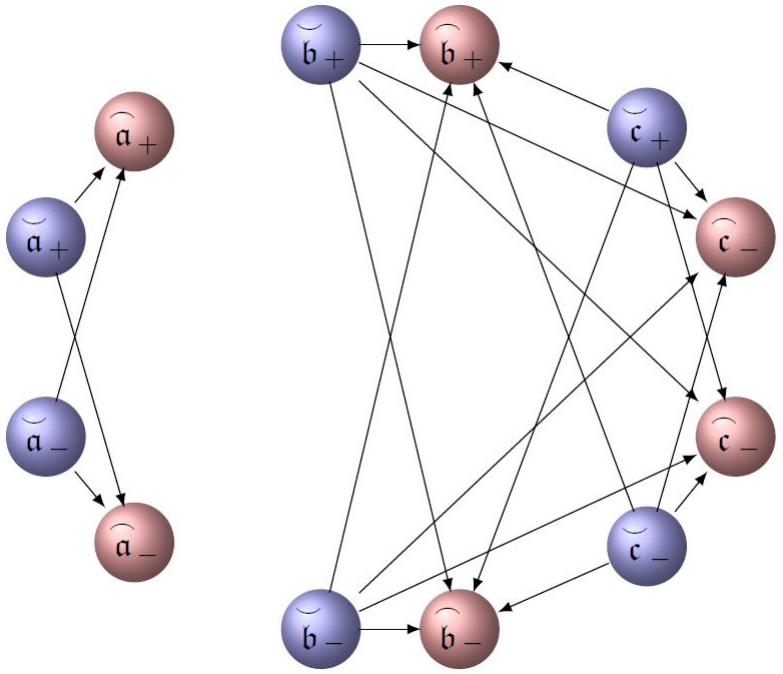

FIGURE 4.18: This graph represents all the possible connections by the partial Poincaré map Φ_1. The arrows correspond to the $\twoheadrightarrow$ symbol. The integer ℓ_1 is not indicated but it can be arbitrarily chosen provided that $T_1 > \ell_1 \tau_1^*$.

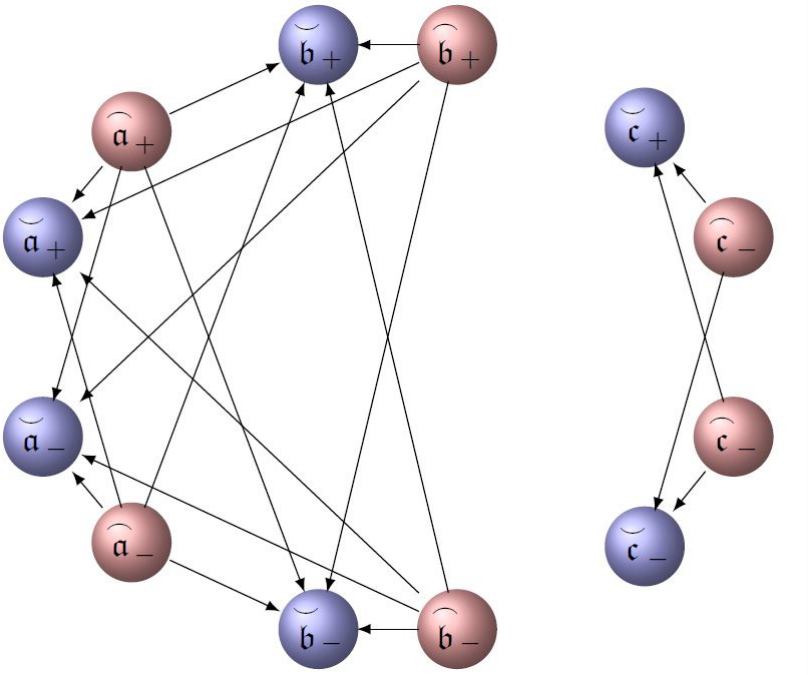

FIGURE 4.19: This graph represents all the possible connections by the partial Poincaré map Φ_2. The arrows correspond to the $\twoheadrightarrow$ symbol. The integer ℓ_2 is not indicated but it can be arbitrarily chosen provided that $T_2 > \ell_2 \tau_2^*$.

Now, we are in position to conclude the proof of our main result.

Proof. [Proof of Theorem 4.8]

Using Lemma 4.12 along with Lemma 4.9 we can guarantee that the Poincaré map $\Phi = \Phi_2 \circ \Phi_1$, as well as $\Phi = \Phi_1 \circ \Phi_2$ induces chaotic dynamics on any finite number of symbols, provided that T_1 and T_2 are large enough.

From the proof of Lemma 4.11 it is clear that the result is stable by small perturbations and the same holds for all the connections considered in Lemma 4.12.

In our case we have several possibilities of producing chaotic dynamics on $m \geq 2$ symbols on a rectangular region $\mathcal{R}$ chosen among the sets $\mathfrak{a}_\pm$, $\mathfrak{b}_\pm$ and $\mathfrak{a}_\pm$. In order to explain better how these possibilities arise, we fix out attention only on the Poincaré map $\Phi = \Phi_2 \circ \Phi_1$ (the other case is treated in a similar manner).

A first and more natural case is to take $\max\{\ell_1, \ell_2\} \geq 2$, so that

$$m = \ell_1 \times \ell_2 \geq 2$$

and, considering the connections described in Lemma 4.12, we immediately see that Lemma 4.9 can be applied for $\widehat{\mathcal{R}}$ any of the sets $\breve{\mathfrak{a}}_\pm$, $\breve{\mathfrak{b}}_\pm$, $\breve{\mathfrak{c}}_\pm$. However, a more careful analysis of the connection diagrams shows that in these sets the SAP property with crossing number greater or equal than two can be obtained also in the case when $\ell_1 = \ell_2 = 1$ (this may be more interesting from the point of view of the applications because we need a lesser restriction on the period). In fact, the following connections are available

$$\begin{array}{ll}
\breve{\mathfrak{a}}_+ \overset{\frown}{\to} \widehat{\mathfrak{a}}_+ \overset{\frown}{\to} \breve{\mathfrak{a}}_+ , & \breve{\mathfrak{a}}_+ \overset{\frown}{\to} \widehat{\mathfrak{a}}_- \overset{\frown}{\to} \breve{\mathfrak{a}}_+ \\
\breve{\mathfrak{a}}_- \overset{\frown}{\to} \widehat{\mathfrak{a}}_- \overset{\frown}{\to} \breve{\mathfrak{a}}_- , & \breve{\mathfrak{a}}_- \overset{\frown}{\to} \widehat{\mathfrak{a}}_+ \overset{\frown}{\to} \breve{\mathfrak{a}}_- \\
\breve{\mathfrak{b}}_+ \overset{\frown}{\to} \widehat{\mathfrak{b}}_+ \overset{\frown}{\to} \breve{\mathfrak{b}}_+ , & \breve{\mathfrak{b}}_+ \overset{\frown}{\to} \widehat{\mathfrak{b}}_- \overset{\frown}{\to} \breve{\mathfrak{a}}_+ \\
\breve{\mathfrak{b}}_- \overset{\frown}{\to} \widehat{\mathfrak{b}}_- \overset{\frown}{\to} \breve{\mathfrak{b}}_- , & \breve{\mathfrak{b}}_- \overset{\frown}{\to} \widehat{\mathfrak{b}}_+ \overset{\frown}{\to} \breve{\mathfrak{b}}_- \\
\breve{\mathfrak{c}}_+ \overset{\frown}{\to} \widehat{\mathfrak{c}}_+ \overset{\frown}{\to} \breve{\mathfrak{c}}_+ , & \breve{\mathfrak{c}}_+ \overset{\frown}{\to} \widehat{\mathfrak{c}}_- \overset{\frown}{\to} \breve{\mathfrak{a}}_+ \\
\breve{\mathfrak{c}}_- \overset{\frown}{\to} \widehat{\mathfrak{c}}_- \overset{\frown}{\to} \breve{\mathfrak{c}}_- , & \breve{\mathfrak{c}}_- \overset{\frown}{\to} \widehat{\mathfrak{c}}_+ \overset{\frown}{\to} \breve{\mathfrak{c}}_-
\end{array}$$

and therefore, we find that

$$\Phi : \breve{\mathfrak{a}}_\pm \overset{\frown}{\to}^2 \breve{\mathfrak{a}}_\pm , \qquad \breve{\mathfrak{b}}_\pm \overset{\frown}{\to}^2 \breve{\mathfrak{b}}_\pm , \qquad \breve{\mathfrak{c}}_\pm \overset{\frown}{\to}^2 \breve{\mathfrak{c}}_\pm .$$

In the last formula we use the convention that $[]_\pm \overset{\frown}{\to} []_\pm$ means that only the two possibilities $[]_+ \overset{\frown}{\to} []_+$ and $[]_- \overset{\frown}{\to} []_-$ are available.

The situation becomes more complicated and interesting if we consider the iterates of the map Φ. For instance, for the map Φ^2, and taking $\widehat{\mathcal{R}} = \breve{\mathfrak{a}}_+$ as a starting set, new connections are available, such as

$$\breve{\mathfrak{a}}_+ \overset{2}{\twoheadrightarrow} \breve{\mathfrak{b}}_\pm \overset{2}{\twoheadrightarrow} \breve{\mathfrak{a}}_+ \quad \text{and} \quad \breve{\mathfrak{a}}_+ \overset{2}{\twoheadrightarrow} \breve{\mathfrak{a}}_\pm \overset{2}{\twoheadrightarrow} \breve{\mathfrak{a}}_+ .$$

Hence, counting all the possible connections for Φ^2, we obtain that

$$\Phi^2 : \breve{\mathfrak{a}}_+ \overset{16}{\twoheadrightarrow} \breve{\mathfrak{a}}_+.$$

In fact, from $\breve{\mathfrak{a}}_+$ we come back again to $\breve{\mathfrak{a}}_+$ by Φ^2 passing through the four sets $\breve{\mathfrak{a}}_\pm$ and $\breve{\mathfrak{b}}_\pm$ and, each time we apply Φ we have two itineraries available. Similar combinations occur for the other oriented rectangles. □

4.5 Final remarks

The existence of chaos in differential systems which are obtained as periodic perturbations of planar autonomous systems exhibiting homoclinic or heteroclinic trajectories is a well established fact (see [44, 76]). The methods of proof applied in those situations, such as the Melnikov method, usually permit to enter in the framework of Smale's horseshoe (cf. [77] and [78]) which guarantees the existence of a compact invariant set for the Poincaré map Φ, where Φ is *topologically conjugate* to the Bernoulli shift on a certain set of symbols. Our result provides a weaker form of chaos since only the semiconjugation is proved. On the other hand, in the concrete applications, some explicit knowledge of the homoclinic (or heteroclinic) solution, in terms of its analytic expression is often needed. A typical example is given by the classical periodically perturbed Duffing equation

$$\ddot{x} - x + x^3 = \varepsilon p(\omega t), \tag{4.65}$$

where the Melnikov function can be explicitly defined (see [76]) thanks to the knowledge of the analytic expression of the homoclinic solutions of

$$\dot{x} = y, \quad \dot{y} = x - x^3.$$

In the model studied in the present paper, two difficulties arise: first, we do not know an explicit form of the homoclinic solutions of system (4.56) and, secondly, the periodic perturbation leading to (4.60) from (4.55), which corresponds to a variation of the form $B_0 \mapsto B_0(t)$ in (4.57), appears to be more complicated than the perturbation considered in equation (4.65). Our approach, even if applied to the simplified situation of a stepwise

function $B_0(t)$, allows to prove the presence of chaotic dynamics using only few geometric information on the geometry of the level curves of the associated energy functions. As already shown in [79] and in [80, Section 8], the choice of a stepwise coefficient has the advantage not only to simplify some technical estimates, but also to put in evidence the presence of interesting bifurcation phenomena for the solutions of the nonlinear equations which are involved.

Chapter 5

Numerical study of other Duffing models

The study of the boundedness of the solutions to the Duffing equation has attracted a lot of interest in the past 60 years. Starting with Littlewood in [6] who raised the questions about boundness of the solutions. The model investigated take the form of

$$\ddot{x} + a(t)g(x) = 0 \tag{5.1}$$

or

$$\ddot{x} + g(x) = p(t) \tag{5.2}$$

with $a,\ p : \mathbb{R} \to \mathbb{R}$ T-periodic functions. Typically, the equation is referred to as superlinear or sublinear according to

1. $\dfrac{g(x)}{x} \to \infty$ for $x \to \pm\infty$,
2. $\dfrac{g(x)}{x} \to 0$ for $x \to \pm\infty$

The simplest example is given by

$$g(x) = |x|^{\alpha}\text{sign}(x) \text{ for } \alpha > 0 \text{ and } \alpha \neq 1 \tag{5.3}$$

where the superlinear and sublinear cases occur for $\alpha > 1$ and $0 < \alpha < 1$, respectively. In [40] Gottlieb and Sprott investigated the Duffing equations

$$\ddot{x} + |x|^{\alpha}\text{sign}(x) = \sin(\omega t) \text{ for } \alpha > 1 \tag{5.4}$$

and gave numerical evidence of the presence of chaotic behaviour, by using estimates on the associated Lyapunov exponents.

5.1 Wang & Yu model

In the next analysis, we consider some more general models including Gottlieb e Sprott [81] as special cases. Normally the following equations are consider

$$\ddot{x} + x^{2n+1} + \sum_{j=0}^{2n} a_j(t)x^j = 0. \tag{5.5}$$

5.1.1 Case I: Parameters are period functions

We restrict to the case $\ddot{x}+x^3+a_2(t)x^2+a_1(t)x+a_0(t) = 0$. Through this subsection we will considered the following trigonometric functions $a_0(t) = \sin(\omega * t)$, $a_1(t) = 0.1 * \sin(\omega * t)$, $a_2(t) = 2 * \cos(\omega * t)$.

In this case the authors of [82] have also proven the boundedness of all the solutions. Here, following Gottlieb e Sprot we study the presence of possible chaos using the Lyapunov exponent and plotting the corresponding Poincaré section. Of particular importance will be the dependence that such chaos indicators have on the control parameters of the model which in this case for simplicity we consider only the frequency ω of the T-periodic functions. In the following we will use the method developed by Skokos [27] for numerically calculating the maximum Lyapunov exponent.

Let us start by studying the dependence of the maximum Lyapunov Characteristic Exponent (mLCE) as defined in Chapter 4 by varying the frequency ω of the T-periodic functions as previously defined. In Fig. 5.1 it is possible to observe that initially for very small values of the frequency the system has a negative mLCE attesting a regular behavior of the system. However, once the period of the system becomes slightly smaller then chaos emerges. In the figure this is illustrated by a positive mLCE in the frequency window $[\ 1,\ 5]$. When the periodicity of the auxilary functions $a_i(t)$ decreases further more then the system regains its regularity as shown by a negative mLCR of the control parameter for $\omega \gtrsim 5$.

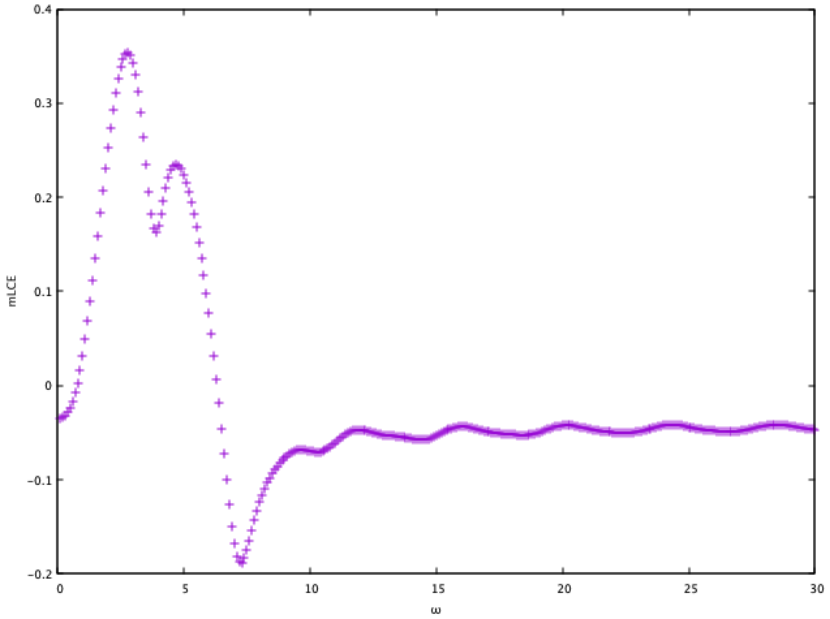

FIGURE 5.1: Maximum Lyapunov Characteristic Exponent (mLCE) (for the case with periodic parameters) as a function of the parameter ω. The system can behave caotically or not depending on the values of the frequency ω indicated respectively by the positiveness or not of the Lyapunov exponent.

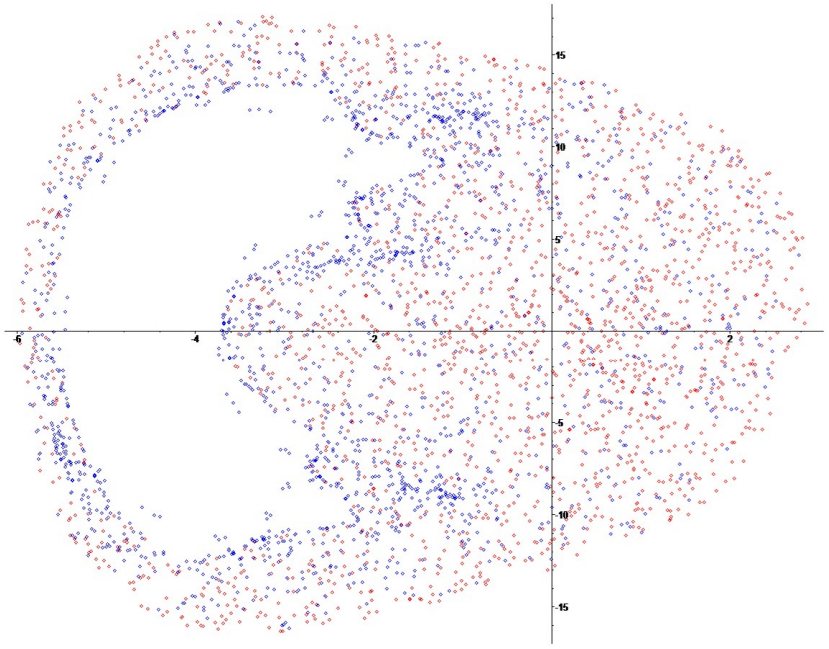

FIGURE 5.2: The Poincaré section for a value of the control parameter $\omega = 3$. In blue are shown the point for an initial value $x(0) = 0$, $\dot{x}(0) = 0$ and in red for $x(0) = 2$, $\dot{x}(0) = 0$. Here are shown only the iteration points from 200 to 2000 steps of integrations.

Qualitatively similar results are obtained even through the Poincaré section plotted in Fig. 5.2. Here we integrate the system for a value of the frequency $\omega = 3$ where chaos invades the phase space. And in fact the Poincaré section is overall dominated by chaotic islands and not a single regular orbits can be noticed. The symbols of two different

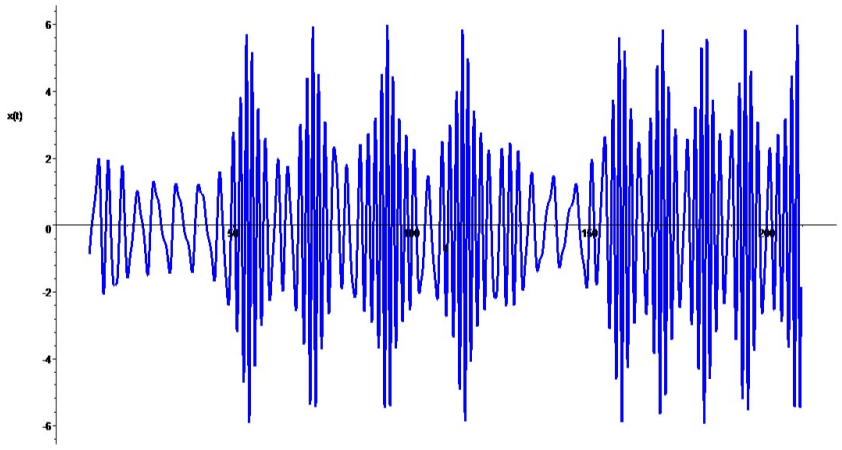

FIGURE 5.3: Temporal evolution of the state variable $x(t)$. Notice the absence of periodicity of the oscillations. A lack of periodicity in the behavior is the proof for the presence of chaos in the dynamics. Here the initial conditions are $x(0) = 2$, $\dot{x}(0) = 0$ and the iteration interval $[T1 - 200, T_1]$, con $T_1 = 200 * \pi/\omega$.

colours in Fig. 5.2 represent two different initial points in the integration process.

Exactly the same behavior can be observed even from the time evolution of the state variable $x(t)$ illustrated in Fig. 5.3 for the same choice of the control parameter as above. It is easy to notice that the systems lacks periodicity and invariance of the amplitude in the time space indicating this way a chaotic behavior.

As a conclusion, we can say that the model (5.5) has the ability to manifest both chaotic and regular behavior depending on the values of the control parameter that in our case was the frequency ω of the T-periodic auxilary functions as previously defined. In fact, initially the system goes to a transition toward chaos when the frequency increases; then when the period of the auxilary trigonometric functions becomes enough large it undergoes a re-entering phase towards the regular behavior.

5.1.2 Case II: Parameters are constant functions

We now consider the case $\ddot{x} + x^3 + a_2(t)x^2 + a_1(t)x + a_0(t) = 0$ where now the parameters are simply constant functions $a_1(t) = 1$, $a_2(t) = 1$, and the external forcing term is defined as $a_0(t) = -8 * \sin(\omega * t)$. Notice that although we are changing the dynamical systems here, it still remains of the Wang & Yu family. This translates that its dynamical behavior is influenced only by the parameters.

We will proceed following the previous line of study by first analysing the dependence of the mLCE indicator as a function of the frequence ω of the forcing term.

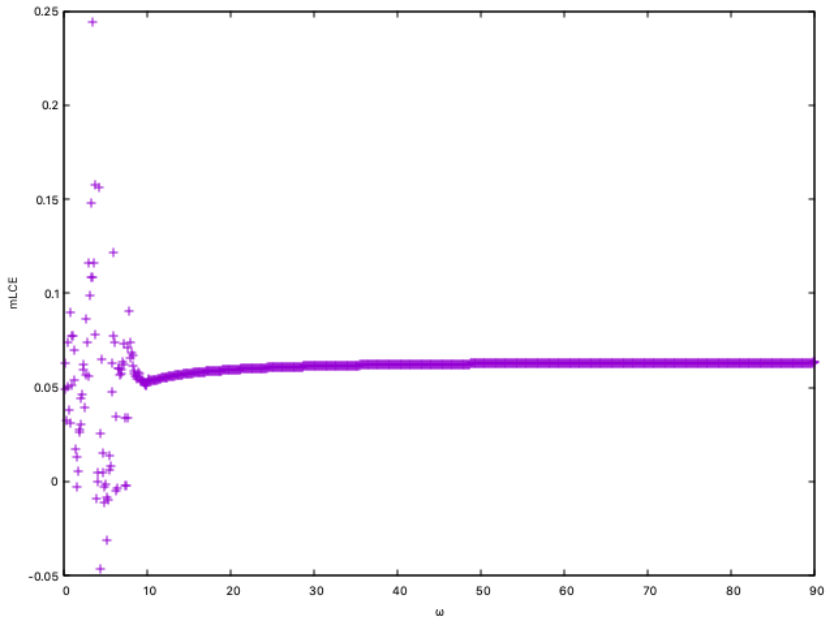

FIGURE 5.4: Maximum Lyapunov Characteristic Exponent (mLCE) (for the case with constant parameters) as a function of the parameter ω. The system can behave caotically or not depending on the values of the frequency ω indicated respectively by the positiveness or not of the Lyapunov exponent.

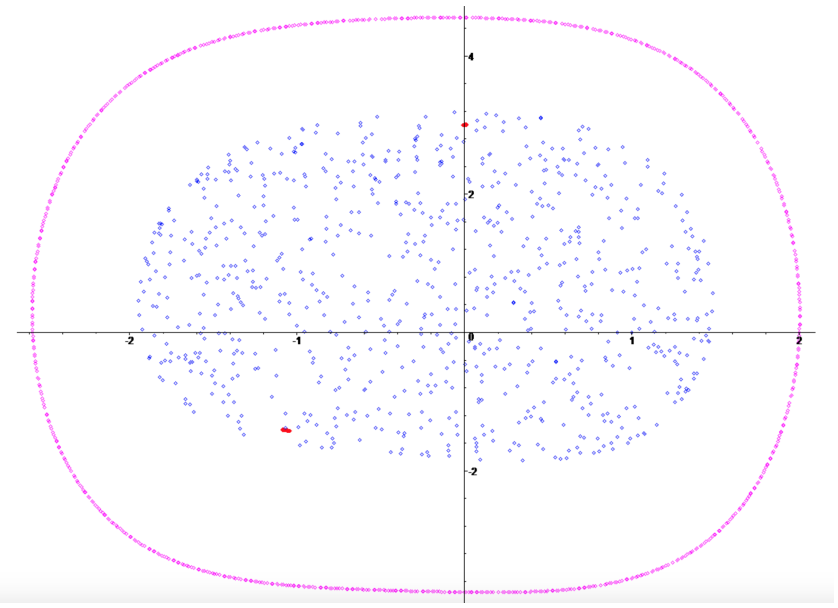

FIGURE 5.5: The Poincaré section for a value of the control parameter $\omega = 0.2$. In blue are shown the point for an initial value $x(0) = 1$, $\dot{x}(0) = 0$, in magenta for $x(0) = 2$, $\dot{x}(0) = 0$, and in red for $x(0) = 0$, $\dot{x}(0) = 3$. Here are shown the iteration points from 0 to $800 * T_0$ steps of integrations where $T_0 = 10 * \pi$ is the period of the forcing term.

In Fig. 5.4 we show the dependence of the maximum Lyapunov Characteristic Exponent (mLCE) by varying the frequency ω of the T-periodic function of the external forcing

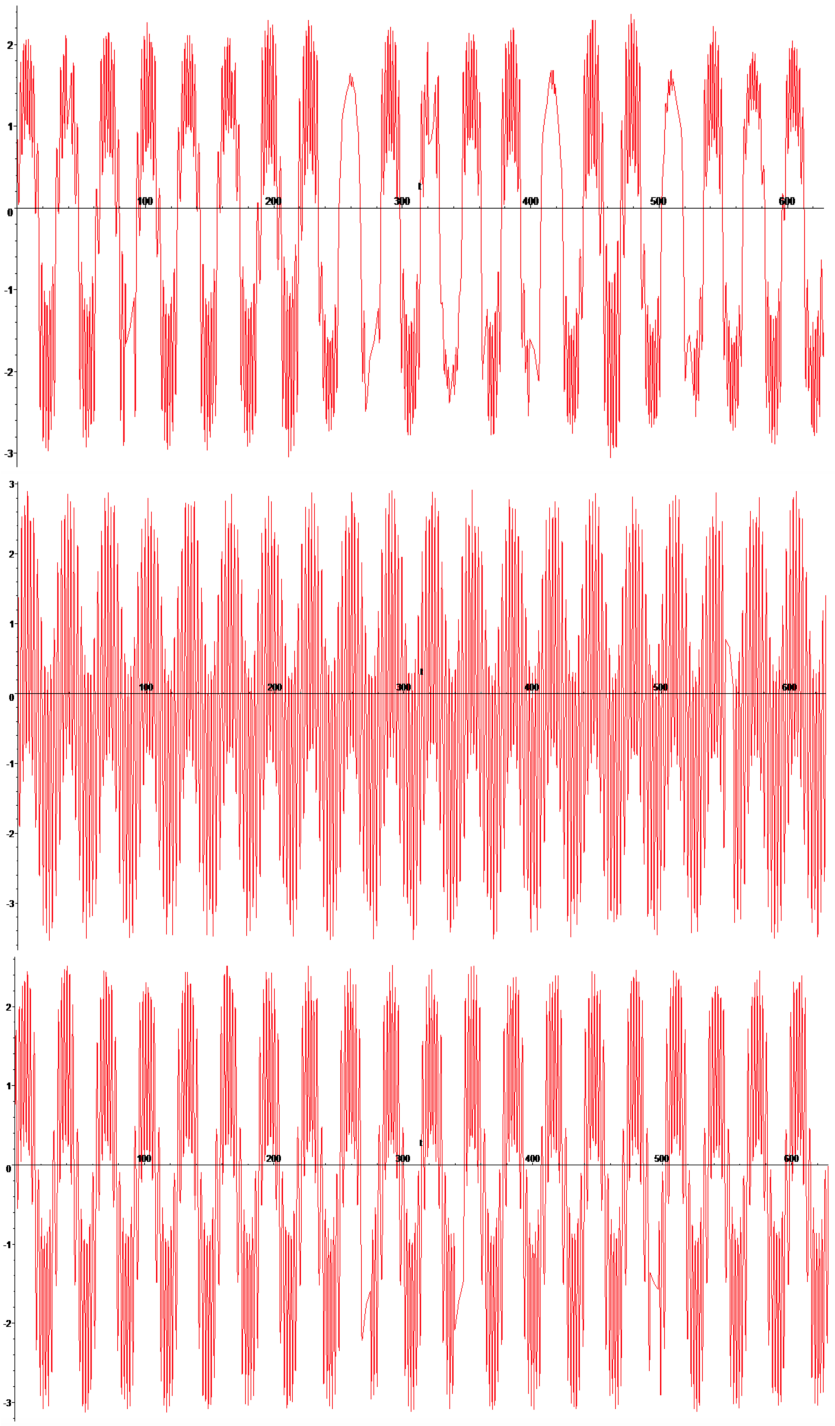

FIGURE 5.6: Temporal evolution of the state variable $x(t)$ corresponding to the intial points as in 5.5. Notice the absence of periodicity of the oscillations in the first panel. which is the proof for the presence of chaos in the dynamics. The situation becomes more regular for the other initial values as the signal regains its periodicity. Here the iteration interval for all the cases is $[0, 20 * T_0]$, con T_0 defined as above.

term. It is shown that for initial very small values of the frequency the system takes positive and negative values of mLCE attesting the possibility of chaotic behavior of the system. However, once the frequency of the system decisively increases, so the control

parameter is $\omega \gtrsim 10$ the orbits clearly remain chaotic.

From the Poincaré section 5.5 it is clear that although we notice that the central part is dominated by a chaotic island (blue symbols), the system has also a larger regular orbits (in magenta) suggesting the presence of subharmonic orbits of very large period. Notice in particular the very small number of red symbols which indicates the presence of subharmonic with a very small period.

The same behavior can be observed even from the time evolution of the state variable $x(t)$ illustrated in Fig. 5.6 for the same choice of the control parameter as above. It is easy to notice that the systems lacks periodicity and invariance of the amplitude in the time space in the first panel corresponding to the initial point $x(0) = 2$, $\dot{x}(0) = 0$ indicating the chaotic behavior for these orbits. However the signal becomes more regular (periodic) for the two other set of orbits.

We conclude that the model of Wang & Yu we considered here when the paramters take constant values has the ability to manifest both chaotic and regular behavior depending on the values of the control parameter that in our case was the frequency ω of the T-periodic auxilary functions as previously defined. In fact, initially the system might be chaotic for small frequencies; then when the period of the external forcing functions becomes enough large it undergoes a re-entering phase towards the chaotic behavior.

5.1.3 Case III: Parameters are constant functions and with different function

We now consider a different case $\ddot{x} + x^5 + a_2(t)x^3 + a_1(t)x + a_0(t) = 0$ where again the parameters are constant functions $a_1(t) = 1$, $a_2(t) = 1$, and the external forcing term is defined as $a_0(t) = -8\sin(\omega t)$. Notice that although we are changing the dynamical systems here, it still remains of the Wang & Yu family. This translates that its dynamical behavior is influence only by the parameters.

As previously we start first by analysing the dependence of the mLCE indicator as a function of the frequence ω of the forcing term.

In Fig. 5.7 we show the dependence of the maximum Lyapunov Characteristic Exponent (mLCE) by varying the frequency ω of the T-periodic function of the external forcing term. It is shown that for initial very small values of the frequency the system has a positive mLCE attesting a chaotic behavior of the system. However, once the period of the system becomes slightly smaller then the orbits stabilise. Even when the periodicity of the forcing function $a_0(t)$ decreases further more the system maintains its regularity as shown by a negative mLCR of the control parameter for $\omega \gtrsim 5$.

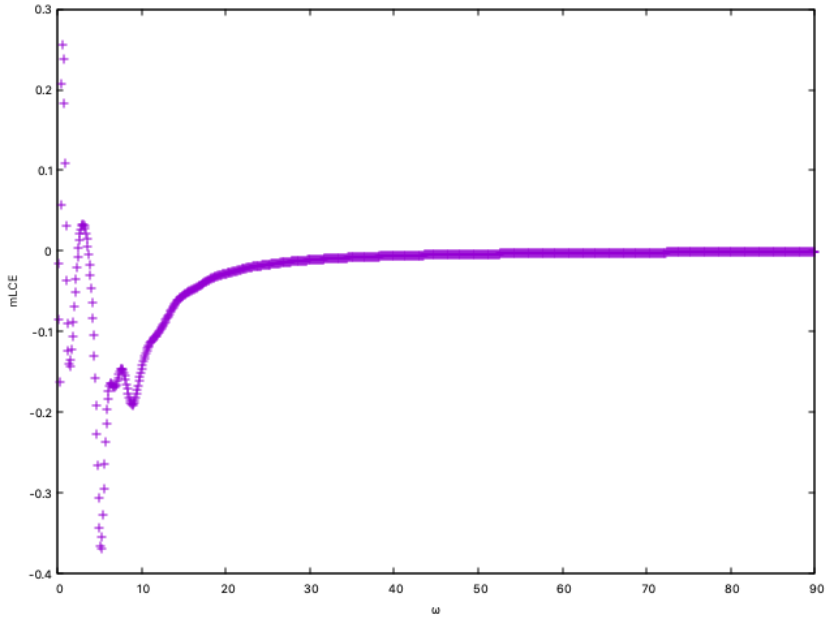

FIGURE 5.7: Maximum Lyapunov Characteristic Exponent (mLCE) (for the case with constant parameters) as a function of the parameter ω. The system can behave caotically or not depending on the values of the frequency ω indicated respectively by the positiveness or not of the Lyapunov exponent.

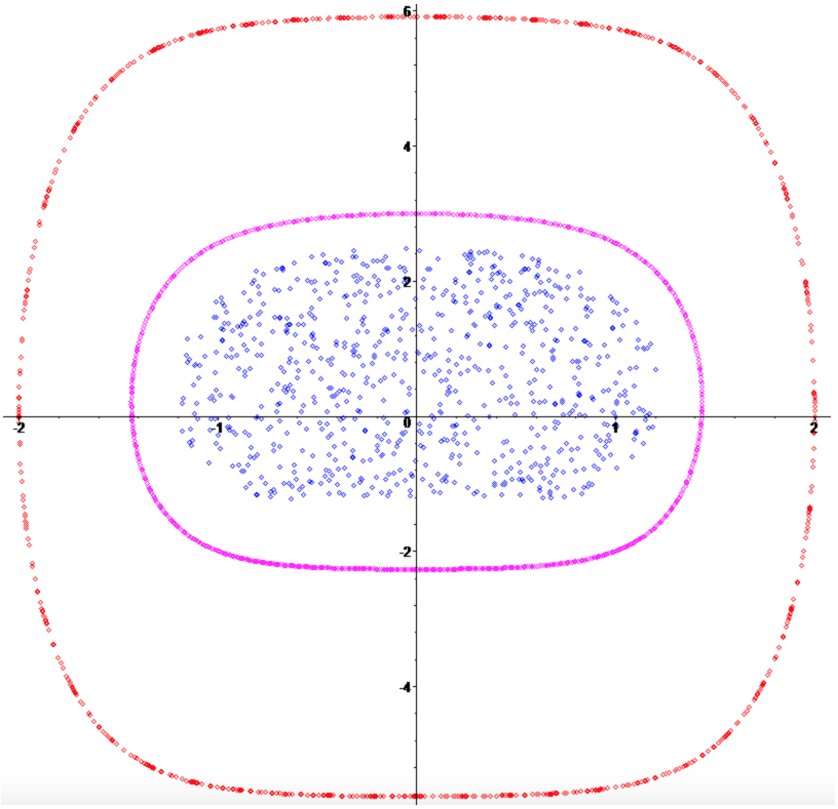

FIGURE 5.8: The Poincaré section for a value of the control parameter $\omega = 0.2$. In blue are shown the point for an initial value $x(0) = 1$, $\dot{x}(0) = 0$, in magenta for $x(0) = 2$, $\dot{x}(0) = 0$, and in red for $x(0) = 0$, $\dot{x}(0) = 3$. Here are shown the iteration points from 0 to $800 * T_0$ steps of integrations where $T_0 = 10 * \pi$ is the period of the forcing term.

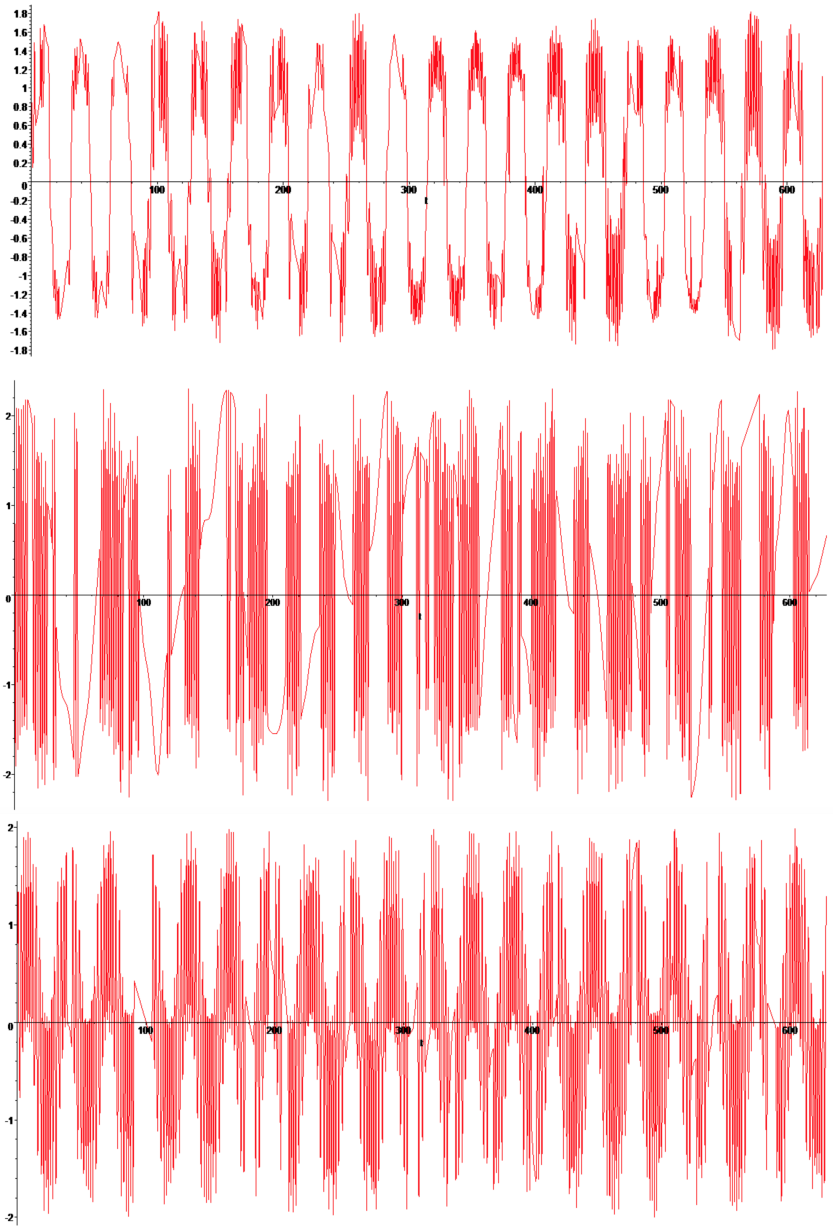

FIGURE 5.9: Temporal evolution of the state variable $x(t)$ corresponding to the intial points as in 5.5. Notice the absence of periodicity of the oscillations in the first panel. which is the proof for the presence of chaos in the dynamics. The situation becomes more regular for the other initial values as the signal regains its periodicity. Here the iteration interval for all the cases is $[0, 20 * T_0]$, con T_0 defined as above.

From the Poincaré section 5.8 it is clear that although we notice that the central part is dominated by a chaotic island (blue symbols), the system has also two larger regular orbits (in magenta and red) suggesting the presence of subharmonic orbits of very high periods.

The same behavior can be observed even from the time evolution of the state variable $x(t)$ illustrated in Fig. 5.9 for the same choice of the control parameter as above. It is easy to notice that the systems lacks periodicity and invariance of the amplitude in

the time space in the first panel corresponding to the initial point $x(0) = 2$, $\dot{x}(0) = 0$ indicating the chaotic behavior for these orbits. However the signal becomes more regular (periodic) for the two other set of orbits.

We conclude that the model of Wang & Yu we considered here when the paramters take constant values has the ability to manifest both chaotic and regular behavior depending on the values of the control parameter that in our case was the frequency ω of the T-periodic auxilary functions as previously defined. In fact, initially the system is chaotic for low frequencies; then when the period of the external forcing functions becomes enough large it undergoes a re-entering phase towards the regular behavior.

5.2 The Tokamak model

The next model that we will analyse here is that of the Tokomak already introduced and discussed in Chapter 1. Here we will complement the analytical study of Chapter 5 with a numerical one. Let us repropose once more the model as follows

$$\ddot{x} + \frac{q(t)}{x^3} + \frac{\log x}{x} = 0. \tag{5.6}$$

Here the function $q(t) : \mathbb{R} \to \mathbb{R}$ is defined as a T-periodic function and is positive $q(t) > 0$, $\forall t \in \mathbb{R}$. In particular, we will consider $q(t) = C + d * \sin(\omega * t + \alpha)$ with $C = 1$, $\alpha = 0$ (or equivalently $\alpha = \pi/2$) and $d \in]0, 1[$.

We will proceed similarly as we did in the previous subsection, so we will start by analysing the dependence that $mLCE$ has on the frequency ω which again will be our control parameter. In Fig. 5.10 is plotted the maximum Lyapunov exponent $mLCE$ as a function of the frequency ω. It can be obviously noted that for the window of the values of the frequency explored $mLCE$ almost does not change at all, remaining around the value 0.5. This is a clear indicator of chaos as we have already discussed several times already in this thesis. In this sense the chaoticity of the system is robust for the control parameter ω.

In our model (5.6), we have also another control parameter, the constant d which also as we have shown in Fig. 5.11 plays an important role in the dynamics. In fact, the $mLCE$ changes when the parameter d varies in the interval $]0, 1[$. Nevertheless as before for the frequency even in this case the chaos dominates the system in a robust way attested by a positive value of $mLCE$ around 0.5. We can conclude that this model is in general strongly chaotic and although it depends in two control parameter they do not influence its chaotic nature.

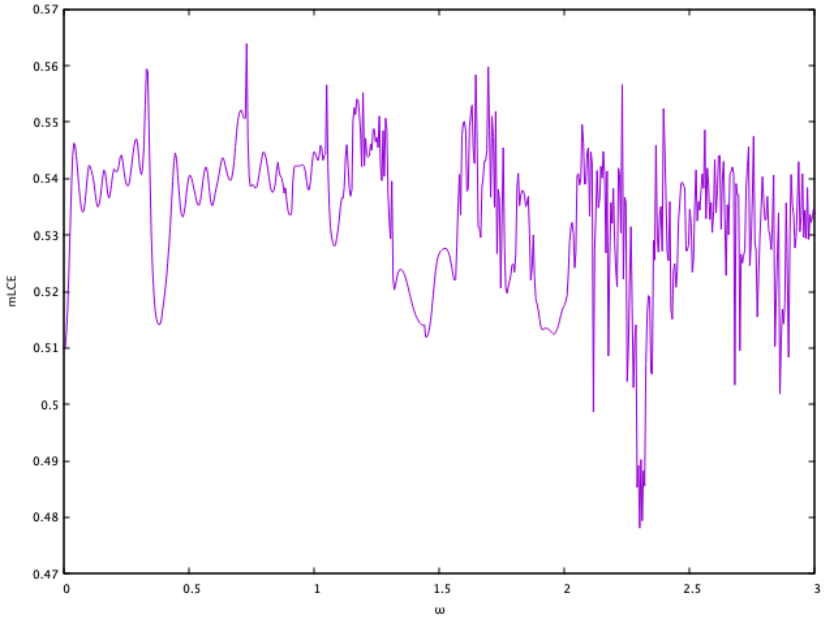

FIGURE 5.10: Maximum Lyapunov Characteristic Exponent ($mLCE$) of the model (5.6) as a function of the control parameter ω and a fixed value of $d = 0.05$. The system behaves chaotically for the values of ω explored here. Such behavior is indicated by the positiveness of the Lyapunov exponent.

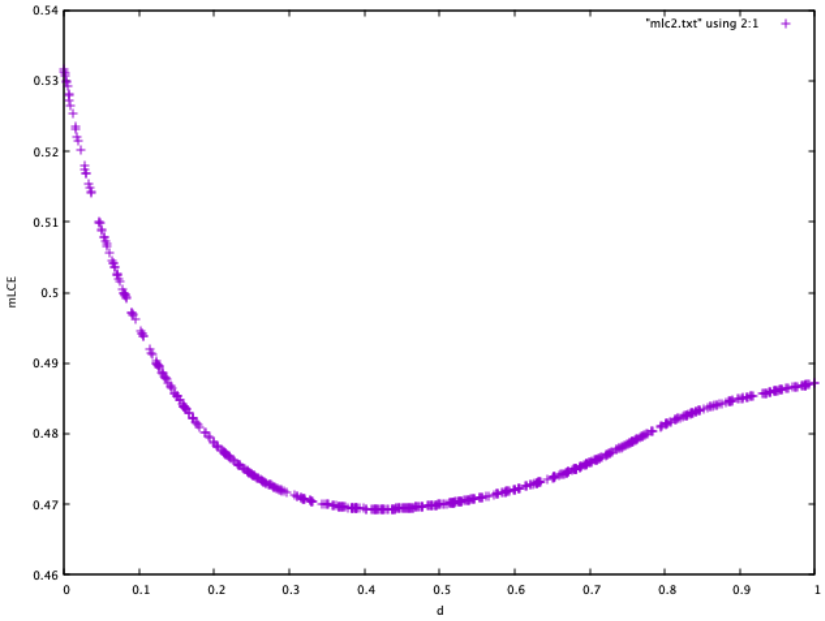

FIGURE 5.11: Maximum Lyapunov Characteristic Exponent ($mLCE$) of the model (5.6) as a function of the control parameter d and a fixed value of $\omega = 0$. The system behaves chaotically for the values of d explored here. Such behavior is indicated by the positiveness of the Lyapunov exponent.

The same result can be obtained even if we explore the Poincaré section of such system. In Fig. 5.12 we show the chaotic orbits that fill densely the Poincare section for the model (5.6). There is no doubt at this point that the orbits behave chaotically in the phase space.

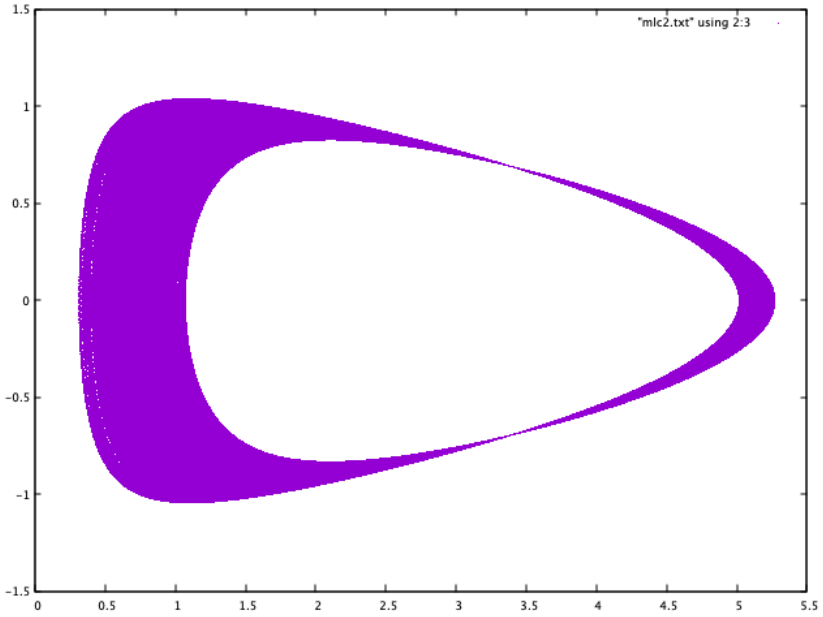

FIGURE 5.12: The Poincaré section for values of the control parameters $\omega = \pi/2$, $d = 0.05$. The orbits behave chaotically in the phase space for the parameters explored here.

Bibliography

[1] Bernard L. Cohen. Breeder reactors: A renewable energy source. *American Journal of Physics*, 51, 1983.

[2] I. L. Caldas, R. L. Viana, M. S. T. Araujo, A. Vannucci, E. C. da Silva, K. Ullmann, and M. V. A. P. Heller. Control of chaotic magnetic fields in tokamaks. *Brazilian Journal of Physics*, 32, 2002.

[3] Benjamin Cambon, Xavier Leoncini, Michel Vittot, Rémi Dumont, and Xavier Garbet. Chaotic motion of charged particles in toroidal magnetic configurations. *Chaos 24*, 2014.

[4] Ch. Skokos. Alignment indices: a new, simple method for determining the ordered or chaotic nature of orbits. *Physics A Journal*, 34, 2001.

[5] Francis F. Chen. Introduction to plasma physics and controlled fusion. *Plasma Physics*, 1 ed, 1984.

[6] Leslie C. Woods. Theory of tokamak transport. new aspects for nuclearfusion reactor design. *Plasma Physics*, 1 ed, 2006.

[7] wikipedia. URL https://en.wikipedia.org/wiki/Lawson${_{-}}$criterion{$#$}/media/File:Fusion${_{-}}$ntau.svg.

[8] B. Cambon, X. Leoncini, M. Vittot, R. Dumont, and X. Garbet. Chaotic motion of charged particles in toroidal magnetic configurations. *Chaos*, 24(3):033101, 11, 2014.

[9] M.Pireddu. Fixed points and chaotic dynamics for expansive- contractive maps in euclidean spaces, with some applications. *Dynamical Systems*, 2009.

[10] T.Y. Li and J.A. Yorke. Period three implies chaos. *Amer. Math. Monthly 82*, 1975.

[11] P. Stefan. A theorem of sarkovskii on the existence of periodic orbits of continuous endomorphisms of the real line. *Comm. Math. Phys. 54*, 1977.

[12] B. Aulbach and B. Kieninger. On three definitions of chaos. *Nonlinear Dyn. Syst. Theory*, 2001.

[13] F. Blanchard, E. Glasner, S. Kolyada, and A. Maass. On li-yorke pairs. *J. Reine Angew. Math.*, 2002.

[14] J. Smital. Chaotic functions with zero topological entropy. *Trans.Amer. Math. Soc.* 297, 1986.

[15] J. Kennedy, S. Kocak, and Y.A. Yorke. A chaos lemma. *Amer. Math. Monthly*, 2001.

[16] J. Banks, J. Brooks, G. Cairns, G. Davis, and P. Stacey. On devaney's definition of chaos. *Amer. Math. Monthly* 99, 1992.

[17] S. Silverman. On maps with dense orbits and the definition of chaos. *Rocky Mountain J. Math.* 22, 1992.

[18] J. Auslander and J.A. Yorke. Interval maps, factors of maps, and chaos. *Tohoku Math. J.* 32, 1980.

[19] F. Balibrea and L. Snoha. Topological entropy of devaney chaotic maps. *Topology Appl.* 133, 2003.

[20] D. Kwietniak and M. Misiurewicz. Exact devaney chaos and entropy. *Qual. Theory Dyn. Syst.* 6, 2005.

[21] S. Li. ω-chaos and topological entropy. *Trans. Amer. Math. Soc.* 339, 1993.

[22] W. Huang and X. Ye. Devaney's chaos or 2-scattering implies li-yorke's chaos. *Topology Appl.* 117, 2002.

[23] C. Conley. Isolated invariant sets and the morse index. *CBMS Regional Conference Series in Mathematics, 38, American Mathematical Society, Providence, R.I*, 1978.

[24] P. Hartman. Ordinary differential equations. *Wiley, New York*, 1964.

[25] P. Hartman. On invariant sets and on a theorem of Ważewski. *Proc. Amer. Math. Soc. 32*, 1972.

[26] Ch. Skokos. The smaller (sali) and the generalized (gali) alignment indices: Efficient methods of chaos detection. *Lect. Notes Phys.*, 915, 2016.

[27] Ch. Skokos. The lyapunov characteristic exponents and their computation. *Lect. Notes Phys.*, 790, 2010.

[28] M.Henon. On the numerical computation of poincaré maps. *Physica D: Nonlinear Phenomena 5*, 1982.

[29] M. Casartelli, E. Diana, L. Galgani, and A Scotti. Numerical computations on a stochastic parameter related to the kolmogorov entropy. *Phys. Rev. A 13*, 1976.

[30] Galgani Benettin, G. and Strelcyn L. Kolmogorov entropy and numerical experiments. *Phys. Rev. A 14*, 1976.

[31] V.I. Oseledec. A multiplicative ergodic theorem. ljapunov characteristic numbers for dynamical systems. *Trans. Moscow Math. Soc. 19, 197–231*, 1968.

[32] A. Giorgilli J.-M. Strelcyn G. Benettin, L. Galgani. Lyapunov characteristic exponents for smooth dynamical systems and for hamiltonian systems; a method for computing all of them. part 1: theory. *Meccanica 15, 9–20*, 1980.

[33] G. Benettin, L. Galgani, A. Giorgilli, J.-M. Strelcyn, C. Antonopoulos, T. Bountis, and M. Vrahatis. Lyapunov characteristic exponents for smooth dynamical systems and for hamiltonian systems; a method for computing all of them. *Part 1: theory. Meccanica*, 1980.

[34] Lunsford G.H. Ford, J. Stochastic behavior of resonant nearly linear oscillator systems in the limit of zero nonlinear coupling. *Phys. Rev. A .*, 59-70, 1970.

[35] C. Skokos. Alignment indices: a new, simple method for determining the ordered or chaotic nature of orbits. *Journal of Physics A: Mathematical and General 34*, 2001.

[36] Ch. Skokos, T.C. Bountis, and Ch. Antonopoulos. Detecting chaos, determining the dimensions of tori and predicting slow diffusion in fermi-pasta-ulam lattices by the generalized alignment index method. *Eur. Phys. J. Spec. Top. 165*, 2008.

[37] W.H. Press, S.A. Teukolsky, W.T. Vetterling, and B.P. Flannery. Numerical recipes in fortran 77: The art of scientific computing. *Cambridge University Press*, 2003.

[38] Athanassoula E. Skokos Ch., Patsis P. A. Orbital dynamics of three-dimensional bars - i. the backbone of three-dimensional bars. a fiducial case. *MNRAS*, 333, 2002.

[39] J. K. Hale. *Ordinary differential equations*. Robert E. Krieger Publishing Co., Inc., Huntington, N.Y., second edition, 1980.

[40] J. Guckenheimer and P. Holmes. *Nonlinear oscillations, dynamical systems, and bifurcations of vector fields*, volume 42 of *Applied Mathematical Sciences*. Springer-Verlag, New York, 1990. Revised and corrected reprint of the 1983 original.

[41] T. R. Ding and F. Zanolin. Subharmonic solutions of second order nonlinear equations: a time-map approach. *Nonlinear Anal.*, 20(5):509–532, 1993.

[42] A. Boscaggin, A. Fonda, and M. Garrione. A multiplicity result for periodic solutions of second order differential equations with a singularity. *Nonlinear Anal.*, 75 (12):4457–4470, 2012.

[43] A. Fonda, R. Manásevich, and F. Zanolin. Subharmonic solutions for some second-order differential equations with singularities. *SIAM J. Math. Anal.*, 24(5):1294–1311, 1993.

[44] K. J. Palmer. Transversal heteroclinic points and Cherry's example of a nonintegrable Hamiltonian system. *J. Differential Equations*, 65(3):321–360, 1986.

[45] F. Battelli and K. J. Palmer. Chaos in the Duffing equation. *J. Differential Equations*, 101(2):276–301, 1993.

[46] A. Pokrovskii, O. Rasskazov, and D. Visetti. Homoclinic trajectories and chaotic behaviour in a piecewise linear oscillator. *Discrete Contin. Dyn. Syst. Ser. B*, 8(4): 943–970, 2007.

[47] F. Battelli and M. Fečkan. On the chaotic behaviour of discontinuous systems. *J. Dynam. Differential Equations*, 23(3):495–540, 2011.

[48] F. Battelli and M. Fečkan. Nonsmooth homoclinic orbits, Melnikov functions and chaos in discontinuous systems. *Phys. D*, 241(22):1962–1975, 2012.

[49] Z. Opial. Sur les périodes des solutions de l'équation différentielle $x'' + g(x) = 0$. *Ann. Polon. Math.*, 10:49–72, 1961.

[50] C. Chicone. The monotonicity of the period function for planar Hamiltonian vector fields. *J. Differential Equations*, 69(3):310–321, 1987.

[51] J. K. Hale. *Ordinary differential equations*. Robert E. Krieger Publishing Co., Inc., Huntington, N.Y., second edition, 1980.

[52] A. C. Lazer and S. Solimini. On periodic solutions of nonlinear differential equations with singularities. *Proc. Amer. Math. Soc.*, 99(1):109–114, 1987.

[53] I. Rachunková, S. Staněk, and M. Tvrdý. *Solvability of nonlinear singular problems for ordinary differential equations*, volume 5 of *Contemporary Mathematics and Its Applications*. Hindawi Publishing Corporation, New York, 2008.

[54] P. J. Torres. *Mathematical models with singularities*, volume 1 of *Atlantis Briefs in Differential Equations*. Atlantis Press, Paris, 2015. A zoo of singular creatures.

[55] A. Margheri and P-J. Torres. Chaotic dynamics of the Kepler problem with oscillating singularity. *Adv. Nonlinear Stud.*, 16(3):551–567, 2016.

[56] U. Kirchgraber and D. Stoffer. On the definition of chaos. *Z. Angew. Math. Mech.*, 69(7):175–185, 1989.

[57] S. Smale. Finding a horseshoe on the beaches of Rio. *Math. Intelligencer*, 20(1): 39–44, 1998.

[58] A. Bacciotti and L. Mazzi. An invariance principle for nonlinear switched systems. *Systems Control Lett.*, 54(11):1109–1119, 2005.

[59] R. L. Devaney. Subshifts of finite type in linked twist mappings. *Proc. Amer. Math. Soc.*, 71(2):334–338, 1978.

[60] H. Aref. Stirring by chaotic advection. *J. Fluid Mech.*, 143:1–21, 1984.

[61] H. Aref. Point vortex dynamics: a classical mathematics playground. *J. Math. Phys.*, 48(6):065401, 23, 2007.

[62] J. M. Ottino. *The kinematics of mixing: stretching, chaos, and transport.* Cambridge Texts in Applied Mathematics. Cambridge University Press, Cambridge, 1989.

[63] R. Sturman, J. M. Ottino, and S. Wiggins. *The mathematical foundations of mixing*, volume 22 of *Cambridge Monographs on Applied and Computational Mathematics.* Cambridge University Press, Cambridge, 2006. The linked twist map as a paradigm in applications: micro to macro, fluids to solids.

[64] S. Wiggins and J. M. Ottino. Foundations of chaotic mixing. *Philos. Trans. R. Soc. Lond. Ser. A Math. Phys. Eng. Sci.*, 362(1818):937–970, 2004.

[65] A. Margheri, C. Rebelo, and F. Zanolin. Chaos in periodically perturbed planar Hamiltonian systems using linked twist maps. *J. Differential Equations*, 249(12): 3233–3257, 2010.

[66] M. Pireddu and F. Zanolin. Chaotic dynamics in the Volterra predator-prey model via linked twist maps. *Opuscula Math.*, 28(4):567–592, 2008.

[67] F. Rothe. The periods of the Volterra-Lotka system. *J. Reine Angew. Math.*, 355: 129–138, 1985.

[68] J. Waldvogel. The period in the Lotka-Volterra system is monotonic. *J. Math. Anal. Appl.*, 114(1):178–184, 1986.

[69] A. Bacciotti. Bounded-input-bounded-state stabilization of switched processes and periodic asymptotic controllability. *Kybernetika (Prague)*, 53(3):530–544, 2017.

[70] B. Aulbach and B. Kieninger. On three definitions of chaos. *Nonlinear Dyn. Syst. Theory*, 1(1):23–37, 2001.

[71] L. S. Block and W. A. Coppel. *Dynamics in one dimension*, volume 1513 of *Lecture Notes in Mathematics*. Springer-Verlag, Berlin, 1992.

[72] A. Medio, M. Pireddu, and F. Zanolin. Chaotic dynamics for maps in one and two dimensions: a geometrical method and applications to economics. *Internat. J. Bifur. Chaos Appl. Sci. Engrg.*, 19(10):3283–3309, 2009.

[73] D. Papini and F. Zanolin. On the periodic boundary value problem and chaotic-like dynamics for nonlinear Hill's equations. *Adv. Nonlinear Stud.*, 4(1):71–91, 2004.

[74] D. Papini and F. Zanolin. Fixed points, periodic points, and coin-tossing sequences for mappings defined on two-dimensional cells. *Fixed Point Theory Appl.*, (2):113–134, 2004.

[75] A. Pascoletti, M. Pireddu, and F. Zanolin. Multiple periodic solutions and complex dynamics for second order ODEs via linked twist maps. In *The 8th Colloquium on the Qualitative Theory of Differential Equations*, volume 8 of *Proc. Colloq. Qual. Theory Differ. Equ.*, pages No. 14, 32. Electron. J. Qual. Theory Differ. Equ., Szeged, 2008.

[76] J. Guckenheimer and P. Holmes. *Nonlinear oscillations, dynamical systems, and bifurcations of vector fields*, volume 42 of *Applied Mathematical Sciences*. Springer-Verlag, New York, 1990. Revised and corrected reprint of the 1983 original.

[77] S. Smale. Differentiable dynamical systems. *Bull. Amer. Math. Soc.*, 73(6):747–817, 1967.

[78] J. Moser. *Stable and random motions in dynamical systems*. Princeton University Press, Princeton, N. J.; University of Tokyo Press, Tokyo, 1973. With special emphasis on celestial mechanics, Hermann Weyl Lectures, the Institute for Advanced Study, Princeton, N. J, Annals of Mathematics Studies, No. 77.

[79] J. López-Gómez, A. Tellini, and F. Zanolin. High multiplicity and complexity of the bifurcation diagrams of large solutions for a class of superlinear indefinite problems. *Commun. Pure Appl. Anal.*, 13:1–73, 2014.

[80] J. López-Gómez, P. Omari, and S. Rivetti. Bifurcation of positive solutions for a one-dimensional indefinite quasilinear neumann problem. *Nonlinear Analysis*, 155: 1–51, 2017.

[81] H. P. W. Gottlieb and J. C. Sprott. Simplest driven conservative chaotic oscillator. *Physics Letters A 291 385–388*, 2001.

[82] Y. Wang and J. You. Boundedness of solutions for polynomial potentials with c^2 time dependent coefficients. *Zeitschrift für angewandte Mathematik und Physik*, 1996.